DIMETHYL ETHER (DME) SYNTHESIS OVER NOVEL MESOPOROUS CATALYSTS

A THESIS SUBMITTED TO
THE GRADUATE SCHOOL OF NATURAL AND APPLIED SCIENCES
OF
MIDDLE EAST TECHNICAL UNIVERSITY

BY

KENAN CEM TOKAY

IN PARTIAL FULFILLMENT OF THE REQUIREMENTS
FOR
THE DEGREE OF MASTER OF SCIENCE
IN
CHEMICAL ENGINEERING

AUGUST 2008

Approval of the thesis:

"DIMETHYL ETHER (DME) SYNTHESIS OVER NOVEL MESOPOROUS CATALYSTS"

submitted by **KENAN CEM TOKAY** in partial fullfillment of the requirements for the degree of Master of Science in **Chemical Engineering Department, Middle East Technical University** by,

Prof. Dr. Canan Özgen _____
Dean, Graduate School of **Natural and Applied Sciences**

Prof. Dr. Gürkan Karakaş _____
Head of Department, **Chemical Engineering**

Prof. Dr. Timur Doğu
Supervisor, **Chemical Engineering Dept., METU** _____

Prof. Dr. Gülşen Doğu
Co-Supervisor, **Chemical Engineering Dept., METU** _____

Examining Committee Members:

Prof. Dr. İnci Eroğlu

Chemical Engineering Dept., METU _____

Prof. Dr. Timur Doğu

Chemical Engineering Dept., METU _____

Assoc. Prof. Dr. Naime Aslı Sezgi

Chemical Engineering Dept., METU _____

Assist. Prof. Dr. Dilek Varışlı

Advanced Technologies, Gazi University _____

Assist. Prof. Dr. Sena Yaşyerli

Chemical Engineering Dept., Gazi University _____

Date: **22.08.2008**

I hereby declare that all information in this document has been obtained and presented in accordance with academic rules and ethical conduct. I also declare that, as required by these rules and conduct, I have fully cited and referenced all material and results that are not original to this work.

Name, Last name: Kenan Cem TOKAY

Signature :

ABSTRACT

DIMETHYL ETHER (DME) SYNTHESIS OVER NOVEL MESOPOROUS CATALYSTS

TOKAY, Kenan Cem
M.Sc., Department of Chemical Engineering
Supervisor: Prof. Dr. Timur DOĞU
Co-Supervisor: Prof. Dr. Gülşen DOĞU

August 2008, 137 pages

Due to overconsumption, fossil reserves are rapidly being depleted and various sources predict that they will not last until the end of 21st century. Moreover, the increase in the rate of global warming and the polluting matter emitted by the vehicles consuming fossil fuels has increased the search for renewable and clean energy sources. Alcohols and ethers, which contain fewer pollutants and have better burning properties, are commonly thought among clean fuel alternatives. Among the potential clean energy sources, dimethyl-ether is already in use in the automotive industries of many countries such as China and Japan, due to its low NO_x and CO_2 emissions, high cetane rating and efficient combustion characteristics, especially in diesel engines.

In this work, dimethyl-ether synthesis is achieved using methanol dehydration reaction over solid acid catalysts. For this purpose, three different

mesoporous MCM-41 type aluminum silicates have been synthesized with direct hydrothermal synthesis method and aluminum is added to the synthesized SBA-15 catalyst using impregnation method. Apart from the catalysts synthesized, different commercial catalysts such as aluminum oxide in different forms (α and γ), Nafion NR-50 and Nafion SAC-13 have also been tested in this reaction. These materials were characterized by methods such as XRD, EDS, SEM, and N_2 physical adsorption and DRIFTS were also investigated in terms of paramters such as the conversion of methanol to products, selectivity and yield.

The analyses have shown that AlSi1 is the most active of all the aluminum silicates synthesized in both 0.136 and 0.27 s.g/cm^3 space times, with up to 80% methanol conversion in all temperatures tested. AlSi1 also has low by-product formation and similar to other aluminum silicates, its dimethyl-ether selectivity approaches 1 at 400^{0}C. Among all synthesized catalysts, the dimethyl-ether yield was seen to be the highest for Al-SBA-15, which approaches 0.5 at 400^{0}C for both space times. For all aluminum silicates synthesized, about 40% dimethyl-ether yield was obtained at the same temperature and space times. Among the aluminum oxides, α-alumina was seen to be superior to others in γ forms in terms of conversion selectivity and yield, especially at low temperatures. As to Nafion catalysts, due to its much higher surface area and high Bronsted acidity, Nafion SAC-13 has shown higher activity compared to Nafion NR-50 for all temperatures and space times tested.

Keywords: DME, methanol dehydration reaction, methanol, mesoporous catalysts.

ÖZ

MEZOGÖZENEKLİ KATALİZÖRLER ÜZERİNDE DİMETİL ETER (DME) SENTEZİ

TOKAY, Kenan Cem
Yüksek Lisans, Kimya Mühendisliği
Tez Danışmanı: Prof. Dr. Timur DOĞU
Eş Danışman: Prof. Dr. Gülşen DOĞU

Ağustos 2008, 137 sayfa

Aşırı tüketime bağlı olarak hızla tükenen fosil yakıt reservlerinin, çeşitli kaynaklarda 21.yüzyıl sonuna kadar bile dayanamayacağı tahmin edilmektedir. Bunun yanı sıra, küresel ısınma hızındaki artış ve de fosil yakıt kullanan taşıtların çevreye yaydıkları kirletici madde salınımı; geleceğe dönük, yenilenebilir, temiz enerji kaynakları arayışını bu günlerde daha da artırmıştır. Daha az kirletici ihtiva eden ve daha iyi yanma özelliklerine sahip alkoller ve eterler, temiz alternatif yakıtlar arasında yaygın olarak düşünülmektedir. Potansiyel temiz enerji kaynakları arasında dimetil eter (DME); düşük NO_x ve CO_2 salınımı, yüksek setan sayısı ve özellikle dizel motorlu araçlarda verimli yanma özellikleri gibi pek çok nedenden ötürü daha şimdiden Çin ve Japonya gibi ülkelerin otomobil endüstrilerinde yerini almıştır.

Bu çalışmada, katı asit katalizörler kullanılarak metanol dehidrasyonu reaksiyonu ile dimetil eter sentezi gerçekleştirilmiştir. Bu amaç doğrultusunda,

direk hidrotermal sentez yöntemiyle 3 farklı mezogözenekli MCM-41 tipi aluminyum silikat sentezlenmiş ve ayrıca sentezlenen SBA-15 katalizörüne impregnasyon (emdirme) yöntemiyle aluminyum eklenmiştir. Sentezlenen katalizörler dışında, ticari firmalardan temin edilen değişik formlardaki (α ve γ) aluminyum oksit, Nafion NR-50 ve Nafion SAC-13 gibi katalizörler bu reaksiyonda denenmiştir. XRD, EDS, SEM, N_2 fiziksel adsorplanmasi ve DRIFTS gibi teknikler kullanılarak karakterize edilen malzemeler, metanolun ürünlere dönüşümü, seçicilik ve de verim parametreleri yönünden incelenmiştir.

Analizler sonucunda, sentezlenen aluminyum silikatlar içerisinde AlSi1 hem 0.136 hem de 0.27 s.g/cm^3 alıkonma süresinde, test edilen tüm sıcaklıklarda %80'e varan metanol dönüşümü ile en aktif katalizör olmuştur. Yan ürün oluşumu da düşük olan AlSi1'de, dimetil eter seçiciliği de diğer aluminyum silikatlar gibi 400^{0}C de 1 e yaklaşmaktadır. Dimetil eter verimi tüm sentezlenen malzemeler arasında 400^{0}C de ve her iki alıkonma süresinde 0.5'e yaklaşan değeriyle en yüksek Al-SBA-15'de gözlenmiştir. Sentezlenen aluminyum silikatlar da ise aynı sıcaklıkta ve alıkonma sürelerinde %40 civarında dimetil eter verimi elde edilmiştir. aluminyum oksitler arasında ise, α-alumina dönüşüm seçicilik ve verim parametrelerinde düşük sıcaklıklarda bile diğer γ formundakilere üstünlük sağlamıştır. Nafyon katalizörler arasında ise; Nafion SAC-13, yüksek yüzey alanı ve Bronsted asiditesi sayesinde Nafion NR-50 ye göre test edilen tüm sıcaklık ve alıkonma sürelerinde daha yüksek aktivite göstermiştir.

Anahtar Sözcükler: DME, metanol dehidrasyon reaksiyonu, metanol, mezo gözenekli katalizörler.

To my family

ACKNOWLEDGEMENTS

First of all, I am very grateful to my supervisor Prof. Dr. Timur Doğu. I learned a lot from him in two years . As all the department is, I am also an admirer of him. I would like to express my special thanks to him for his inspiration to me and guidance for my thesis.

Also, I would like to thank my co-supervisor Prof. Dr. Gülşen Doğu for her valuable advices and supplying technical support about the analyses in Gazi University.

In addition to this, I would like to thank Prof. Dr. Hilmi Önder Özbelge and Prof. Dr. Tülay Özbelge for introducing me to Prof. Dr. Timur Doğu. They always ask me whether I have a problem or not wherever we meet in the department :). Besides, I would like to thank Assoc. Prof. Dr. Nail Yaşyerli for behaving me in a friendly manner whenever I go to his office. Also, I am giving thanks to Assoc. Prof. Dr. Naime Aslı Sezgi for her behavior to me. In addition, I am grateful to Prof. Dr. İsmail Tosun. I learned very much about "Transport Phenomena". Also, I am thankful for his precious guidance to me from the beginning of my graduate study.

Special thanks go to Kasnakoğlu family for their support and being my other family.

For their eternal friendship, I thank to my lab mates Dr. Dilek Varışlı, Zeynep Obalı, Canan Martı, Ekin Özdoğan, Ayşegül Çiftçi and Ayça Arınan. Especially, I thank Dilek Varışlı for helping me every time about my subject; Zeynep Obalı, "director of our laboratory" :), and Canan Martı are always

helpful not only for the synthesis and analyses but also supporting me with their optimistic behavior. I'll never forget you.

TABLE OF CONTENTS

ABSTRACT…….. iv
ÖZ…….. vi
DEDICATION…….. viii
ACKNOWLEDGEMENTS…….. ix
TABLE OF CONTENTS…….. x
LIST OF TABLES…….xiii
LIST OF FIGURES…….. xiv
NOMENCLATURE…….. xvi
CHAPTER
1- INTRODUCTION……. 1
2- USAGE OF ALCOHOLS……. 3
2.1. Alcohols as Transportation Fuels……3
2.2. Present Uses of Methanol……... 5
2.3. Physical Properties of DME……... 6
2.4 DME Markets……...8
2.5. DME as Fuel……... 8
3- CATALYTIC DEHYDRATION OF METHANOL ……... 10
3.1. Routes of DME Synthesis…….....10
3.1.1. Indirect Synthesis Method……..... 10
(Methanol Dehydration)
3.1.2. Direct DME Synthesis (Syngas to DME)……..…….....16
3.2. Thermodynamics of the Reaction……... 22
4- M41S MESOPOROUS MATERIALS…….....25
4.1. Mesoporous Materials…….....25
4.2. M41S Family……..... 26
5- CHARACTERIZATION OF THE MATERIALS…… 31

5.1. X-Ray Diffraction (XRD)……...31
5.2. N_2 Physisorption…… 32
5.3. Scanning Electron Microscopy (SEM)……... 33
5.4. Energy Dispersive Spectrum (EDS)……... 33
5.5. Diffuse Reflectance FT-IR (DRIFTS)…… 33
6- EXPERIMENTAL STUDIES …….. 35
6.1. Catalyst Synthesis…….....35
6.1.1. Synthesis of Mesoporous Aluminum Silicates…… 35
6.1.2. Synthesis of SBA-15…….. 39
6.1.3. Aluminum Impregnation in Synthesized SBA-15…….....40
6.2. Catalyst Characterization…….....40
6.2.1. X-Ray Diffraction (XRD)…….....40
6.2.2. N_2 Physisorption…….. 41
6.2.3. Energy Dispersive Spectrum (EDS)…… 41
6.2.4. Scanning Electron Microscopy (SEM)…….....41
6.2.5. Diffuse Reflectance FT-IR (DRIFTS)……41
6.3. Experimental Setup……41
6.3.1. Chemicals and Experimental Parameters…….44
7- RESULTS AND DISCUSSION……46
7.1. Characterization Results of the Catalysts……... 46
7.1.1. Characterization Results of Aluminum Silicates……46
7.1.1.1. XRD……..46
7.1.1.2. EDS…….. 49
7.1.1.3. N_2 Physisorption……... 50
7.1.1.4. SEM…….. 52
7.1.1.5. DRIFTS…….54
7.1.2. Characterization Results of SBA-15 and……. ……... 57
Al-SBA-15
7.1.2.1. XRD…….....57
7.1.2.2. EDS……... 58
7.1.2.3. N_2 Physisorption……... 59
7.1.2.4. SEM……...61
7.1.2.5. DRIFTS……62

7.1.3. Characterization Results of Aluminum Oxide……..…..... 63
Catalysts
7.1.3.1. N_2 Physisorption…….. 63
7.1.3.2. SEM……..... 66
7.1.3.3. DRIFTS…….... 68
7.1.4. Characterization Results of Nafion Catalysts…….. 70
7.1.4.1. N_2 Physisorption……..... 70
7.1.4.2. SEM…….. 72
7.1.4.3. DRIFTS……..... 73
7.2. Results of Methanol Dehydration Reactions…….. 73
7.2.1. Results of Methanol Dehydration Reaction over……..... 75
Aluminum Based Catalysts
7.2.2. Results of Methanol Dehydration Reaction over……..... 77
Synthesized Aluminum Silicates and Aluminum
Impregnated SBA-15 (Al-SBA-15)
7.2.3. Results of Methanol Dehydration Reaction over……..... 88
α and γ Forms of Aluminum Oxides
7.2.4. Results of Methanol Dehydration Reaction over……. 96
Nafion Catalysts
8- CONCLUSION……. 108
9- REFERENCES…….. 110
10- APPENDIX…….....117
A.1. EDS RESULTS……..117
A.2. SEM IMAGES……..... 121
B.1.CALIBRATION FACTORS OF THE
SPECIES FOR CHROMOTOGRAPHIC ANALYSIS……..... 131
B.2. SAMPLE CALCULATIONS……..... 132
OF THE REACTION PARAMETERS
B.3.OTHER MEOH DEHYDRATION REACTION RESULTS..... 134

LIST OF TABLES

Table 1. Comparison of Dimethyl Ether's Physical and Thermo-Physical.. 7
Properties to Commonly Used Fuels
Table 2. Silica and Aluminum Sources Used in Synthesized Catalysts……37
Table 3. d_{100} and a Values for the Catalysts……..49
Table 4. EDS Analyses of the Synthesized Aluminum Silicate……50
Samples Having Different Al Loadings
Table 5. Physical Properties of the Synthesized Aluminum Silicates…….. 52
Table 6. EDS Analysis of the Synthesized Al-SBA-15…… 59
Table 7. Physical Properties of Synthesized SBA-15 and Al-SBA-15…….60
Table 8. Physical Properties of the Catalysts…… 66
Table 9. Physical Properties of the Catalysts…… 71
Table 10. Experimental Conditions for Aluminum Based Catalysts…… 76
Table 11. Variation of Methanol Conversion with Different Space Times.. 80
Table 12. Variation of DME and FA Selectivity over……. 83
Al-SBA-15 with 0.27 s.g/cm^3
Table 13. Variation of DME and FA Selectivity over AlSi1 and…… 85
AlSi2 with Different Space Times.
Table 14. Variation of DME and FA Yield Over……..86
Al-SBA-15 with 0.27 s.g/cm^3
Table 15. Variation of DME and FA Yields over Aluminum Silicates…... 87
with Different Space Times.
Table 16. Variation of Methanol Conversion over α and γ Forms……...89
of Aluminum Oxides with Different Space Times.
Table 17. Variation of DME Selectivity over α and γ Forms……... 91
of Aluminum Oxides with Different Space Times
Table 18. Variation of FA Selectivity over α and γ Forms……... 93

of Aluminum Oxides with Different Space Times
Table 19. Variation of DME Yield over α and γ Forms……... 95
of Aluminum Oxides with Different Space Times
Table 20. Variation of FA Yield over α and γ Forms……... 95
of Aluminum Oxides with Different Space Times
Table 21. Experimental Conditions for Nafion Catalysts……. 97
Table 22. Variation of Methanol Conversion over Nafion…….. 98
Catalysts with Different Space Times
Table 23. Variation of DME and Formaldehyde Selectivity over…… 103
Nafion Catalysts with Different Space Times
Table 24. Variation of DME and Formaldehyde Yield over…….106
Nafion Catalysts with Different Space Times
Table 25. Calibration Factors of the Components…….....132

LIST OF FIGURES

Figure 1. X-ray Diffraction Pattern of Calcined MCM-41…….. 28
Figure 2. Adsorption Isotherm of Nitrogen on MCM-41……. 29
with 4.0 nm Pores at 77 K
Figure 3. Synthesis Steps of Mesoporous Aluminum Silicates....…..... 36
Figure 4. Experimental Setup……43
Figure 5. A Photo of Experimental Setup……44
Figure 6. Chemical Structure of Nafion……45
Figure 7. XRD Pattern of AlSi1 catalyst…….. 47
Figure 8. XRD Pattern of AlSi2 catalyst…….. 47
Figure 9. XRD Pattern of AlSi3 catalyst…….. 48
Figure 10. Adsorption-Desorption Isotherm of Synthesized…… 51
Aluminum Silicates
Figure 11. Pore Size Distribution of Synthesized Aluminum Silicates…… 51
Figure 12. SEM Image of AlSi1……... 53
Figure 13. SEM Image of AlSi2……... 53
Figure 14. SEM Image of AlSi3……... 54
Figure 15. DRIFT Spectra of AlSi1…….. 55
Figure 16. DRIFT Spectra of AlSi2…….. 55
Figure 17. DRIFTS Spectra of AlSi3……56
Figure 18. XRD Pattern of SBA-15……..57
Figure 19. XRD Pattern of Al-SBA-15…….58
Figure 20. Adsorption-Desorption Isotherm of Synthesized SBA-15…….. 59
and Al-SBA-15
Figure 21. Pore Size Distribution of Synthesized SBA-15…….. 60
and Al-SBA-15
Figure 22. SEM Image of SBA-15……61

Figure 23. SEM Image of Al-SBA-15…….. 62
Figure 24. DRIFTS Spectra of Al-SBA-15…….. 62
Figure 25. Adsorption-Desorption Isotherm of α-Al……... 63
Figure 26. Adsorption-Desorption Isotherm of γ-Al-1…… 64
Figure 27. Adsorption-Desorption Isotherm of γ-Al-2……. 64
Figure 28. Adsorption-Desorption Isotherm of γ-Al-3……. 65
Figure 29. Pore Size Distribution of Aluminum Oxides……..65
Figure 30. SEM Image of α-Al……. 67
Figure 31. SEM Image of γ-Al-1…….. 67
Figure 32. SEM Image of γ-Al-2…….. 68
Figure 33. DRIFTS Spectra of α-Al……..69
Figure 34. DRIFTS Spectra of γ-Al-1…….. 69
Figure 35. Adsorption-Desorption Isotherm of Nafion NR-50…….70
and SAC-13
Figure 36. Pore Size Distribution of Nafion NR-50 and SAC-13……71
Figure 37. SEM Image of Nafion NR-50……..72
Figure 38. SEM Image of Nafion SAC-13……... 72
Figure 39. DRIFTS Spectra of Nafion SAC-13…… 73
Figure 40. Conversion of Methanol over AlSi1 and AlSi2…….. 77
at 0.136 s.g/cm^3
Figure 41. Conversion of Methanol over Synthesized Aluminum……... 78
Silicates and Al-SBA-15 at 0.27 s.g/cm^3
Figure 42. Variation of MeOH Conversion Over AlSi1 and AlSi2……..81
at Different Space Times
Figure 43. Selectivity of DME and Formaldehyde with AlSi1…….82
and AlSi2 at 0.136 s.g/cm^3
Figure 44. Selectivity of DME and Formaldehyde with Aluminum…….84
Silicates and Al-SBA-15 at 0.27 s.g/cm^3
Figure 45. Yield of DME and Formaldehyde with……... 85
AlSi1 and AlSi2 at 0.136 s.g/cm^3
Figure 46. Yield of DME and Formaldehyde with Aluminum Silicates….. 85
and Al-SBA-15 at 0.27 s.g/cm^3
Figure 47. Conversion of Methanol over α and γ Forms…….. 88

of Aluminum Oxides at 0.136 s.g/cm^3
Figure 48. Conversion of Methanol over α and γ Forms of……. 90
Aluminum Oxides at 0.27 s.g/cm^3
Figure 49. Selectivity of DME and Formaldehyde with…….. 91
α and γ Forms of Aluminum Oxides at 0.136 s.g/cm^3
Figure 50. Selectivity of DME and Formaldehyde with…….. 92
α and γ Forms of Aluminum Oxides at 0.27 s.g/cm^3
Figure 51. Yield of DME and Formaldehyde with α and γ Forms of…….. 94
Aluminum Oxides at 0.136 s.g/cm^3
Figure 52. Yield of DME and Formaldehyde with α and γ Forms of……...94
Aluminum Oxides at 0.27 s.g/cm^3
Figure 53. Conversion of Methanol over A-Al and AlSi1……96
at 0.27 s.g/cm^3
Figure 54. Conversion of Methanol over Nafion Catalysts…….. 99
at 0.27 s.g/cm^3
Figure 55. Conversion of Methanol over Nafion Catalysts…….. 100
at 0.68 s.g/cm^3
Figure 56. Conversion of Methanol over Nafion Catalysts…….. 101
at 1.36 s.g/cm^3
Figure 57. Conversion of Methanol over Nafion SAC-13……102
at different catalyst loading
Figure 58. Selectivity of DME and Formaldehyde with…….. 102
Nafion Catalysts at 0.27 s.g/cm^3
Figure 59. Selectivity of DME and Formaldehyde with…….. 104
Nafion Catalysts at 0.68 s.g/cm^3
Figure 60. Yield of DME and Formaldehyde with…….. 105
Nafion Based Catalysts at 0.27 s.g/cm^3
Figure 61. Yield of DME and Formaldehyde with…….. 107
Nafion Based Catalysts at 0.68 s.g/cm^3
Figure 62. EDS of AlSi1……...117
Figure 63. EDS of AlSi2……...118
Figure 64. EDS of AlSi3……...119
Figure 65. EDS of Al-SBA-15……..120

Figure 66. SEM Image of AlSi1 (a)……..121
Figure 67. SEM Image of AlSi1 (b)……..121
Figure 68. SEM Image of AlSi1 (c)……..121
Figure 69. SEM Image of AlSi2 (a)……..122
Figure 70. SEM Image of AlSi2 (b)…… 122
Figure 71. SEM Image of AlSi2 (c)……..122
Figure 72. SEM Image of AlSi2 (d)……..122
Figure 73. SEM Image of AlSi2 (e)……..122
Figure 74. SEM Image of AlSi3 (a)……..123
Figure 75. SEM Image of AlSi3 (b)……..123
Figure 76. SEM Image of AlSi3 (c)……..123
Figure 77. SEM Image of α-Al (a)……124
Figure 78. SEM Image of α-Al (b)……124
Figure 79. SEM Image of α-Al (c)……124
Figure 80. SEM Image of α -Al (d)…….. 124
Figure 81. SEM Image of α-Al (e)……124
Figure 82. SEM Image of α-Al (f)…… 124
Figure 83. SEM Image of α-Al (g)……125
Figure 84. SEM Image of γ -Al-1 (a)……... 125
Figure 85. SEM Image of γ -Al-1 (b)……125
Figure 86. SEM Image of γ-Al-1 (c)……125
Figure 87. SEM Image of γ-Al-1 (d)……125
Figure 88. SEM Image of γ-Al-2 (a)……126
Figure 89. SEM Image of γ-Al-2 (b)……126
Figure 90. SEM Image of γ-Al-2 (c) ……... 126
Figure 91. SEM Image of γ-Al-2 (d)……126
Figure 92. SEM Image of NR-50 (a)…… 127
Figure 93. SEM Image of NR-50 (b)…… 127
Figure 94. SEM Image of NR-50 (c)…… 127
Figure 95. SEM Image of NR-50 (d)…… 127
Figure 96. SEM Image of NR-50 (e) ……... 127
Figure 97. SEM Image of NR-50 (f)……127
Figure 98. SEM Image of SAC-13 (a)…….. 128

Figure 99. SEM Image of SAC-13 (b)……..128
Figure 100. SEM Image of SAC-13 (c)…… 128
Figure 101. SEM Image of SAC-13 (d)…… 128
Figure 102. SEM Image of SAC-13 (e)…… 128
Figure 103. SEM Image of SBA-15 (a)……... 129
Figure 104. SEM Image of SBA-15 (b)……...129
Figure 105. SEM Image of SBA-15 (c)……... 129
Figure 106. SEM Image of SBA-15 (d)……...129
Figure 107. SEM Image of Al-SBA-15 (a)……...130
Figure 108. Conversion of Methanol over AlSi1 and AlSi2…….134
at 0.2 s.g/cm^3.
Figure 109. Selectivity of DME and Formaldehyde with…….....134
AlSi1 and AlSi2 at 0.2 s.g/cm^3.
Figure 110. Yield of DME and Formaldehyde with……. 135
AlSi1 and AlSi at 0.2 s.g/cm^3.
Figure 111. Conversion of Methanol over α and γ Forms…… 135
of Aluminum Oxides at 0.2 s.g/cm^3.
Figure 112. Selectivity of DME and Formaldehyde with…….136
α and γ Forms of Aluminum Oxides at 0.2 s.g/cm^3.
Figure 113. Yield of DME and Formaldehyde with……. 136
α and γ Forms of Aluminum Oxides at 0.2 s.g/cm^3
Figure 114. Selectivity of DME and Formaldehyde with…….137
Nafion Based Catalysts at 1.36 s.g/cm^3
Figure 115. Yield of DME and Formaldehyde with……. 137
Nafion Based Catalysts at 1.36 s.g/cm^3

NOMENCLATURE

A-Al: Alpha alumina

CIDI: Compression Ignition Direct Injection

DME: Dimethyl Ether

DRIFTS: Diffuse Reflectance FT-IR

EDS: Energy Dispersive Spectroscopy

FA: Formaldeyhde

G-Al: Gamma alumina

ICE: Internal Combustion Engine

IUPAC: International Union of Pure and Applied Chemistry

MCM: Mobil Composition of Matter

MeOH: Methanol

S: Selectivity

SEM: Scanning Electron Microscopy

X: Conversion

XRD: X-Ray Diffraction

Y: Yield

CHAPTER 1

INTRODUCTION

Dimethyl ether is considered as an excellent clean burning transportation fuel alternate for compression-ignition engines, a fuel for household use, as an alternate to LPG and also for power generation [1]. Its high cetane rating of 55-60, high oxygen content and clean burning characteristics with very low NO_x and soot emissions and no SO_2 emissions make DME as a sustainable fuel alternate of the future [2].

Solid acid catalysts can be used for dehydration of alcohols. In this study, activities of different solid acid catalysts, such as Nafion NR-50, Nafion SAC-13, Mesoporous aluminum silicates, pure and aluminum impregnated SBA-15 and different aluminum oxides in α and γ forms were tested for the dehydration reaction of methanol to synthesize DME. Mesoporous aluminum-Silicates, SBA-15 and Al-SBA-15 were synthesized following a hydrothermal synthesis procedure using Cetyltrimethylammonium bromide as the surfactant, following a similar procedure reported in Dogu et al.'s earlier studies for the synthesis of MCM-41 [3]. All the other catalysts were obtained from the commercial suppliers.

Chapter 2 deals with alcohols in transportation sector in the past and for the future. Also, present uses of methanol and physical properties of DME are given. In addition to this, the chapter deals with DME as a fuel.

In Chapter 3, DME synthesis routes, which are direct DME synthesis (syngas to DME) and indirect synthesis method (methanol dehydration), are investigated in detail. This chapter reviews the thermodynamics of DME synthesis of both routes.

Chapter 4 presents what mesoporous materials are and where they are used. Also, it discusses the members of M41S family including MCM-41, MCM-48 and MCM 50. Moreover, it reviews the studies related to SBA-15 and aluminum impregnated SBA-15 (Al-SBA-15).

Chapter 5 presents theoretical information about the characterization methods that are used for the catalysts of both synthesized and commercial ones. Chapter 5 also describes the experiments performed. Synthesis procedures of mesoporous aluminum silicates, SBA-15 and Al-SBA-15 are clarified. The equipments that are used for characterization of the materials are also explained.

Chapter 6 is the “results and discussion” part of the study. Results that were obtained with the experiments are analyzed and interpreted. The effect of temperature and the amount of catalyst for methanol dehydration are examined. In order to explain the behavior of the catalysts that were tested, characterization results with comments are presented. Conclusions and recommendations are presented in the final part.

CHAPTER 2

USAGE OF ALCOHOLS

2.1. Alcohols as Transportation Fuels

At the end of the 19th century, ICEs (Internal Combustion Engines) were designed to run on alcohol by Nicholos Otto and the others. They would not only be replacing steam engines but also used in automobiles. These alcohol engines were launched as less polluting than that of the gasoline ones. Especially the European countries that have no or restricted oil resources were much more anxious to develop alcohols as fuels than the other countries, because they could be distilled from different agricultural products. On the other hand, ethanol could hardly compete with gasoline on economic bases because of the abundant petroleum resources available especially in the United States [4].

At the beginning of 1920, consumption of alcoholic beverages and alcohol production was prohibited even for fuel usage. Nevertheless, some of the European countries such as England, Germany and France as well as Brazil and New Zealand insisted on encouraging the production of alcohols and blending them with gasoline. Among these countries, Germany desired to be influential in the field of energy because of their failure in World War I due to fuel shortages. During these years, methanol was produced increasingly from coal via syn-gas using the process invented by BASF. Before World War II, the ratio of alternative fuels that were used in Germany's total light motor fuel consumption reached

50%. After the world war, demand for alcohols decreased due to cheap oil prices even with the oil crises in 1970's and concerns about pollution. In 1997/1998, the amount of ethanol production from sugar cane and its residues reached a value of about 15 million m^3/day (220.000 barrels of oil). During the same years, total sale of alcohol-fueled motor cars decreased significantly due to the low oil prices and large reserves. With the increase in oil prices, the interest in alcohol production again increased and the mixture of ethanol and gasoline was used to run vehicles. On the other hand, ethanol became attractive because of an oxygenated additive that was substituted to methyl tert-buthyl ether (MTBE). Although, automotive sector also focused on methanol which could be obtained from a variety of source such as natural gas, coal, wood, agricultural and municipal waste, etc. at a cost lower than that for ethanol. In 1973, Thomas Reed, a researcher at the Massachusetts Institute of Technology (MIT) published a paper about the usage of methanol as fuel and its advantages in Science magazine [5]. He stated that methanol gasoline mixture (10 % methanol in gasoline) not only improved performance and gave better mileage but also reduced pollution. In 1975, Volkswagen (VW) tested and operated successfully its vehicles using a 15% blend of methanol in gasoline. Furthermore, VW tested pure methanol rather than gasoline. They exceeded the cold start problem due to lower volatility of methanol by adding butane or pentane. Although American motor car manufacturers had little interest in methanol fueled cars, research programs were started in 1978 at the University of Santa Clara. The tests with Ford and VW showed that the vehicles which run on pure methanol had good fuel economy and engine durability than that of the gasoline vehicles. At the time, in 1980, 200 methanol fueled vehicles got a mileage of 30 million km on the roads. At 1980s, with the new pollution standards, most of the car companies such as General Motors, Ford, Mercedes, Volvo, Chrysler, etc. began to develop methanol fueled vehicles. Most of the models were designed as Flexible Fuel Vehicle due to the lack of methanol blended fuel filling stations. In 1997, the use of methanol fueled vehicles reached a maximum of still minor 20.000 units. During the 1990s, the interest in methanol-based fuels decreased because of the improvements in emission problems and different technological advances such as direct fuel injection, three way catalytic converters, reformulated gasoline, etc [4].

Finally, the fate of methanol is dependent on economic factors, especially oil prices. Furthermore, the introduction of methanol is delayed intentionally with political considerations. Nevertheless, methanol will play a major role in the near future due to the fact that the price of oil is dramatically increasing and anthropogenic climate changes will be the driving force for the researchers to come up with alternative fuels [4].

2.2. Present Uses of Methanol

Methanol is a primary feedstock for today's chemical industry. As methanol is produced in large quantities (In 2004, over 32 million tons per year [1]), it is not only used as an intermediate input for variety of chemicals but also a feedstock for chloromethanes, methylamines, methyl methacrylate, and dimethyl terephthalate, etc. After these intermediates are processed, they can be used for manufacturing many products such as paints, resins, silicones, plastics, antifreeze, adhesives, etc [4].

Today, methanol is used in internal combustion engines. Although methanol as a fuel is environmentally safe, a drawback is present in conventional generation of methanol from natural gas. Also, with the energetic efficiency rate at methanol generation reaching only 68%, a challenge is waiting for methanol to confront the present petrol generation from crude oil (<80%). Concerning the whole energy chain, none or only minor advantages of fuel cell powered vehicles can be expected with respect to the energy balance, the CO_2 emissions and the efficient use of resources [6]. Due to these reasons, the efficient way to produce methanol from the source materials like biomass or renewable energy as a long term option.

Because methanol and derived dimethyl ether (DME) have excellent combustion characteristics for the internal combustion engines (ICE) and for fuel

cell powered cars for the future, they will play significant role as a transportation fuel in the near future [4, 6].

2.3. Physical Properties of DME

Dimethyl ether (CH_3OCH_3), the simplest invisible gaseous ether compound under ambient conditions has no known side effect [7]. The physical properties of DME are very similar to those of liquefied petroleum gas (LPG) which is composed of propane and butane. In addition to this, it can be handled and stored as LPG. Thus, with a little modification, DME can be appropriated not only for land usage but also for ocean transportation. That's why it can be used as an alternative for LPG. Also, DME can be liquefied easily as its vapor pressure is about 0.6 MPa at 25^0C [8]. In contrast to methane, DME does not require an odorant as it has a sweet ether-like odor. The physical properties of DME and other fuels are listed in Table 1 [8].

Table 1. Comparison of Dimethyl Ether's Physical and Thermo-Physical Properties to Commonly Used Fuels (Adapted from [8]).

	Methane	Methanol	**DME**	Ethanol	Gasoline	Diesel
Formula	CH_4	CH_3OH	**CH_3OCH_3**	CH_3CH_2OH	C_7H_{16}	$C_{14}H_{30}$
Molecular weight($g.mol^{-1}$)	16.04	32.04	**46.07**	46.07	100.2	198.4
Density ($g.cm^{-3}$)	0.00072[a]	0.792	**0.661**[b]	0.785	0.737	0.856
Normal boiling point (^0C)	-162	64	**-24.9**	78	38-204	125-400
LHV($kj.cm^{-3}$)	0.0346[a]	15.82	**18.92**	21.09	32.05	35.66
LHV($kj.g^{-1}$)	47.79	19.99	**28.62**	26.87	43.47	41.66
Exergy ($MJ.L^{-1}$)	0.037	17.8	**20.63**	23.1	32.84	33.32
Exergy ($MJ.kg^{-1}$)	51.76	22.36	**30.75**	29.4	47.46	46.94
Carbon content (wt.%)	74	37.5	**52.2**	52.2	85.5	87
Sulfur content (ppm[c])	~7-25	0	**0**	0	~200	~250
Explosion limit[d]	5-15	5.5-36	**3.4-17**	-	-	0.6-6.5
Ignition temperature (K)[e]	905	743	**623**	-	-	-
Cetane number[f]	0	5	**55-60**	-	-	40-5

[a] Values per cm^3 of vapor at standard temperature and pressure.
[b] Density at P=1 atm and T=-25 ^0C.
[c] Mass basis.
[d,f] Data taken from [9].
[e] Data taken from [2].

2.4. DME Markets

DME can be used for various fields such as power generation, transportation, home heating, cooking, etc. [9]. DME is used as fuel in diesel engines, gasoline engines and gas turbines. In addition to this, it is used as a refrigerant, solvent, extraction agent, (-co) blowing agent for foam, propellant for aerosol products, chemical reaction medium, and fuel for welding, cutting and brazing [10].

2.5. DME as a Fuel

Due to fast consumption and diminishing of petroleum resources and environmental pollution due to the fossil fuels, researches on alternative fuels gained much attention. Volatile organic compounds (VOCs) cause serious environmental problems due to their carcinogenic and mutagenic properties. DME is also a volatile organic compound but is non-carcinogenic, non-mutagenic and non-toxic [8]. In addition to these, it has a characteristic of rapid evaporation, low noise level combustion and it is considered to be an environmentally safe material [11]. In the process of the search for more advanced energy technologies (e.g., fuel cells) to increase the efficiency of energy use, DME has attracted much attention [8].

DME can also be used as a transportation fuel, especially as a diesel substitute because it is clean burning, produces no soot, black smoke or SO_2 and especially has a high cetane rating of 55-60. The high cetane number of DME as compared to conventional fuels makes it ideal for use in compression ignition engine [9]. Also, the boiling point of DME (-24.9 ^{0}C) provides fast fuel/air mixing, reduced ignition delay and great cold starting properties [12]. Furthermore, it causes very low amounts of NO_x and other emissions [4]. Xu et al [13] stated that preliminary engine tests showed that engine operation with

thermal efficiencies equivalent to traditional diesel fuel can achieve these emissions with little fuel system modifications. However, DME has a crucial disadvantage compared to diesel. DME has lower energy content per volume unit. This means that to get the same energy as diesel, larger amount of fuel must be supplied to the engine [14]. Semelsberger et al stated that in order to achieve equivalent driving range as that of a CIDI (compression ignition direct injection) diesel, a DME fuel storage tank must be twice the size of a conventional diesel fuel tank given the lower energy density of DME compared with diesel fuel [8]. On the other hand, according to Semelsberg et al [8], since DME harms elastomers that is because any rubber and plastic components must be replaced. Furthermore, DME has a low lubricity so some additives should be added to prevent any injection problem [14].

CHAPTER 3

CATALYTIC DEHYDRATION REACTION OF METHANOL TO DME

3.1. Routes of DME Synthesis

3.1.1. Indirect Synthesis Method (Methanol Dehydration)

Dimethyl ether can be produced by two methods: Indirect synthesis method and direct synthesis method. In indirect synthesis method, also named as dehydration reaction of methanol, DME is produced by a two step method where methanol is first produced from syngas and then dehydrated to form DME [15].

The methanol dehydration reaction is as follows:

$$2CH_3OH \rightarrow CH_3OCH_3 + H_2O$$

Ramos et al. [16] studied several mixtures composed of a methanol synthesis catalyst (ACZ) and solid acid catalysts in order to understand the role of the catalyst acid for the direct synthesis of DME. Depending on the objective, commercial materials were taken and the mixture of ACZ/acid catalyst ratios were kept constant in all the experiments. The surface areas of the solid acid catalysts including Al_2O_3, ZrO_2, ZSM-5 changed from 94 to 341 m^2/g.

FTIR analysis were done in order to get the spectra of pyridine adsorbed on the solid acid catalysts. They observed that Al_2O_3 has Lewis acid sites in the bands of 1450, 1490, 1575, 1595 and 1613 and a shoulder at 1620 cm^{-1}. Bronsted acid sites were present at the bands of 1490, 1540, 1640 cm^{-1}. However, the contributions of both Bronsted and Lewis acid sites were observed for HZSM-5 and also for tungsten and sulfate loaded zirconium samples. They observed the same number of Lewis acid sites that were present for HZSM-5 and zirconium-based solids, and also indicated that their acidity strength were quite different, more acidic for doped zirconium. On the other hand, stronger Bronsted acid sites were observed for HZSM-5 than that for zirconium based samples [16].

According to the same catalytic behavior of methanol dehydration reactions that Ramos et al observed were indeed clarified as the reason of the identical Lewis acidity distribution determined for alumina samples. Also, from pyridine adsorption analysis, they realized that the activity of a solid acid is mainly determined by the number of its more acidic sites rather than total acid sites from the correlation between Bronsted acidity and methanol dehydration rate [16].

Yaripour et al. [17] studied a series of solid acid catalysts with different components contents that were prepared by coprecipitation (sol-gel) method. These include γ-alumina and modified Al_2O_3 with silica. They studied dehydration reaction of methanol to DME in a fixed bed flow reactor under atmospheric pressure at 300^0C with a catalyst loading of 0.5 g. They also tested aluminum silicate samples which had surface areas higher than 250 m^2/g. High acidity was obtained by modifying γ-alumina with silica. Also, surface acidity was increased by increasing silica loading for aluminum silicate catalysts.

With the experimental analysis of dehydration reaction of methanol, Yaripour et al observed that the catalytic activity of γ-alumina has increased by modifying silica. This is clarified as the surface acidity of aluminum silicates

increased with increasing silica (3-6 wt %) loading. Furthermore, no by product formation was observed with this range of silica loadings. They also emphasized that dehydration reactions take place mainly on Bronsted acid sites. On the other hand, they concluded that excess amount of silica occupies the active acid sites on the surface of the catalyst. According to the literature that Yaripour et al. surveyed, it was reported that methanol was dehydrated to form DME with weak and medium acid sites of the catalysts [17].

Xu et al. [13] studied methanol dehydration reaction over different solid acid catalysts such as γ-Al_2O_3, H-ZSM-5, amorphous silica-alumina, as well as titania modified zirconium. The aim of their study was to relate the catalytic activity for methanol to DME and acid base property of the catalysts. The reactions were conducted with a temperature of 280^0C in order to find out the most suitable one for syngas to DME catalyst. The reaction was performed with a plug flow reactor system.

For γ-Al_2O_3, they reached a methanol conversion of about 90% at 250 ^{0}C which is mentioned as the equilibrium limitation temperature of the reaction. They also tested the influence of water on catalytic activity over γ-Al_2O_3. As a result of the experiments, it was observed that partial pressure of water has a negative effect on the catalytic activity. As they increased the partial pressure of water, methanol conversion has decreased and the temperature had to be increased in order to achieve the same methanol conversion in the presence of excess water. It was also argued that addition of water increased the activation energy for DME formation because of the fact that water blocks the active catalytic sites [13].

For titanium modified zirconium that Xu et al. tested, a 50 mol % TiO_2/ZrO_2 showed enhanced catalytic activity than that of pure TiO_2. However, ZrO_2 is much less active compared to γ-Al_2O_3 that is because ZrO_2 has weaker acid sites but stronger basic sites and has smaller concentration of acid sites than γ-Al_2O_3 [13].

It was indicated that HZSM-5 catalyst has both Lewis and Bronsted acid sites -according to the extra framework aluminum- rather than γ-Al_2O_3 which has only Lewis acid site. It is clarified that because of the fact that water reduces the number of Lewis acid sites but Bronsted acid sites, water addition slightly affects HZSM-5 than that of γ-Al_2O_3 as the only acid site is Lewis [13].

According to Xu et al. both Lewis and Bronsted acid sites were present in amorphous silica-alumina (SiO_2/Al_2O_3). When they increased silica content, the number of acid sites in SiO_2/Al_2O_3 increased. They tested the catalysts within the temperature range of 140-190 ^{0}C. In general, methanol conversion increases as the acidity of the catalyst increases. In contrast to this, methanol conversion has decreased with increasing silica content. They thought the reason might be that the number of Lewis acid sites could be reduced, transformed to Bronsted acid sites. Another reason might be that the number of basic sites could be decreased as acid-base pair is essential for the dehydration reaction of methanol. On the other hand, amorphous silica-alumina is found to be very selective for DME formation over a wide range of temperature [13].

In another study, Fei et al. [18] studied the synthesis of DME on modified HY zeolite and modified HY zeolite supported Cu-Mn-Zn catalysts. It is argued that the activity of active alumina is lower compared with HZSM-5 and HY zeolites for methanol dehydration to DME. The experiments were conducted in a high pressure microreactor system. In each sample that they tested, the conversion of methanol dehydration to DME decreased with Fe-HY, Co-HY, Cr-HY, HY, Ni-HY, Zr-HY after 3 hours on stream. However, Ni-HY and Zr-HY were very stable even 15 hours on stream depended on lower amount of strong acid sites. Also, coke formation was very limited with Ni-HY and Zr-HY.

Jiang et al. [19] worked with Zeolite SUZ-4 as a selective dehydration catalyst for methanol conversion to DME. SUZ-4, which is reported in 1992, has a potential as a catalyst and indicated that it shows extraordinary shape-selective properties in comparison with other zeolites. It is reported as a

promising support for lean NO_x catalysts for high temperature applications. Following the pyridine adsorption analysis, it was reported that the presence of strong acid sites were comparable as HZSM-5 with Bronsted acidity. The dehydration reaction was carried out with a fixed bed reaction system at atmospheric pressure. SUZ-4 showed catalytic activity within the temperature range of 470-570 K. Also, SUZ-4 exhibited similar catalytic activity with HZSM-5 after 520 K. Moreover, the DME selectivity of these catalysts are about 100% till 520 K. After that temperature HZSM-5's selectivity quickly decreased. SUZ-4 is said to be very stable for more than 40 hours even without coke formation.

In 2005, Yaripour et al. [17] published a paper related to their study on DME synthesis over aluminum phosphate and silica-titania catalysts. It was studied in a fixed-bed reactor under 300^0C atmospheric pressure conditions. A series of solid-acid catalysts with different content of components by co-precipitation (sol-gel) method was prepared.

According to the previous findings of Yaripour et al., it is well known that γ-Al_2O_3 is an excellent catalyst for the methanol dehydration. In contrast to this, it undergoes a fairly rapid, irreversible deactivation due to the deposit of heavy secondary products (HCs) inside the pores generally known as coke. It is clarified as; since HCs are formed on the strong acid sites, in order to avoid the formation of coke and to increase the DME selectivity to 100%, the strength of the acid sites must be reduced. From the published papers, it has been found that if the reaction of methanol dehydration takes place on the modified-alumina catalysts with phosphorus can reduce the amounts of coking and by-products [17].

From the experimental results, silica-titania catalysts have shown low activity for DME compared to the untreated γ-Al_2O_3. However, phosphorus modified catalysts have shown better performance than γ-Al_2O_3. It is stated that the surface areas increased with increasing the molar ratio of aluminum to phosphorus. On the other hand, with increasing in the molar ratio of Al/P,

Yaripour and the others observed that the surface acidity of the catalysts decreased. They got the best conversion with the molar ratio of Al/P = 2 without any by product [17].

Another study on dehydration reaction of methanol is by Fu et al. [20]. They specifically focused on the nature, strength and number of acid sites for H-ZSM-5, steam de-aluminated H-Y zeolite (SDY), γ-Al_2O_3 and $Ti(SO_4)_2$/ γ-Al_2O_3 catalysts. The reactions were carried out in a fixed bed micro-reactor. Also, the acidity test were done using an adsorptive microcalorimeter.

After the experiments and tests were performed, they concluded that H-ZSM-5 and SDY catalysts have strong Bronsted acid sites. Due to this, they showed high activity. It is indicated that the addition of $Ti(SO_4)_2$ increased the catalytic activity. Methanol conversion reached a value of about 85% at 513K. However, at the same temperature pure γ-Al_2O_3 exhibited low catalytic activity, as a methanol conversion of 3%. The reason for this was the water molecules that adsorbed on the strong Lewis acid sites and blocked the active sites of the catalyst [20].

Jun et al. [21] studied methanol dehydration reaction with γ-alumina, silica-alumina and modified γ-alumina with B_2O_3, ZrO_2 and SiO_2 catalysts. They tried to find a suitable catalyst for synthesis of DME with one step (syngas to DME). Accordingly, they concentrated on water effect. The reactions were performed by using a fixed bed reactor.

According to Xu et al. in 1997 [13], the active sites inside the catalyst were blocked by water throughout the reaction period due to the competitive adsorption with methanol on the surface. Xu et al also indicated that the calcination temperature of the catalyst is so crucial that at low calcination temperatures, the hydrophilicity of the catalyst may increase and also the strength of the acidity may change.

From Jun et al's results [21], it was concluded that the presence of water deactivates γ-alumina. The performance of γ-alumina increased with high calcination temperatures. Among different modified γ-alumina, modified with 1 wt% SiO_2 showed the best performance.

3.1.2. Direct DME Synthesis (Syngas to DME)

In the direct synthesis method, also named as syngas-to-dimethyl ether (STD), DME is synthesized by combining the methanol synthesis and dehydration steps in a single process. Nowadays, STD process has received more attention [15]. There are mainly two overall reaction routes that synthesize DME from synthesis gas ($H_2 + CO$ gas): Reaction 1 and reaction 2 [2].

(1) $3CO + 3H_2 \rightarrow CH_3OCH_3 + CO_2$

(2) $2CO + 4H_2 \rightarrow CH_3OCH_3 + H_2O$

(3) $2CO + 4H_2 \rightarrow 2CH_3OH$ (Methanol synthesis reaction)

(4) $2CH_3OH \rightarrow CH_3OCH_3 + H_2O$ (Methanol dehydration reaction)

(5) $CO + H_2O \rightarrow CO_2 + H_2$ (Water-gas shift reaction)

DME synthesizes in three steps which are methanol synthesis reaction (reaction 3), dehydration reaction of methanol (reaction 4) and water gas shift reaction (reaction 5) by the route of reaction 1. In the case of water gas shift reaction does not take place, then reaction 3 and reaction 4 are combined to form reaction 2 is the other DME synthesis route [2].

Kim et al. [22] experimented with Na-ZSM-5 and H-ZSM-5 catalysts with different Si/Al ratios for methanol dehydration and direct DME synthesis.

For methanol synthesis, $Cu/ZnO/Al_2O_3$ was used and physically mixed with ZSM-5 catalysts that they were synthesized. The reaction was carried out with a fixed bed high pressure reactor. Methanol dehydration was done at atmospheric pressure. H-ZSM-5 showed much higher activity than that of Na-ZSM-5 catalysts. The activity of H-ZSM-5 and Na-ZSM-5 increased with decreasing Si/Al ratio. However, they observed that Na-ZSM-5 catalyst showed no activity with Si/Al ratio of 100. It was indicated that Na-ZSM-5 catalyst had acid sites with moderate acid strength. In respect of NH_3-TPD spectra, the acid sites which appeared below 450 ^{0}C, estimated to be not important for dehydration reaction of methanol. They had the highest activity with the ratio of Si/Al=30 of Na-ZSM-5.

For the direct DME synthesis, Na-ZSM-5 with Al/Si ratio of 30 (Na-ZSM-5(30)) showed the highest activity. Moreover, Na-ZSM-5 with Al/Si ratio of 30 exhibited higher DME yield than that of Na-ZSM-5 with Al/Si ratio of 50 (Na-ZSM-5(50)). At 260 ^{0}C, the conversion of CO to DME is in the order of Na-ZSM-5(50)>Na-ZSM-5(30)>Na-ZSM-5(100) [20].

According to the acidity tests, H-ZSM-5(30) was the most acidic and Na-ZSM-5(100) was the least acidic ones among the tested catalysts. Finally, Kim et al. concluded that acid strength of the solid acid catalysts are directly related with the dehydration of methanol rate. However, the conversion of CO to DME was shown to be independent of the acid strength of H-ZSM-5 catalysts [22].

In Ng et al.'s study [23] of kinetics and modeling of DME from synthesis gas, methanol and water-gas shift reaction was synthesized with $CuO/ZnO/Al_2O_3$ and methanol dehydration reaction was carried out by an acidic component (i.e. γ-alumina). The aim of the study was to search thoroughly the process variables which influence the reaction kinetics for the syn-gas to DME process. CO_2 feed concentration, CO_x/H_2 ratio and the catalyst loading ratio effects were reported. They studied in a continuous, internal-recycle reactor. By using synthesis gas with 2-5% CO_2, Ng et al. obtained the

highest methanol production which was mentioned as a common industrial feed condition.

As a result, the total methanol yield was found to be about three times higher than that of methanol (only) synthesis for syngas of low CO_2 content. Selectivity to DME was favored under conditions of rich CO end where dehydration reaction was not affected by water. For the conditions of high CO_2, water-gas shift reaction was favored and high fraction of unconverted methanol obtained due to the inhibition effect of water. To understand the influence of CO_x/H_2 ratio, Ng et al. first used usual industrial methanol synthesis feed conditions (CO=16.2%, CO_2=1.8%, H_2=72%, He=10%) and then the content of hydrogen was reduced, finally H_2 was replaced by helium. According to the results, when H_2 to CO_x ratio increased, methanol yield increased, but DME yield decreased. They also investigated the influence of varying catalyst ratio and realized that total methanol yield and selectivity to DME increased as the ratio of methanol synthesis to dehydration catalyst increased till the ratio of 1:1/2. After that ratio, the catalyst was supposed to be deactivated due to the high space velocities [23].

In another study, Mao et al. [24] reported the results for the direct synthesis of DME from syngas over hybrid catalysts with sulfate modified γ-Al_2O_3 as methanol dehydration components. They analyzed the acidic properties of the SO_4^{2-}/γ-Al_2O_3 that were synthesized with different sulfate contents and calcined temperatures. In addition to this, they determined the life time of the most active and selective catalyst. The catalytic activity test was carried out in a fixed bed reactor. Acidity tests were done by temperature programmed desorption of ammonia (NH_3-TPD).

Sulfate modified γ-Al_2O_3 showed better activity than that of untreated γ-Al_2O_3. SO_4^{2-}/γ-Al_2O_3, yielded a DME selectivity of about 60% with by-products of some hydrocarbons and CO_2, and then decreased with increasing sulfate content. CO conversion also increased with increasing sulfate content to 10 wt.% but remained constant after this concentration. According to Mao et al.,

not only the number of acid sites but also their strength increased after sulfate addition of γ-Al_2O_3. On one hand, it was clarified that strong acid sites decreased the selectivity of DME because it increases the formation of CO_2 and light olefins. However, the stability of 10 wt % sulfate modified γ-Al_2O_3 calcined at 550 ^{0}C exhibited high stability [24].

Another study on direct DME synthesis came from Omata et al. [25]. The aim of this study was to develop a catalytic process to reach high conversion to DME and CO_2 from syngas ($3CO + 3H_2 \rightarrow CH_3OCH_3 + CO_2$). They used temperature-gradient reactor (TGR) as the performance of the catalyst would be much effective than that of isothermal fixed bed flow reactor. In addition to this; with TGR, the equilibrium limitation would be overcome. Omata et al prepared Cu-Zn based catalysts by oxalate-ethanol method. As a methanol dehydration catalyst, γ-Al_2O_3 was mixed. They reached high CO conversion as 90 % by using TGR with the conditions of 510-550 K, 3MPa in syngas.

Sun et al. [26] studied direct synthesis of DME from CO_2 hydrogenation with their synthesized catalysts of Pd modified CuO-ZnO-Al_2O_3-ZrO_2/HZSM-5 (CZZA/H) catalysts. They indicated that, in the literature there are few studies for DME synthesis from CO_2 hydrogenation and these are conducted with CuO-ZnO based catalysts. Catalytic activities were tested with conventional fixed bed flow reactor. The BET surface areas of the materials varied between 120-140 m^2/g. According to the catalytic tests, Pd addition enhanced DME synthesis and slowed down CO formation. Although this was the situation, DME selectivity reached only to a maximum value of 74 with 50 wt% loading into CZZA/H. Much effort must be spent in order to solve the uncertainties for the effects of Pd for this system.

In Sun's another study in 2003 [27], Cu-ZnO-ZrO_2/HZSM-5 catalysts were synthesized by co-precipitating sedimentation method for the DME synthesis by STD process. It is stated that zirconium is suitable for methanol

synthesis from both CO and CO_2 hydrogenation. The influence of zirconium on DME synthesis is tried to be indentified in this study. From the analysis, the optimum zirconium loading found was 8 wt. % for the highest DME yield. Also, they clarified that by adding zirconium, the stability of Cu-ZnO/HZSM-5 catalysts increased. It was reported that the addition of ZrO_2 is important for the formation and stabilization of Cu^+ on the surface of Cu particles-the active sites for methanol according to Okamoto et al.- that is crucial for increasing the catalytic activity. On one hand, in a recent study Toyir et al. reported that the coexistence of ZnO with Cu enhances the possibility of adsorbing CO species on Cu particles.

In 2006, Wang et al. [15] studied a series of CuO-ZnO catalysts (with different molar ratios for CuO/ZnO/HZSM-5) and tested the influence of reaction conditions in the syngas-to-DME process.

Finally Wang et al. concluded that changing the molar ratio of Cu/Zn affected methanol synthesis and water-gas shift reaction. For methanol synthesis, high Cu/Zn ratio would be the choice for satisfactory activities but low Cu/Zn ratio would be ideal for water-gas shift reaction. Increasing CO_2 concentration reported to have negative effects (retardation and inhibition at high concentrations) on both methanol formation and water-gas shift reaction. Also, for getting high activity, the space velocity of the reaction should be lowered [15].

In the work of Moradi et al. [28] various hybrid catalysts as a general form of $CuO/ZnO/Al_2O_3$ were synthesized by different methods such as co-precipitation by Na_2CO_3, $NaAlO_2$, co-precipitation impregnation and a novel method of sol-gel impregnation. Also, various contents of γ-Al_2O_3 were prepared at a fixed ratio of CuO/ZnO in order to find out the effect of γ-Al_2O_3. The catalysts were tested in a micro slurry reactor at 240^0C, 40 bar.

Following the reactivity tests, among different catalyst preparation methods, sol-gel impregnation method performed better than the others due to

the well dispersion of Cu. In other words, specific surface area of Cu was the highest in this method. γ-Al_2O_3 is said to be advantageous for preparation methods because it supplied active sites for methanol synthesis and methanol dehydration. 60% by weight of Al_2O_3 was established to be optimum for fixed and conventional ratio of CuO/ZnO=2 [28].

Erena et al. [29] studied the effects of operating conditions over CuO-ZnO-Al_2O_3/NaHZSM-5 bifunctional catalyst. From the experimental results, they concluded that the catalyst is appropriate for direct DME synthesis. Due to this catalysts' feature of not having strong acid sites but moderate ones, by product formations were diminished. Also, the catalytic activity related with the catalyst wasn't retarded by water adsorption according to the high concentration of H_2 present in the reaction medium. 80% DME yield was achieved at the temperature of 275^0C.

In Fei et al.'s study [18], the effects of copper content on the activity of Cu-Mn-Zn/zeolite-Y catalysts were investigated. The reactions were performed in a high pressure micro reactor. CO conversion increased with increasing copper content while DME selectivity remained constant. When the content increased to 0.6 from 0.4, the conversion of CO changed from about 66% to 79%. However, when the ratio increased to 0.7, the conversion increased slightly. As a result, Cu content increased CO conversion for the direct synthesis of DME from CO hydrogenation.

In 2005, a modification of Cu based methanol synthesis catalyst was done by Tan et al. [30] for DME synthesis from syngas in slurry phase. The modification was done by adding Mn for getting higher activity and stability. Li et al. stated that Mn has been used as a promoter within CuZnAl which is a methanol synthesis catalyst for getting resistance against high heat and improvement of dispersion of the catalyst. The activity of the catalysts were carried out in an autoclave.

Based on their analyses, for slurry phase DME synthesis, Tan et al. concluded that Mn addition provides an enhancement for the catalytic activity of CuZnAl catalyst. DME selectivity was reached a maximum at the temperature of 260^0C. The catalyst that Mn was added with co-precipitation showed better activity than impregnation method. The CuO-ZnO eutectic that could be seen from the XRD pattern revealed the active sites of the catalyst. Mn addition also exhibited a good stability for slurry phase DME synthesis [30].

In the study of Mao et al. [31], HZSM-5 zeolites were modified with different contents of magnesium oxide with a novel impregnation technique. In order to synthesize DME from syngas, they combined modified HZSM-5 with CuO-ZnO-Al_2O_3. The reactions were carried out under pressurized fixed bed flow conditions.

The results from Mao et al showed that the addition of MgO less than 5 wt% exhibited high conversion of CO and selectivity of DME increased. However, higher contents of MgO (>5 wt%) decreased the conversion of CO and DME selectivity. This situation explained that the activity of the modified catalyst was dependent not only the acid sites but also the basic sites of it. It was emphasized that if the basic sites are too strong then the conversion to DME from CO hydrogenation couldn't be accomplished sufficiently. It is also stated that appropriate amounts of MgO addition removed strong Bronsted acid sites and moderate Lewis acid sites on the modified catalyst lead the catalytic activity [31].

3.2. Thermodynamics of DME Synthesis Reaction

Since dehydration reaction of methanol is exothermic and reversible, thermodynamic limitation of this reaction is a fact beyond doubt. Although in the literature, kinetic studies related with both direct and indirect synthesis of DME are present, there are hardly enough investigations on the thermodynamics.

In order to understand the operational conditions, thermodynamic analysis were done by Shikada et al. [32]. The effect of initial H_2/CO ratio in feed gas on both the conversion and selectivity to DME were investigated. The studies were carried out with hybrid catalyst in a slurry bubble column reactor.

$$3CO + 3H_2 \rightarrow CH_3OCH_3 + CO_2 \qquad +245.7 \text{ kj/mol} \qquad (1)$$

$$2CO + 4H_2 \rightarrow CH_3OCH_3 + H_2O \qquad +204.8 \text{ kj/mol} \qquad (2)$$

$$CO + 2H_2 \rightarrow CH_3OH \qquad +90.7 \text{ kj/mol} \qquad (3)$$

$$2CH_3OH \rightarrow CH_3OCH_3 + H_2O \qquad +23.4 \text{ kj/mol} \qquad (4)$$

$$CO + H_2O \rightarrow CO_2 + H_2 \qquad +40.9 \text{ kj/mol} \qquad (5)$$

Equilibrium conversion of syngas was calculated via reaction 1 and 2, that are DME synthesis reactions, and via reaction 3 for methanol synthesis reaction with different H_2/CO ratio. Maximum conversion was reached with the ratio of 1.0 for reaction 1, with the ratio of 2.0 for reactions 2 and 3 at 280^0C and 50 atm. About 80% conversion was obtained with reaction 1, however, with reaction 2 maximum conversion was only about 60% and about 40% for reaction 3 [32].

According to the experimental analyses conducted at 260^0C and 50 atm, they used a physical mixture of CuO-ZnO-Al_2O_3 and γ-alumina supported copper as catalyst. The results matched with the thermodynamic calculations. The catalyst showed a satisfactory activity. 56% conversion and 96% selectivity was found at the initial H_2/CO ratio of 1 [32].

Diep et al. [33] studied thermodynamic equilibrium of methanol-dimethyl ether-water system over γ-alumina by using a pressurized flow reactor system of 200 kPa. Equilibrium constants were obtained between the temperatures of 498-623 K. According to their derived equations similar to previous studies, equilibrium constant values were temperature dependent. However, the temperature dependence of equilibrium constant changes whether

the heat of reaction (ΔH_R) is assumed to be constant ($\ln K_p = \frac{\Delta H_R}{RT} + C$) over the temperature range or not ($\frac{d \ln K_p}{dT} = \frac{\Delta H_0}{RT^2} + \frac{1}{RT^2}\int_0^T \Delta C p dT$). They compared equilibrium conversion values that were found experimentally with the studies of Hayashi et al. [34] and Given et al. [35]. They concluded that, equilibrium data from the experimental studies that were obtained with both of these equations matched with the above references.

CHAPTER 4

M41S
MESOPOROUS MATERIALS

4.1. Mesoporous Materials

IUPAC definition classified porous materials into three groups; microporous materials that have pore diameters less than 20 Å; mesoporous materials have pore diameters between 20-500 Å, and macroporous materials have larger than 500 Å [36].

Zeolites are the well known members of the microporous materials that have superior catalytic properties due to having crystalline aluminum Silicate network. However, small pore openings are their major drawback and limit their application areas. Therefore, enlargement of the pores is the major challenge in zeolite chemistry [37].

The researchers at Mobil Research and Development Corporation almost ended the concerns through the studies from the late 1980s to 1992. In 1992, the researchers discovered the synthesis of a group of mesoporous materials stated as M41S [38].

4.2. M41S Family

M41S family, the nano structured mesoporous materials, has three main members as MCM-48 which has three dimensional cubic ordered pore structure, MCM-41 which has one dimensional hexagonally ordered pore structure, and MCM-50 which has an unstable lamellar structure. M41S materials have some characteristics. Rather than zeolites, M41S materials have amorphous pore wall structure. Ordering is based on the pore arrangements [32]. Also, these materials have not only high surface area and pore volumes but also tunable pore sizes that seemed to be attractive for scientists and researchers [37]. In addition to this, broad pore openings that mesoporous materials have reduce mass transfer problems [39].

MCM type mesoporous materials have been studied especially in catalytic reactions. When MCM was first discovered, it was assumed that the acid sites inside these materials are as strong as zeolites have. But today it is well known that MCM-41 can only be used in catalysis with incorporation of aluminum into the silica walls. Therefore, it is understood that in the absence of aluminum, MCM-41 materials have only weak acid sites. So they can only be used for the reactions that do not require high acidity to catalyze [37]. On the other hand, addition of aluminum has some drawbacks. Incorporation of high aluminum into the silica walls causes pore structure irregularity and uniformity. However, Al in the structure is stated to improve the stability [40]. Therefore, synthesis conditions and procedures are very crucial in order to get an applicable material.

In Russo et al.'s study [40], it was indicated that Khushalani et al. [41] synthesized large pore MCM-41s with suitable structural ordering by post synthesis method. Russo et al. studied the effect of hydrothermal treatment on the structure, stability and acidity of Al containing MCM-41 and MCM-48 materials. They synthesized different Al-MCM-41 materials containing Si/Al ratios of 30 and 15. Surfactants of having different alkly chain size were tested. It was clarified that, the quality of the pores depends not only on the amount of

aluminum incorporation but also on the source of aluminum. According to the XRD results, among different amount of aluminum additions, the lowest amount of aluminum showed better resolution than that of the others. Also, the loss of structural regularity was minimum by using aluminum sulfate as aluminum source. Structural ordering was said to be dependent on hydrothermal treatment but Si/Al ratio or template alkly chain length.

Another study in 2007 by Carrott et al. [42] investigated the influence of the synthesis conditions on the pore structure and stability of MCM-41 materials containing different metal ions. The quality of pore structure was observed to be lost with increasing of metal content. But, it is indicated that the negative effect of aluminum incorporation was more drastic than that of titanium. However, structural stability was enhanced with the addition of both Al and Ti.

The investigation of different silicon sources and Si/Al ratios is present in a study of Blanco et al. [43]. MCM-41 materials were synthesized hydrothermally at 423 K. Like some other studies, Blanco et al. concluded that the quality of the materials increased and appearance of diffraction peaks cleared as aluminum in the structure decreased. Also, according to adsorption isotherms, as aluminum increased, adsorption of nitrogen at the same relative pressure increased. They obtained the highest surface area with the smallest Si/Al molar ratio. Most of the samples that they synthesized showed narrow pore size distributions.

For industrial applications, they can be used as a refining catalyst, a petrochemical catalyst and an adsorbent for separation processes. They can also be used as sensors, optical guides and fuel cell electrodes [38].

The characterization of MCM-41 needs three main techniques of X-ray diffraction (XRD), transmission electron microscopy (TEM), and adsorption analysis. A typical XRD pattern can be seen in Fig.1. Generally there can be reflections changing from 3 to 5 between Bragg angle $2\theta = 2^0$ and 5^0.

According to the ordered hexagonal array of parallel silica tubes, these reflections occurred. On one hand, any reflection can be seen at higher angles because of the fact that at the atomic level, the materials are not crystalline [37].

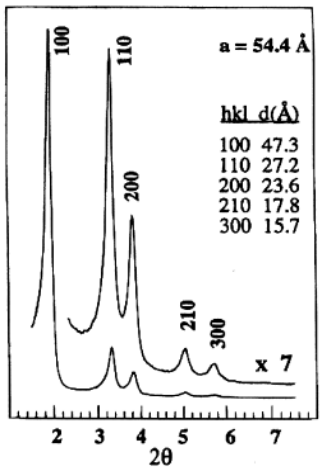


Figure 1. X-ray Diffraction Pattern of Calcined MCM-41 [37].

TEM is used in order to clarify the pore structure of MCM-41. Although, one cannot do very effective analysis of pore size and thickness of the pore walls due to the focus problem, 4 nm sized pores can be seen in a TEM image. Also, lamellar and fingerprint like structures can be seen from the images. MCM-41 shows a typical type IV isotherm (Fig.2) for the nitrogen adsorption as described by the IUPAC classification [37].

The wall thickness can be calculated in a way that the repeating distance "*a*" between the two pore centers (i.e. characteristic lattice parameter was calculated from the following equation, $a = \frac{2}{\sqrt{3}} d_{(100)}$) is subtracted from pore size [37].

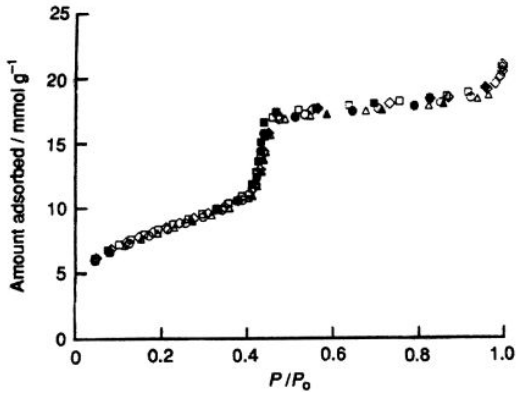


Figure 2. Adsorption Isotherm of Nitrogen on MCM-41 with 4.0 nm pores at 77 K [37].

After the discovery of hexagonally ordered mesoporous silica, MCM-41, the efforts to go over ordered mesoporous materials would be the new area of research. Following surfactant templated synthesis of mesoporous materials, polymer templated of these materials, namely SBA-15, attracted attention. It featured larger mesopores, thicker pore walls, and higher hydrothermal stability than that of MCM-41. Like MCM-41, SBA-15 has 2 dimensional hexagonally ordered cylindrical pores. On the contrary of MCM-41, SBA-15 is interconnected by irregular micropores. Adsorption, catalysis, separations are some of the application areas of SBA-15 [44, 45].

Block copolymers such as poly ethylene oxide (PEO) and poly butylene oxide (PBO) are utilized as templates in the synthesis of mesoporous silica materials [45]. In Yu et al.'s study, several commercial poly triblock copolymer surfactants were used in order to synthesize mesoporous silica. As a conclusion, block copolymers including PEO and PBO showed appropriateness with final silica mesostructures according to the micelle concentration values. Moreover, it was realized that pore size of the synthesized mesoporous materials were dependent of the molecular weight of hydrophobes of block copolymer templates. Also, synthesized mesoporous silicas by using diblock copolymer showed larger pore size than that of the materials using triblock copolymer.

According to Zhao et al. [46], well ordered mesoporous silica structures with large uniform pore sizes up to 300 Å were obtained by using amphiphilic block copolymers. These organic structure agents are attributed as good candidates because of enhancing structural properties and their low cost availability. Tetraethoxysilane (TEOS), tetramethoxysilane (TMOS), and tetrapropoxysilane (TPOS) are common silica sources for the synthesis procedures.

In 2000, Kruk et al [47], in their published study, drew crucial conclusions about understanding the structure of SBA-15 and characterization of this material. Pore size of SBA-15 was said to be directly related with synthesis temperature. Washing of synthesized SBA-15 causes removal of considerable part of polymeric template. Synthesis temperature and washing were attributed as the parameters that change the degree of penetration of poly chains within the silica walls.

Kumaran et al. [48] synthesized Al-SBA-15 with different Al/Si ratios using tri- block copolymer P123. Al was incorporated by using Al-isopropoxide according to the direct synthesis method. It was observed that aluminum did not deteriorate the mesoporous structure of pure SBA-15. Strong acid sites were formed with different Al/Si ratios.

Various Al containing SBA-15 were synthesized with different Al/Si ratios in another study by Cazalilla et al. [49]. Sodium silicate and amphiphilic block copolymer were used as silica source and structure directing agent respectively. According to the analyses, Bronsted acid sites with mildly acidity were observed to be useful in catalytic reactions that need some acidity. In addition to this, according to Hu et al, no Lewis acid sites were observed in aluminum containing SBA-15 [49, 50].

CHAPTER 5

CHARACTERIZATION OF THE MATERIALS

5.1. X-Ray Diffraction (XRD)

X-Ray Diffraction is a characterization technique that is used to identify bulk phases, to monitor the kinetics of bulk transformations, and to determine particle sizes. XRD is the flexible scattering of X-ray photons by atoms in a periodic lattice. Diffraction of X-rays by crystal planes allows one to derive lattice spacing by using the Bragg relationship:

$n \times \lambda = 2dSin\theta$; n= 1,2,…

where;

λ is X-ray wavelength;

d is the distance between two lattice planes;

θ is the angle between the incoming X-rays and the normal to the reflecting plane;

n is the integer called the order of the reflection.

The Bragg relationship gives the corresponding lattice spacing, which are characteristic for a certain compound. With a stationary X-ray source and a moveable detector that scans the intensity of the diffracted radiation as a function of the angle 2Θ between the incoming and the diffracted beams, XRD pattern of a powdered sample is measured.

Although XRD is such a useful technique, it has one considerable limitation. Clear diffraction peaks are only observed when the sample possesses

sufficient long-range order. The advantage of this limitation is that the width (or rather the shape) of diffraction peaks carries information on the dimensions of the reflecting planes.

The relation between crystal size and line width can be obtained from the Schrerrer equation;

$$<L> = \frac{K\lambda}{\beta \cos\theta}$$

where;

<L> is a measure for the dimension of the particle in the direction perpendicular to the reflecting plane,

λ is the X-ray wavelength,

β is the peak width,

Θ is the angle between the beam and the normal on the reflecting plane,

K is a constant usually taken as a value between 0.89 and 1 [51].

5.2. N_2 Physisorption

Surface areas of the materials are determined by physisorption. This method is commonly used to obtain the amount of available catalyst surface for interaction with reactant molecules [48]. The technique is generally based on how much N_2 is adsorbed onto a certain amount of material. The uptake is measured as a function of N_2 pressure at a constant low temperature (i.e., 80 K), and is usually very well described by the Brunauer-Emmett-Teller (BET) isotherm. After determining the number of N_2 molecules that form a monolayer on the support, one obtains the total area by setting the area of a single N_2 molecule to 0.16 nm^2 [51].

5.3. Scanning Electron Microscopy (SEM)

Scanning electron microscopy (SEM) is used by scattering a tight electron beam over the surface, and detecting the yield of either secondary or backscattered electrons as a function of the position of the primary beam [51]. For understanding the surface structure of a material, SEM images supply three dimensional appearances with wide range of magnifications. For the principle of the system, the primary beam causes the ejection of inner shell electrons from the material. Then, X-rays are emitted and used to explain the composition of the material [53].

5.4. Energy-Dispersive X-Ray Spectroscopy (EDS)

Atoms in a material emit characteristic X-rays when they are ionized by a high-energy radiation. EDS is based on the collection and energy dispersion of characteristic X rays. An ordinary EDS system consists of three main parts which are high energy radiation source (electrons), a sample, a solid state detector generally made from lithium-drifted silicon, Si (Li) and signal processing electrons. X rays enter the Si (Li) detector and are converted into signals. These signals can be processed by the electronics into an X-ray energy histogram. According to the type and relative amount of each element in the sample, X-ray spectrum gives different peaks that represent the elements. The number of counts in each peak can then be converted into elemental weight concentration as compared with the standards [51].

5.5. Diffuse Reflectance Infrared Fourier Transform Spectroscopy (DRIFTS)

DRIFTS can be used for the sample forms of loose powders. This method is easy to apply and tedious preparation of wafers is unnecessary. Also, diffusion limitations associated with tightly pressed samples are avoided. It can

be used for strongly scattering and absorbing particles. By using an ellipsoidal mirror, the diffusively scattered radiation is gathered and focused on the detector. Kubelka-Munk function is described for the infrared absorption spectrum:

$$\frac{K}{S} = \frac{(1 - R_\infty)^2}{2R_\infty}$$

where:

K is the absorption coefficient, a function of the frequency;

S is the scattering coefficient;

R_∞ is the reflectivity of a sample of infinite thickness, measured as a function of the frequency [51].

CHAPTER 6

EXPERIMENTAL STUDIES

6.1. Catalyst Synthesis

Three different mesoporous aluminum silicates (AlSi1, AlSi2, AlSi3) were synthesized according to the hydrothermal synthesis method described by Şener et al. [54]. Also, SBA-15 and aluminum impregnated SBA-15 were synthesized in this study.

6.1.1. Synthesis of Mesoporous Aluminum Silicates

Chemical Reagents

Chemical Reagents that are used for the synthesis of mesoporous aluminum silicates are as follows;

- Surfactant source: Cetyltrimethylammonium bromide (CTMABr), $C_{16}H_{33}(CH_3)_3NBr$, 99% pure, Merck.
- Silica source: Sodium silicate solution, $Na_2Si_3O_7$, 27 wt.% SiO_2, Aldrich; Tetraethyl orthosilicate (TEOS) solution, Merck.
- Aluminum source: aluminum nitrate nonahydrate, $Al(NO_3).9H_2O$, Merck.
- Base source: NaOH (2M), Merck.

- Solvent source: Deionized water, Millipore Ultra-Pure Water System (Milli-QPlus).

Procedure

Procedure for the synthesized mesoporous aluminum silicates consists of 5 main steps including preparation of the synthesis solution, hydrothermal synthesis, washing, drying and calcination. Schematic illustration of the procedure can be seen in Fig.3.

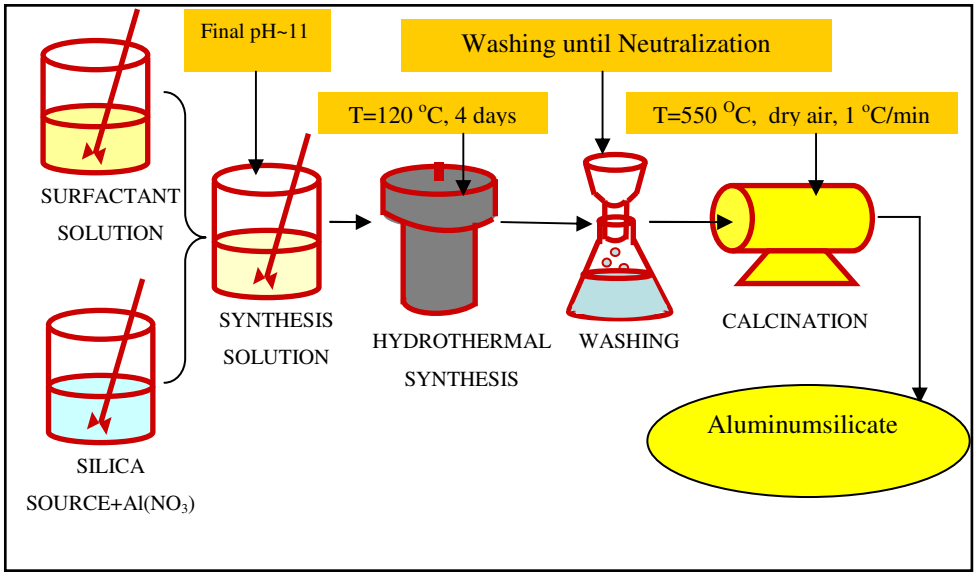


Figure 3. Synthesis Steps of Mesoporous Aluminum Silicates.

The silica and aluminum sources used in synthesized catalysts are given in Table 2 .

Table 2. Silica and Aluminum Sources Used in Synthesized Catalysts

Sample Name	Al/Si	Si Source	Al Source
AlSi1	0.1	Sodium Silicate $Na_2Si_3O_7$	Aluminum nitrate nanohydrate $Al(NO_3).9H_2O$
AlSi2	0.2	Sodium Silicate $Na_2Si_3O_7$	Aluminum nitrate nanohydrate $Al(NO_3).9H_2O$
AlSi3	0.1	Tetraethyl orthosilicate (TEOS)	Aluminum nitrate nanohydrate $Al(NO_3).9H_2O$

Preparation of the Synthesis Solution

- **Using Sodium Silicate as Silica Source**

The synthesis began with dissolving 13.2 g of cetyltrimethylammonium bromide in 87 ml of deionized water. The surfactant solution was stirred continuously with a rate of 500 rpm and at a temperature of 30^0C until a clear solution was obtained.

The process was followed by adding 11.3 ml sodium silicate to the surfactant solution. After adding sodium silicate, pH of the synthesis solution increased to 12.

Then, certain amount of aluminum nitrate solution (2.648 g and 5.296 g for Al/Si mole ratio of 0.1 and 0.2, respectively) was added to the synthesis solution. pH of the synthesis solution decreased below 7 after adding aluminum nitrate solution. In order to adjust the pH around 11, NaOH was added to the solution and stirred for 1 h.

- **Using TEOS as Silica Source**

Again, the synthesis began with dissolving 13.2 g of cetyltrimethylammonium bromide in 87 ml of deionized water. The surfactant solution was stirred continuously with a rate of 500 rpm and at a temperature of 30^0C until a clear solution was obtained.

This time, Tetraethyl Orthosilicate (TEOS) solution was used as silica source and added drop wise to the surfactant solution. After adding TEOS, the pH of the synthesis mixture decreased to 7.

Then, certain amount of aluminum nitrate solution (2.648 g for Al/Si mole ratio of 0.1) was added to the synthesis solution. pH of the synthesis solution decreased to a value around 2. In order to adjust the pH around 11, NaOH was added to the solution and stirred for 1 h.

Hydrothermal Synthesis

After the preparation step, the solution was taken into a Teflon bottle and placed in a stainless-steel autoclave. The hydrothermal synthesis was carried out at 120°C for 96 h.

Washing

After hydrothermal synthesis step, the solid was kept by filtration and washed with deionized water to get rid of Na^+ and the excess template. Because the synthesized material was too concentrated that water couldn't penetrate into the pores, it was transferred into a beaker and washed with the help of a vacuum pump. This was repeated until the pH of the residual water remained constant. For each washing, about 500 ml of water was used and it was taken

about half an hour for one of them. After washing, the material was dried at 40°C.

Calcination

It is the final step of synthesizing mesoporous aluminum silicates. The aluminum silicates were placed in a quartz tube with a membrane filter. The quartz tube which was positioned in a furnace was heated to 550°C at a rate of 1°C/min and kept at 550°C for 8 h in a flow of dry air. At the end of calcination, furnace was switched but air was continuing to flow during cooling of furnace to prevent accumulating moisture.

6.1.2. Synthesis of SBA-15

Chemical Reagents

Chemical Reagents that are used for the synthesis of SBA-15 is as follows;

- Surfactant source: Triblockcopolymer (P123), $(C_3H_6O.C_2H_4O)x$, Aldrich (Surfactant).
- Silica source: Tetraethyl orthosilicate (TEOS) solution, Merck.
- Acid source: HCl.
- Solvent source: Deionized water, Millipore Ultra-Pure Water System (Milli-QPlus).

Procedure

Procedure of the synthesized SBA-15 is almost the same as that of mesoporous aluminum silicates except the hydrothermal synthesis and calcination steps. 4 g of triblock copolymer was dispersed in 120 ml of 2M HCl and stirred for 4 h at 40^0C. Then, 8.54 g of TEOS was added to the solution while stirring at 350 rpm. The resulting gel was aged at 40°C for 2 h. After that, the hydrothermal synthesis was carried out at 100^0C for 2 days. The solid was kept by filtering and dried at 80^0C. The calcination was done at 540^0C with the same conditions as aluminum silicates.

6.1.3. Aluminum Impregnation in Synthesized SBA-15

Synthesized SBA-15 was held at 110^0C under vacuum for 2 hours. 30 ml of water was added to the solid (SiO_2) and stirred for 2 hours. Certain amount of aluminum (aluminum nitrate nanohydrate, $Al(NO_3).9H_2O$) (0.376 g for Al/Si molar ratio of 0.1) was added to the solution. After this process, the solution was stirred for 24 hours. Then, the solution was dried at 80^0C. The calcination was done at 540^0C with the same conditions.

6.2. Catalyst Characterization

X-ray diffraction (XRD), nitrogen physisorption, energy dispersive spectroscopy (EDS), scanning electron microscopy (SEM) and diffuse reflectane FT-IR (DRIFTS) of pyridine adsorption analysis were done for the characterization of both the synthesized materials and commercial ones.

6.2.1. X-Ray Diffraction (XRD)

X-ray diffraction was performed by Rigaku D/MAX2200 diffractometer using CuK_{α} in Metallurgical and Materials Engineering at METU. Diffraction data were recorded in different Bragg angle (2θ) range at an interval of 0.01° with a scanning speed of 1° per minute.

6.2.2. Nitrogen Physisorption

By using the nitrogen adsorption technique, BET and single point surface areas of all the materials were found. The measurements of BET and single point surface area were performed by Quantachrome Corporation, Autosorb-1-C/MS at METU Central Laboratory and Quantachrome Autosorb 1C at Gazi University, respectively. The samples were dried at 110^0C for one night before the analyses. For single point surface area analyses, the samples were put in de-gas unit at a temperature of 140^0C in order to remove humidity of the samples.

6.2.3. Energy Dispersive Spectroscopy (EDS)

In order to measure chemical composition of the synthesized materials, the JEOL 6400 apparatus at METU was used. The samples were coated with gold for the analyses.

6.2.4. Scanning Electron Microscopy (SEM)

For SEM photographs of the materials, JSM-6400 (JEOL) equipped with NORAN system Six that is present in the department of Metallurgical and Materials Engineering at METU was used.

6.2.5. Diffuse Reflectance FT-IR (DRIFTS)

Perkin Elmer (Spectrum One) FTIR Spectrometer with a Graseby Specac DRIFT accessories present in the Department of Chemical Engineering is used for the analysis of DRIFTS.

6.3. Experimental Setup

Vapor phase dehydration of methanol was carried out in a tubular reactor placed into a temperature controlled oven. Stainless steel tubular reactor having an internal diameter of ¼ in was used. Catalyst was placed in the middle of the reactor in order to prevent the effects of temperature gradients. Quartz wool was placed at the end of the placed catalyst to fix it at the center. Then the reactor was located into the oven in order to adjust the reaction temperature. The reaction temperature was changed from 120^{o}C to 450^{o}C. Liquid methanol was first pumped into an evaporator by a syringe pump. The evaporation chamber was kept at 150^{o}C. Vaporized alcohol was mixed with a He stream within the evaporator to adjust its composition and this mixture was then fed to the tubular reactor. After leaving the reactor, products and the unreacted feed passed through the gas chromotograph. Varian CP 3800 GC equipped with a Poropak T column was used for online analysis of the product stream composition. In order to prevent condensation of the alcohol mixture, the temperature of the line for the whole system was kept at 150^{0}C by using heating tapes and isolations on them.

Helium was used as the carrier gas with a constant flow rate of 30 cc /min for the gas chromatograph. Thermal conductivity detector (TCD) was used and the temperature of the TCD detector and the gas sampling valve were kept at 225 ^{0}C and 200^{0}C respectively. To separate the products from each other, temperature-ramped program was used. The column temperature is initiated at 75^{0}C and it was held for 2 minutes. Then it was raised to 170^{o}C with a ramp rate of 10^{0}C/min. The program was holding the column at this temperature for

3 minutes. During this period, peaks corresponding to products and unreacted feed were obtained clearly. After the experiments, He gas has swept the whole system for 1 hour to prevent any condensation in the line. The schematic presentation and a photo of the experimental setup are given in Fig.4 and Fig.5, respectively.

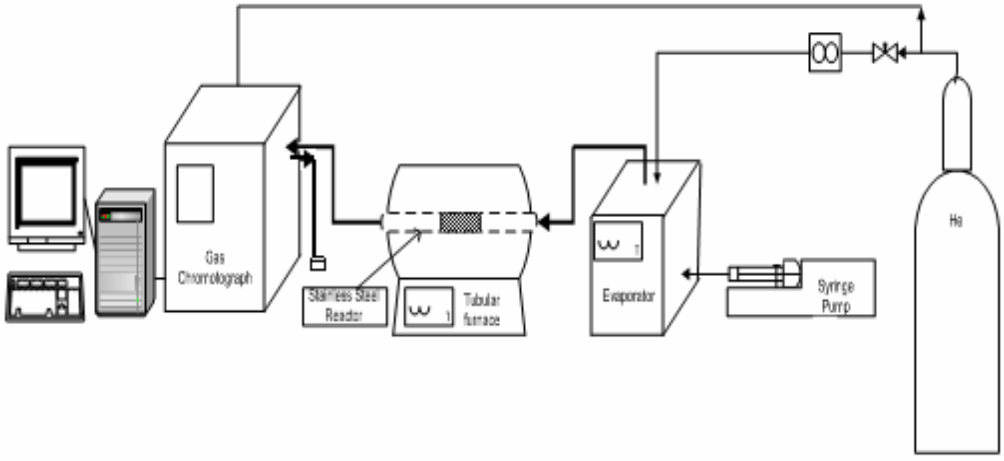


Figure 4. Experimental Setup



Figure 5. A Photo of Experimental Setup

6.3.1. Chemicals and Experimental Parameters

In all experiments, high purity helium gas was used for feed stream and also as a carrier gas for GC. Pure methanol (99.9%) from Merck were used.

Solid acid catalysts were tested according to the activity tests for the dehydration reaction of alcohols. Other than synthesized catalysts, the ones obtained from commercial suppliers were γ-Al (Sigma Aldrich), γ-Al (Damla Kimya), α-Al (Toyo Engineering), Nafion NR-50 (Fluka), Nafion SAC-13 (Sigma Aldrich).

Nafion is a polymer which contains flor and sulfonic acid. General structure can be seen in Fig.6.

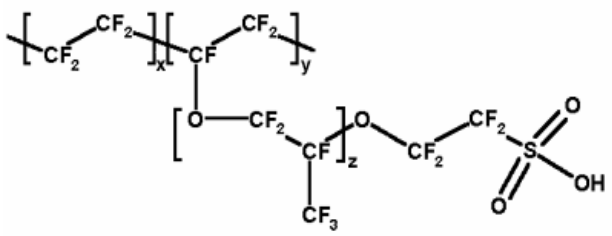


Figure 6. Chemical Structure of Nafion [55]

As nafion has a property of superacidic, high Bronsted acidity and is insoluble in polar solvents, it shows activity in dehydration reaction of alcohols. The activity of nafion is limited due to the low surface area value (0.02 m^2/g). Therefore, in order to extend the usage of nafion as a an active catalyst, nafion can be synthesized by entrapping nafion resin particles within a porous silica network. In their study of Harmer et al., using a sol-gel technique, the surface area of the synthesized materials were ranged between 150-500 m^2/g. The catalytic activity of these materials was shown to be increased according to the accessibility of acid groups improved [56].

Two parameters were studied over both synthesized and commercial catalysts. One of the parameters was reaction zone temperature. For synthesized catalysts and different aluminum oxides in γ and α forms, the reaction temperature ranged between 200 ^0C and 400 ^0C. For Nafion type catalysts, the tests were conducted at the temperature range between 120 ^0C and 220 ^0C. The other parameter is the amount of catalyst that is the effect of space time. Also, the effect of water in feed stream was investigated for Nafion NR-50. Synthesized catalysts and different aluminum oxides in γ and α forms were tested with 0.1 g (0.136 $s.g/cm^3$), 0.15 g (0.2 $s.g/cm^3$) (Appendix B.3) and 0.2 g (0.27 $s.g/cm^3$). Nafion type catalysts were tested with 0.2 g and 0.5 g (0.68 $s.g/cm^3$). In addition to this, 1 g (1.36 $s.g/cm^3$) of Nafion SAC-13 was tested (Appendix B.3).

CHAPTER 7

RESULTS AND DISCUSSION

This chapter presents methanol dehydration reaction results and effect of operating conditions over synthesized and commercial catalysts. Also, the results of characterization techniques are reported.

7.1. Characterization Results of the Catalysts

In this part, characterization analyses of XRD, N_2 Physisorption, SEM, EDS and DRIFTS are presented.

7.1.1. Characterization Results of Aluminum Silicates

7.1.1.1. XRD

The XRD patterns corresponding to aluminum silicate catalysts of AlSi1, AlSi2 and AlSi3 are given in Figure 7, 8, and 9, respectively.

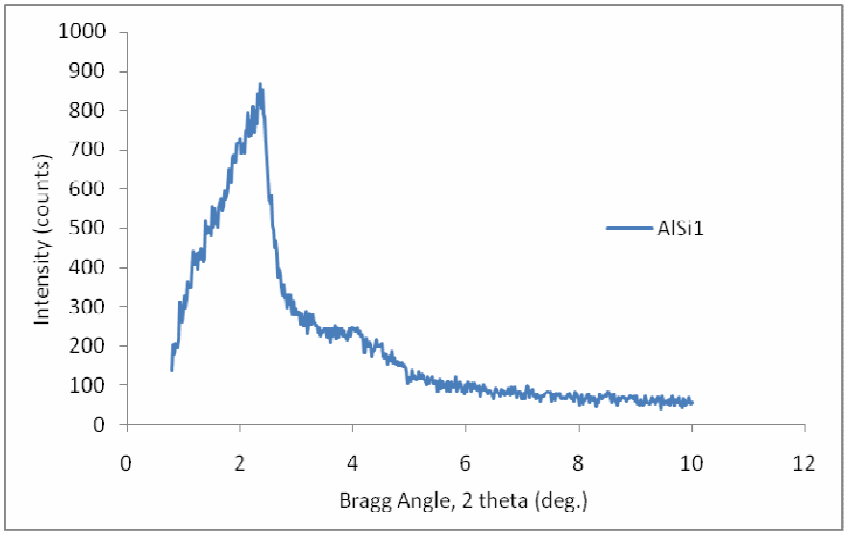


Figure 7. XRD Pattern of AlSi1 Catalyst

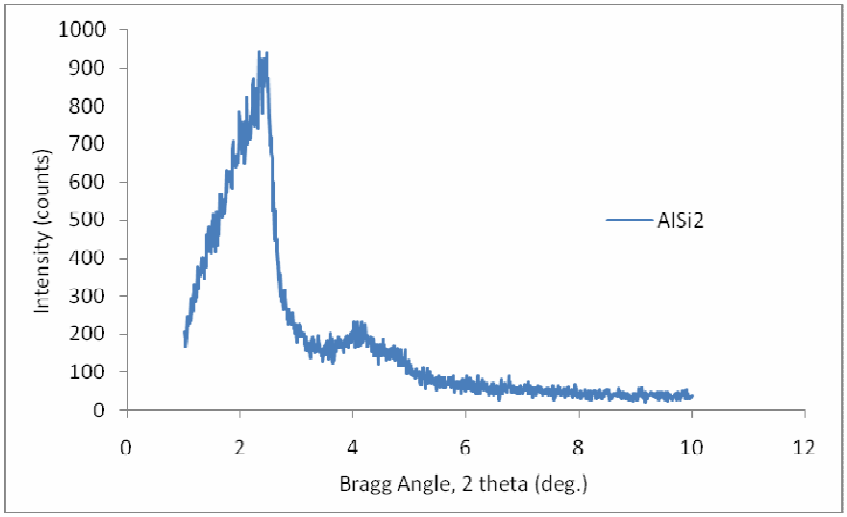


Figure 8. XRD Pattern of AlSi2 Catalyst

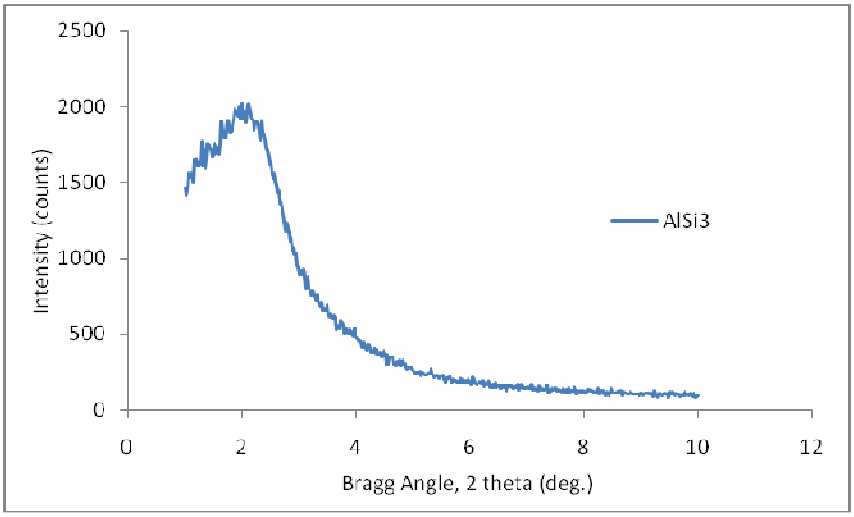


Figure 9. XRD Pattern of AlSi3 Catalyst

A typical MCM-41 material should have a major peak at a 2θ value of 2.5° in the XRD patterns and three reflections at 4.2°, 4.9° and 6.5°. Since mesoporous materials have major and reflection peaks in low Bragg angle range, the major peaks were observed at a 2θ value of 2.36°, 2.45° and 2.20° for AlSi1, AlSi2 and AlSi3, respectively. Also, the reflection peaks were observed at values of 4.0°, 4.02°, and 3.96° respectively. These major peaks that were observed between 2.20°-2.45° and the reflections observed at about 4° are characteristic peaks for the ordered mesoporous structure of MCM-41 like materials. The third and fourth characteristic peaks of the pure MCM material could not be observed. Intensities of these peaks were not as high as pure MCM-41. These results indicated some distortion of the long range ordering of the mesoporous structure. This is due to the incorporation of aluminum into the silicate walls, causing structural irregularity. In addition to this, much wider and less intense main peaks obtained from synthesized aluminum silicates support this claim. Additionally, better XRD pattern was observed at the same Al/Si ratio when sodium silicate was used as silica source (Fig.7). Therefore, silica source used in synthesizing the mesoporous materials also affects the structure of the material.

For these synthesized catalysts, the repeating distance "*a*" between the two pore centers of this material calculated from $a = \frac{2d_{100}}{\sqrt{3}}$ are presented in Table 3.

Table 3. d_{100} and a Values for the Catalysts

Catalyst	**d_{100} (nm)**	**a (nm)**
AlSi1	3.8	4.4
AlSi2	3.6	4.2
AlSi3	4.0	4.6

7.1.1.2. EDS

The results of EDS analyses are presented in Table 4. According to EDS analyses, atomic and weight ratios of Al to Si were evaluated.

EDS results and Al/Si ratios of the synthesis solutions were quite close to each other but AlSi3. According to the EDS analyses; the catalysts of AlSi1, AlSi2 and AlSi3 synthesized with solutions containing Al/Si ratios of 0.1, 0.2 and 0.1 gave 0.09, 0.18 and 0.05 respectively in the final product. The incorporation of aluminum into silicate walls of the synthesized catalysts of AlSi1 and AlSi2 were highly successful. Almost half of the aluminum was not incorporated into the structure for AlSi3. This was the case because the aluminum might be removed during washing step or dealumination might occur during calcination step. Using sodium silicate as silica source gave better results than that of TEOS. EDS patterns of all synthesized aluminum silicate materials are given in Appendix A1.

Table 4. EDS Analyses of the Synthesized Aluminum Silicate Samples Having Different Al Loadings

Sample	Element	Weight Conc. (%)	Atom Conc. (%)	Al/Si Ratio		Solutions Containing Al/Si Ratio
				Weight	Atomic	
AlSi1	Al	8.24	8.55	0.090	0.093	0.1
	Si	91.76	91.45			
AlSi2	Al	14.91	15.43	0.175	0.182	0.2
	Si	85.09	84.57			
AlSi3	Al	4.26	4.43	0.045	0.046	0.1
	Si	95.74	95.57			

7.1.1.3. N_2 Physisorption

Nitrogen adsorption and desorption isotherms of AlSi1, AlSi2 and AlSi3 are given in Fig.10.

The nitrogen adsorption isotherm of these aluminum silicates were Type IV as described by the IUPAC classification (Fig.10), indicating mesoporous structure and the pore size distributions were quite narrow. Hysteresis was formed due to capillary condensation of N_2 in mesoporous of the structure. These pore size distributions also indicated the presence of some larger pores in the order of magnitude of 100 nm (Fig.11). Based on the distributions, it can be argued that AlSi1 and AlSi2 show much similar narrow pore size distributions than that of AlSi3. Having the same Al/Si ratio of AlSi1 and AlSi3, this situation estimated due to the silica source variation. Physical properties of these synthesized

mesoporous aluminum silicate materials used in the methanol dehydration reaction are reported in Table 5.

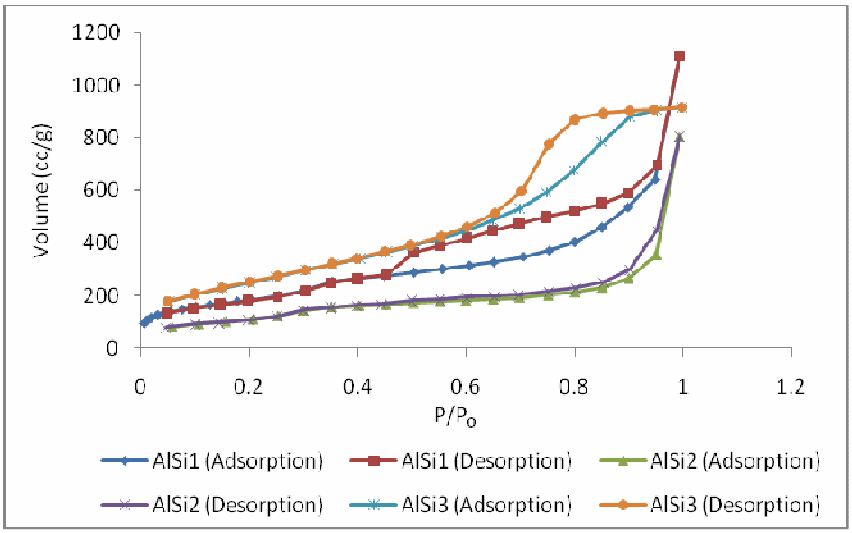


Figure 10. Adsorption-Desorption Isotherm of Synthesized Aluminum Silicates

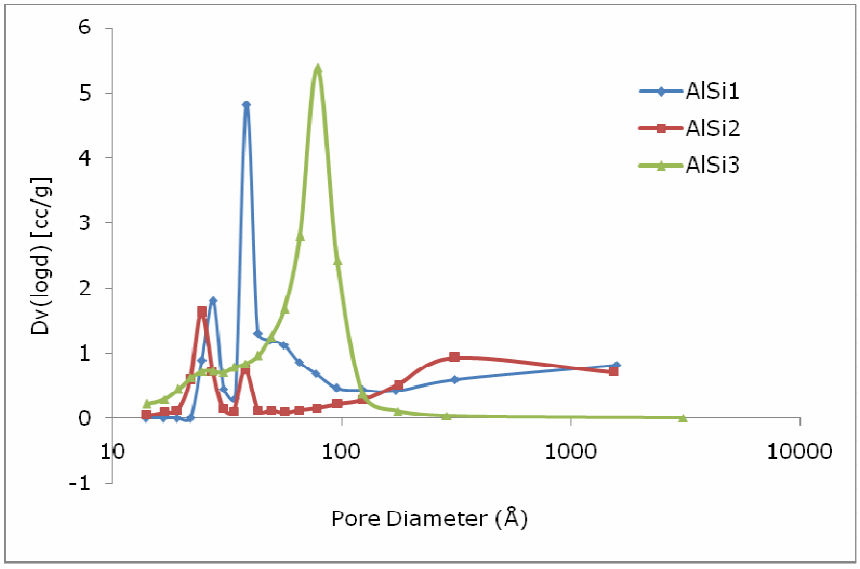


Figure 11. Pore Size Distribution of Synthesized Aluminum Silicates

Table 5. Physical Properties of the Synthesized Aluminum Silicates

Catalyst	Single Point Surface Area (m^2/g)	BET Surface Area (m^2/g)	BJH Ads. Surface Area (m^2/g)	BJH Ads. Pore Volume (cc/g)	BJH Ads. Pore Diameter (nm)	Lattice Parameter *a* (nm)	d_{100} (nm)
AlSi1	610	673	1008	1.80	2.7	4.4	3.8
AlSi2	471	414	463	1.25	2.4	4.2	3.6
AlSi3	904	937	1070	1.45	2.5	4.6	4.0

As seen from Table 5, increasing the alumina content of the catalyst resulted in a decrease in the surface area of the catalyst. AlSi3, containing an Al/Si atomic ratio of 0.046 had the highest BET surface area value of about 937 m^2/g. However, AlSi1 and AlSi2 containing Al/Si ratios of 0.09 and 0.18 had BET surface area of 673 and 414 m^2, respectively.

7.1.1.4. SEM

Some of the SEM images of the catalysts are given in Fig.12, 13 and 14. According to the SEM images, it can be said that synthesized aluminum silicates generally agglomerated. Average particle size of AlSi1 and AlSi2 was 0.33 and 1.9 µm, respectively. In Appendix A2, some other SEM images of these catalysts are also presented.

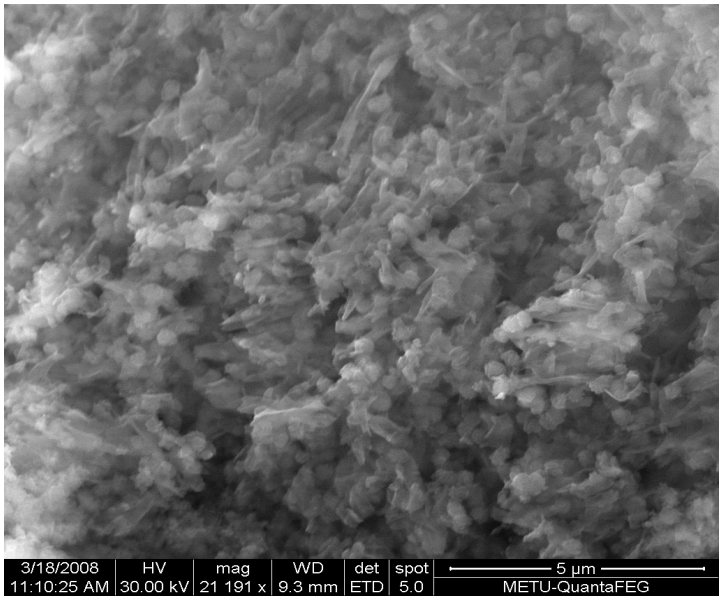


Figure 12. SEM Image of AlSi1

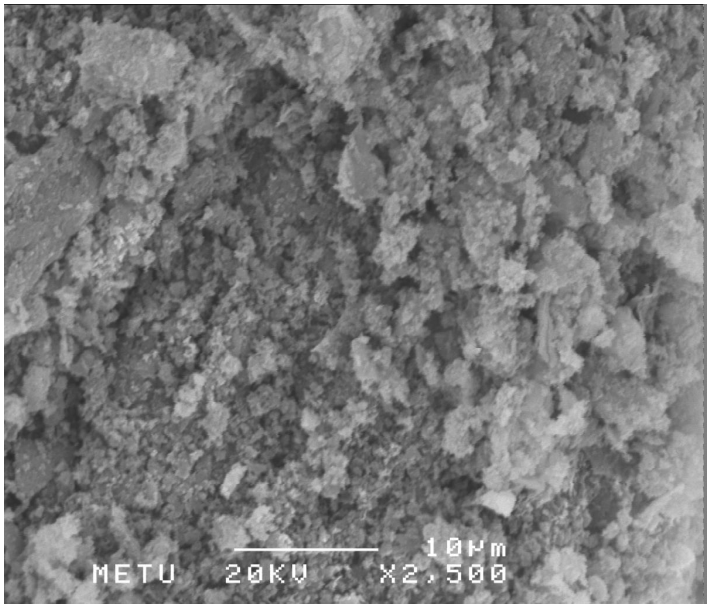


Figure 13. SEM Image of AlSi2

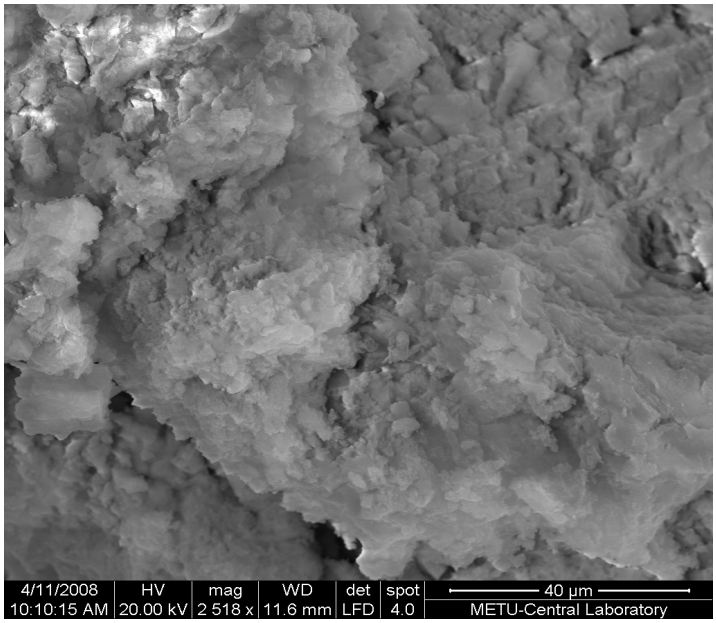


Figure 14. SEM Image of AlSi3

7.1.1.5. DRIFTS

Since surface acidity of the catalyst is expected to play an important role in the methanol dehydration, DRIFTS analyses of fresh and pyridine adsorbed catalysts were carried out in order to investigate the acidic characteristic of the aluminum silicate catalysts. The difference of these fresh and pyridine adsorbed spectra (Figure 15, 16, 17) gave information about the acid sites. DRIFTS bands observed at 1447 cm^{-1} and 1598 cm^{-1} correspond to the Lewis acid sites. Bands observed at 1540 cm^{-1} and 1640 cm^{-1} correspond to Bronsted acid sites and the band observed at 1489 cm^{-1} was reported to be due to both Lewis and Bronsted acid sites [57].

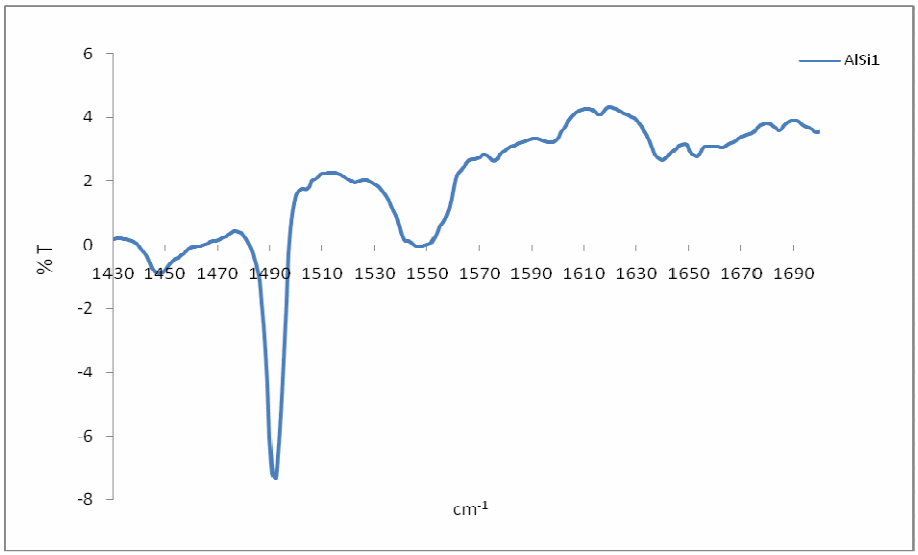


Figure 15. DRIFTS Spectra of AlSi1

According to DRIFTS spectra of AlSi1, Lewis acid sites existed in the band of 1447 cm^{-1}. At the band of 1547.5 and 1639 cm^{-1}, Bronsted acid sites were present. Besides, the contribution of both Lewis and Bronsted acid sites were observed at the band of 1491 cm^{-1}.

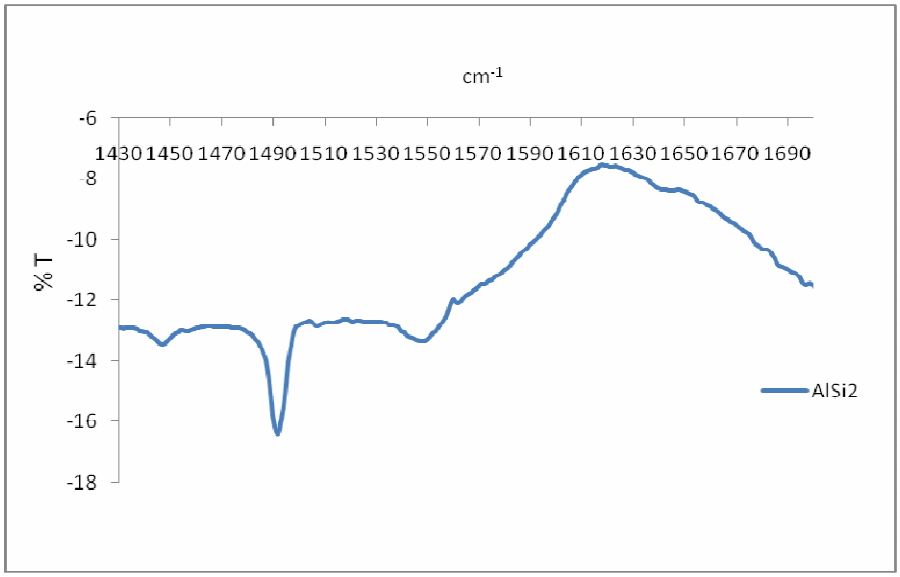


Figure 16. DRIFTS Spectra of AlSi2

In Fig.16, DRIFTS spectra of AlSi2 can be seen. The intensity of Lewis acid site observed at the band of 1447 cm^{-1} was a little less than that of AlSi1. Also, Bronsted acid sites that were observed at the band of 1547 and 1640 cm^{-1} were also less intense than that of AlSi1. In addition to this, the contribution of both Lewis and Bronsted acid sites correspond to the bands of 1491 cm^{-1} was higher for AlSi1 than the corrsponding band of 1490 cm^{-1} for AlSi2. Both for AlSi1 and AlSi2, the bands at 1547 cm^{-1} are stronger than the bands at 1447 cm^{-1}, indicating the presence of more Bronsted acid sites than Lewis acid sites.

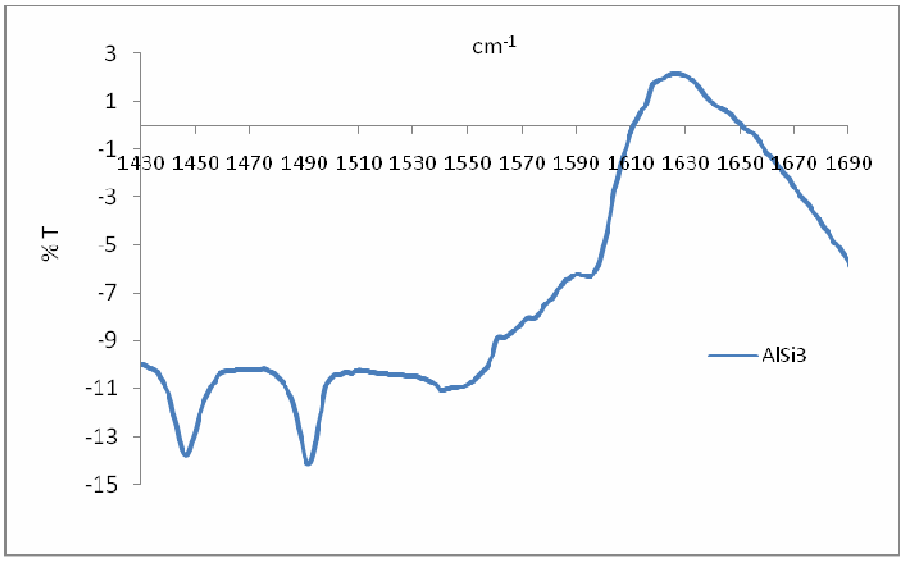


Figure 17. DRIFTS Spectra of AlSi3

In Fig.17, the DRIFTS spectra of the final synthesized aluminum silicate material of AlSi3 is presented. The intensity of 1447 cm^{-1} band corresponding to Lewis acid site was much higher than that of both AlSi1 and AlSi2. However, the contribution of Bronsted acid sites are not as much as obtained from that of AlSi1. No clear spectra of bronsted acid site was observed at the band of 1540 or 1640 cm^{-1}.

In conclusion, it can be said that for AlSi1 and AlSi2 Bronsted acid sites are stronger than Lewis acid sites. However, for AlSi3 Bronsted acid sites are not as strong.

7.1.2. Characterization Results of SBA-15 and Al-SBA-15

7.1.2.1. XRD

The XRD pattern corresponding to SBA-15 and aluminum impregnated SBA-15 (Al-SBA-15) are presented in Fig.18 and Fig.19, respectively.

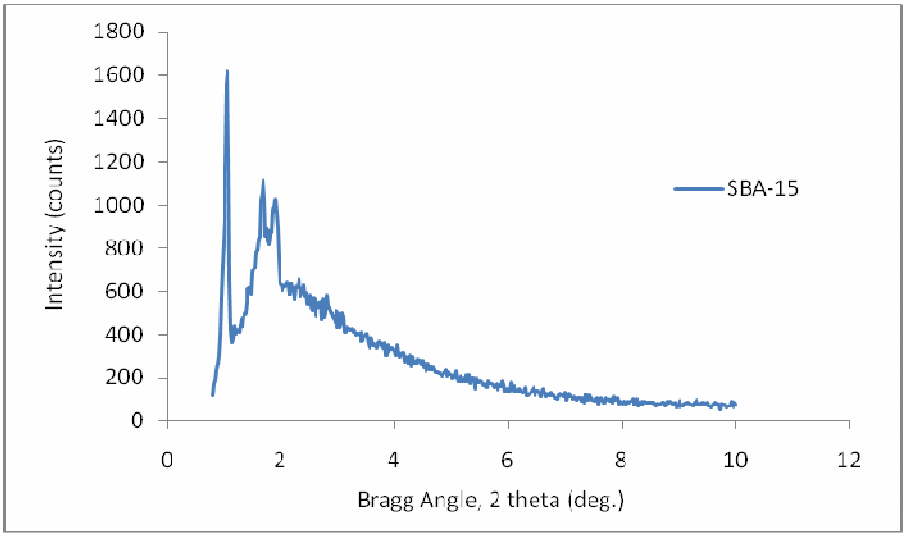


Figure 18. XRD Pattern of SBA-15

Synthesized SBA-15 gave a characteristic single strong peak at a Bragg angle, 2θ value of 1. Also, it had 2 reflections that were observed at 2θ value of 1.66 and 1.9. Therefore, the hexagonally ordered structure of pure SBA-15 exhibited 3 characteristic peaks. The XRD pattern did not show any other reflection peaks for 2θ values higher than 1.9.

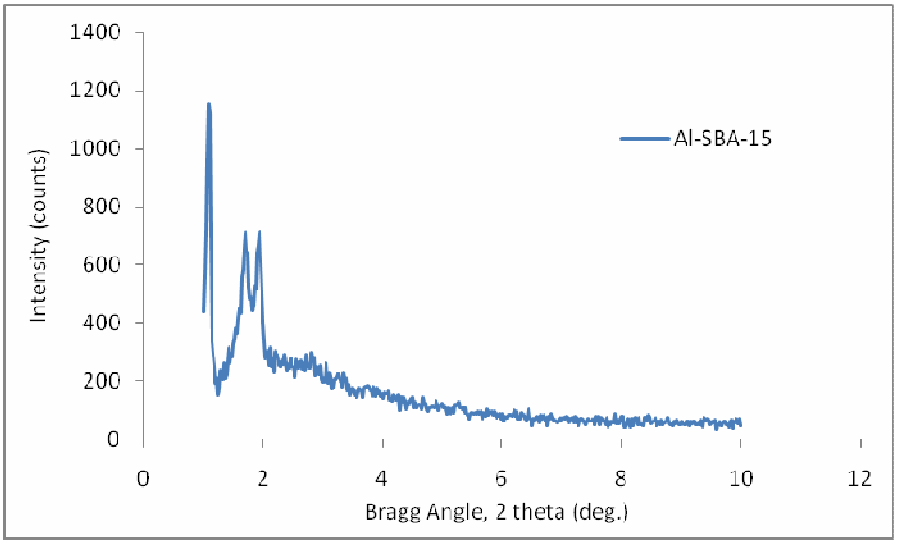


Figure 19. XRD Pattern of Al-SBA-15

According to the XRD pattern of Al-SBA-15, the same three peaks were observed at similar 2θ values. As a result, it can be said that the ordered mesoporous structure was preserved after aluminum impregnation into the structure. However, the relative intensities of the peaks were lowered after adding aluminum.

7.1.2.2. EDS

EDS analysis of Al-SBA-15 was performed in order to see whether aluminum incorporation into SBA-15 was succesful or not. The result of the analysis was given in Table 6.

Al was incorporated with the Al/Si ratio of 0.1 and gave Al/Si ratio of 0.1 in the final product. Therefore, all of the aluminum can said to be succesfully incorporated into the structure.

Table 6. EDS Analysis of the Synthesized Al-SBA-15

Sample	Element	Weight Conc. (%)	Atom Conc. (%)	Al/Si Ratio	
				Weight	Atomic
Al-SBA-15	Al	8.87	9.20	0.097	0.101
	Si	91.13	90.80		

7.1.2.3. N_2 Physisorption

The adsorption and desorption isotherm of SBA-15 and Al-SBA-15 featured hysteresis loops with sharp branches (Fig.20). Type IV isotherm was obtained according to the IUPAC definition. No drastic change was encountered for the mesoporous network of SBA-15 after aluminum incorporation.

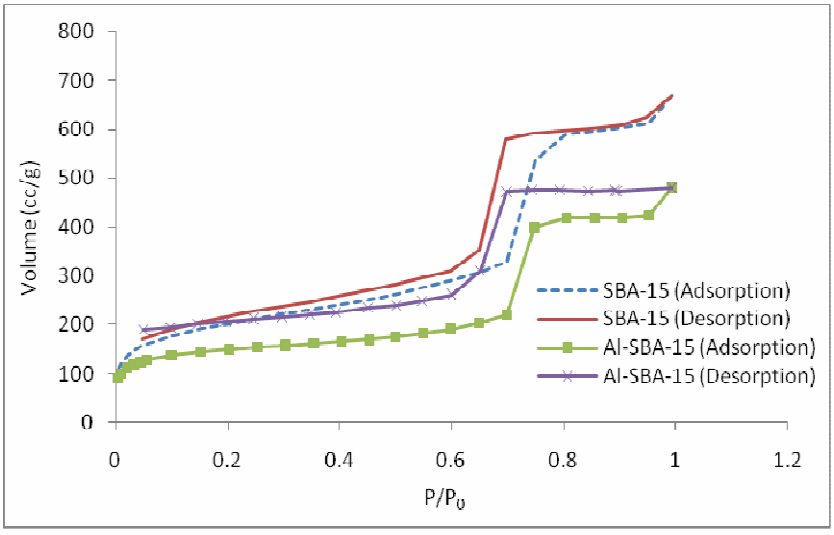


Figure 20. Adsorption-Desorption Isotherm of Synthesized SBA-15 and Al-SBA-15

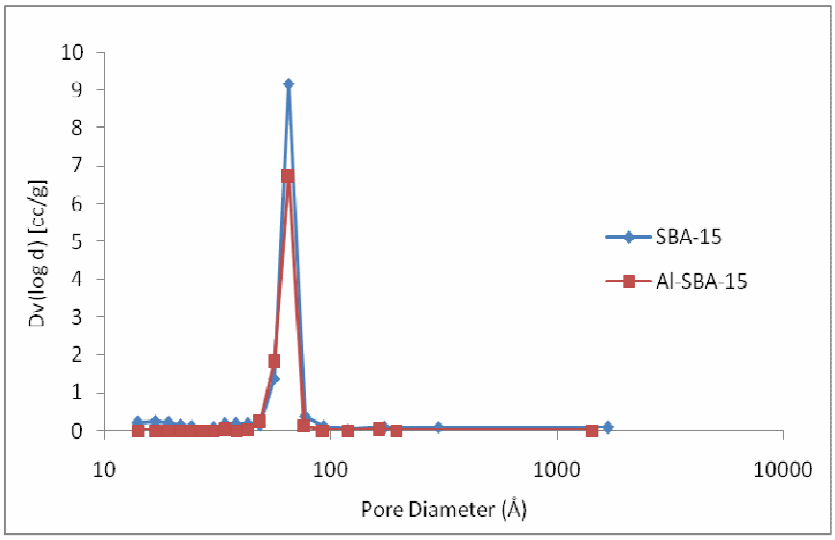


Figure 21. Pore Size Distribution of Synthesized SBA-15 and Al-SBA-15

According to pore size distribution of SBA-15 and Al-SBA-15, both of the synthesized materials had larger pores in the order of magnitude of 100 nm. These materials also had narrow pore size distributions (Fig.21). The sharpness of the adsorption branches verified this situation. Both SBA-15 and Al-SBA-15 exhibited similar distributions, the maxima decreased after adding aluminum into the structure.

Table 7. Physical Properties of Synthesized SBA-15 and Al-SBA-15

Catalyst	Single Point Surface Area (m^2/g)	BET Surface Area (m^2/g)	BJH Ads. Surface Area (m^2/g)	BJH Ads. Pore Volume (cc/g)	BJH Ads. Pore Diameter (nm)	Lattice Parameter *a* (nm)	d_{100} (nm)
SBA-15	662	699	1158	1.1	0.9	9.8	8.5
Al-SBA-15	500	515	783	0.8	0.9	5.3	4.6

Surface area, pore volume and pore diameter values were obtained according to the N_2 physisorption analysis and presented in Table 7. As expected, metal incorporation into the structure decreased surface area values. 0.9 nm of adsorption pore diameter was obtained for both SBA-15 and Al-SBA-15. Moreover, the repeating distance "*a*" between the two pore centers of these materials were calculated again from $a = \frac{2d_{100}}{\sqrt{3}}$.

7.1.2.4. SEM

SEM images of SBA-15 and Al-SBA-15 are shown in Fig.22 and Fig.23, respectively. Other SEM images of these catalysts are also given in Appendix A.2.

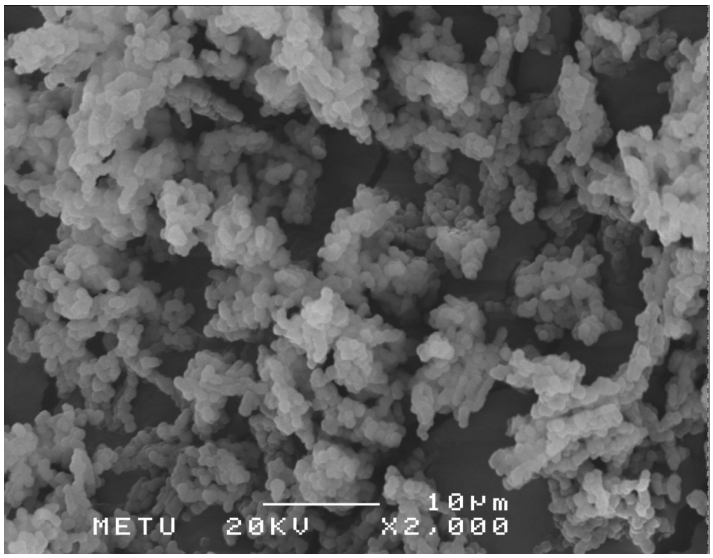


Figure 22. SEM Image of SBA-15

According to the images of pure SBA-15 and aluminum impregnated SBA-15, it can be interpreted that aluminum incorporation into the structure caused no morphological change in the structure of SBA-15. Aggregates of

regular rod-shaped particles retained after alumination. However, a cloudy structure was obtained after the addition of aluminum and nothing remained of the clear structure of SBA-15. Average particle size of SBA-15 and Al-SBA-15 was 1.89 and 1.17 µm, respectively.

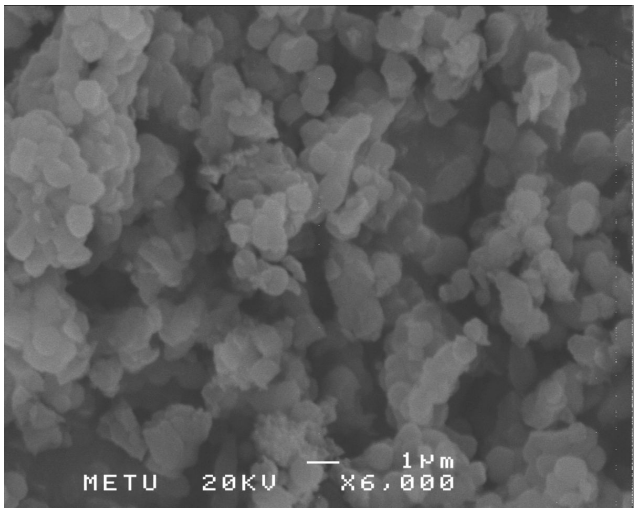


Figure 23. SEM Image of Al-SBA-15

7.1.2.5. DRIFTS

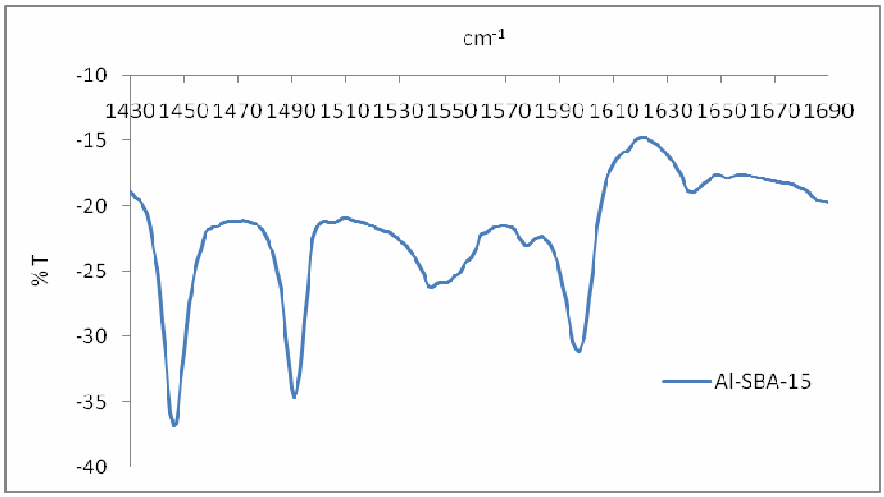


Figure 24. DRIFTS Spectra of Al-SBA-15

According to the DRIFTS spectra of pyridine adsorbed Al-SBA-15, large Lewis acid site bands were observed at 1447 and 1598 cm^{-1}. Also, at the bands of 1540 and 1640, Bronsted acid sites were established. The contribution of both Lewis and Bronsted acid sites were observed at the band of 1489 cm^{-1} with a very high intensity.

7.1.3. Characterization Results of Aluminum Oxide Catalysts

7.1.3.1. N_2 Physisorption

Adsorption-desorption isotherms of different forms of aluminum oxides are reported and graphed below. α and γ forms are represented as A and G in the figures, respectively.

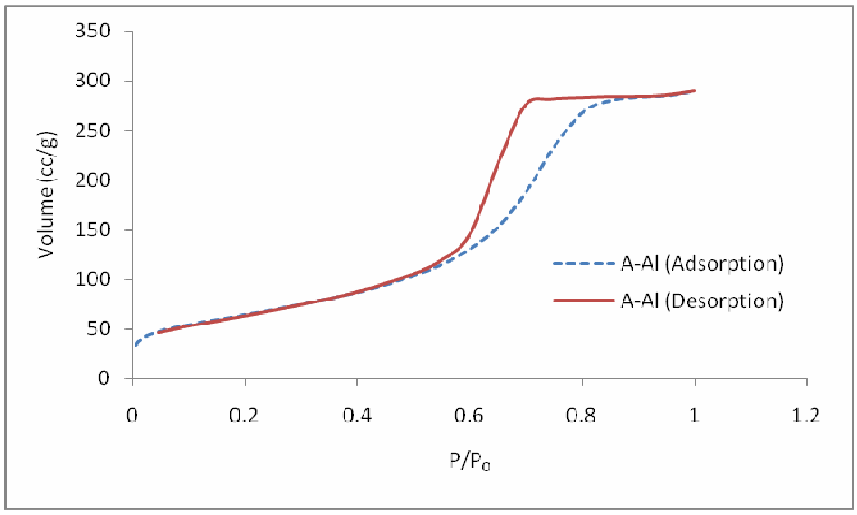


Figure 25. Adsorption-Desorption Isotherm of α-Al

In Fig.25, adsorption desorption isotherm of α-Al is presented. The nitrogen adsorption results indicated close to type V isotherm not only for α-Al

but also for γ-forms of aluminum oxides (Fig.26, 27, 28) according to the IUPAC classification. Like type IV, type V represents adsorption isotherms with hysterises. However, different from type IV, type V describe mesoporous adsorbents with weak affinities.

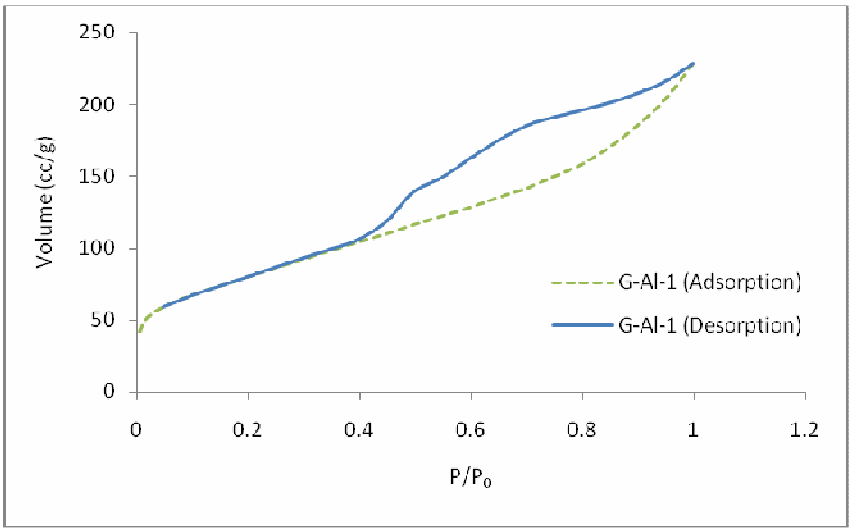


Figure 26. Adsorption-Desorption Isotherm of γ-Al-1

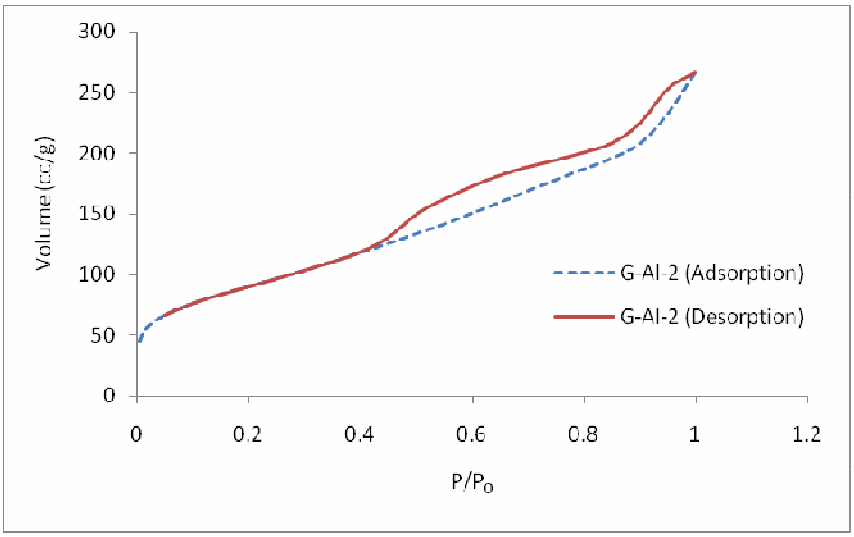


Figure 27. Adsorption-Desorption Isotherm of γ-Al-2

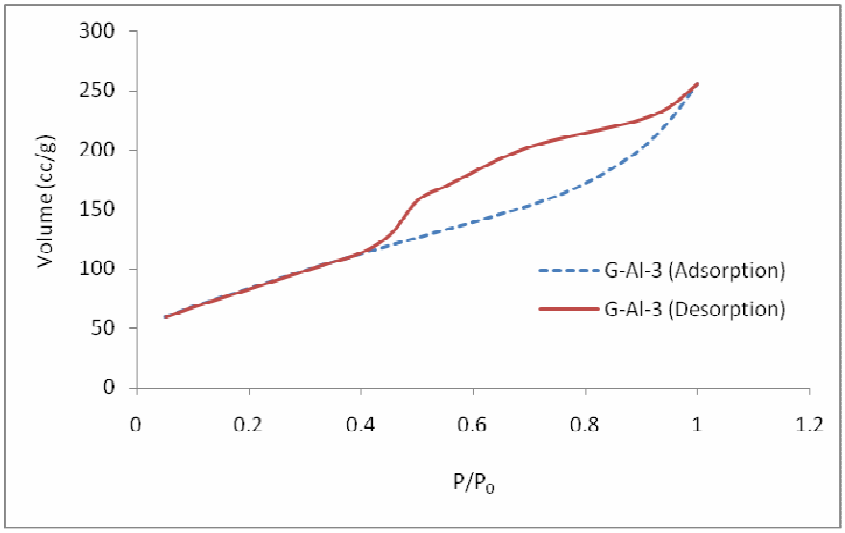


Figure 28. Adsorption-Desorption Isotherm of γ-Al-3

Pore size distribution of different forms of aluminum oxides are given in Fig.29. α-alumina had larger pores in the order of magnitude of 100 nm. γ-Al-1 and γ-Al-3, that showed very similar pore size distribution, also had larger pores in the order of magnitude of 100 nm. However, γ-Al-2 had larger pores in the order of magnitude of almost 10 nm. Both of these catalysts showed narrow pore size distributions. The physical properties of the catalysts are presented in Table 8.

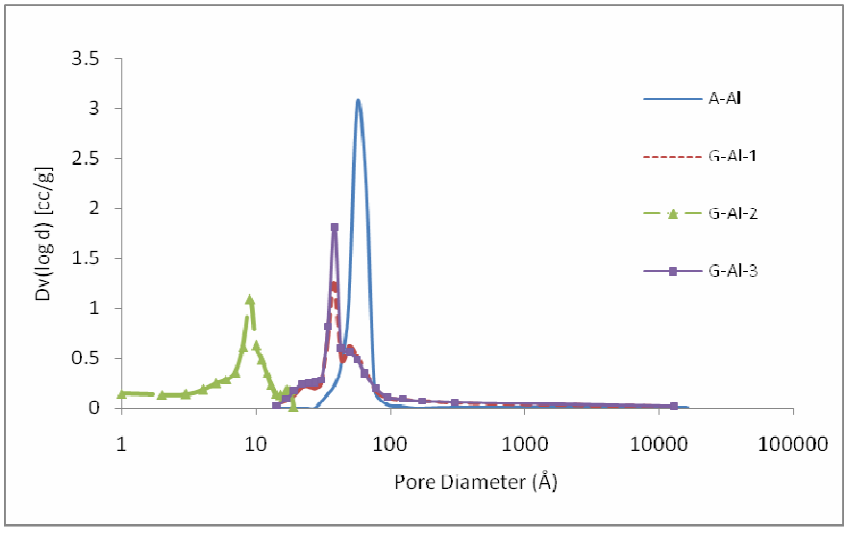


Figure 29. Pore Size Distribution of Aluminum Oxides

Table 8. Physical Properties of the Catalysts.

Catalyst	Single Point Surface Area(m^2/g)	BET Surface Area (m^2/g)	BJH Ads. Surface Area (m^2/g)	BJH Ads. Pore Volume (cc/g)	BJH Ads. Pore Diameter(nm)
α-Al	215	232	441	0.47	6.5
γ-Al-1	294	289	232	0.38	0.9
γ-Al-2	314	323	515	0.45	0.9
γ-Al-3	274	287	342	0.40	2.2

According to BET surface area values, γ forms of aluminum oxides had higher BET surface areas than that of α form of aluminum oxide. Among two forms of aluminum oxides, γ-Al-2 had higher BET surface area taking a value of higher than 320 m^2/g. Almost the same surface areas were obtained for γ-Al-1 and γ-Al-3 with the value of almost 290 m^2/g. Although α-Al had lower surface area, it had very large pore diameter than that of γ forms of aluminum oxides. According to the pore diameter values of γ-Al-1 and γ-Al-2, it can be declared that these catalysts had some micropores in their structure. Pore volume of the catalysts were similar, almost 0.4 cc/g.

7.1.3.2. SEM

SEM images of α-Al, γ-Al-1, γ-Al-2 are shown in Fig.30, 31, 32, respectively. Average particle size of α-Al, γ-Al-1 and γ-Al-2 was 1 cm, 2.85 and 3 mm, respectively. Some of the SEM images of these catalysts are also given in Appendix A.2.

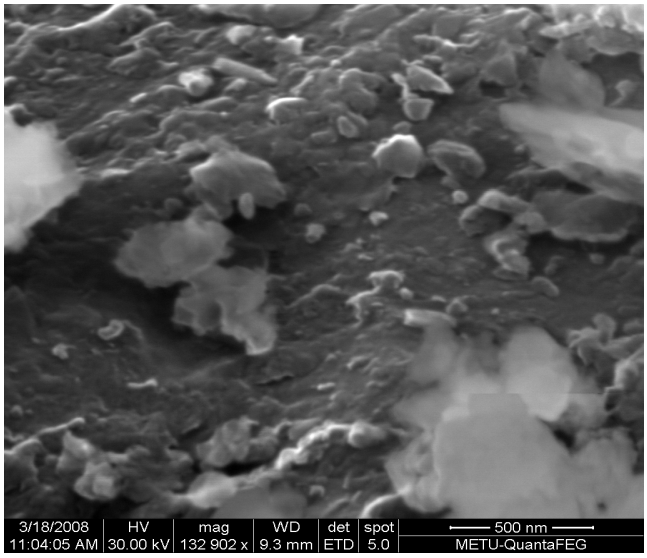


Figure 30. SEM Image of α-Al

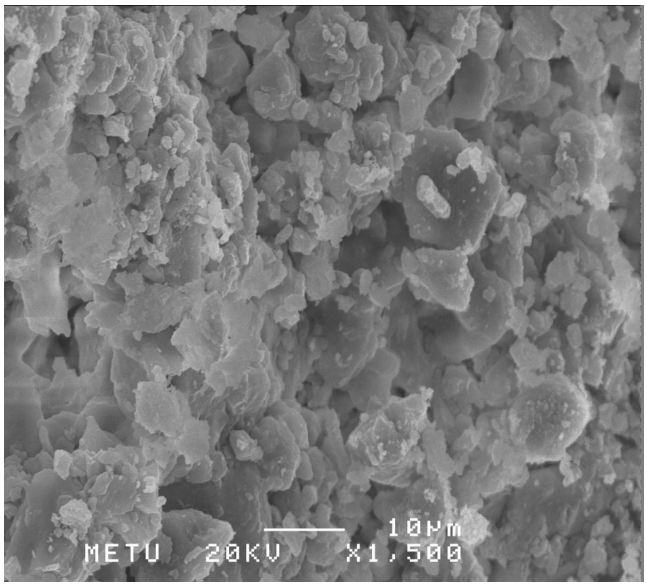


Figure 31. SEM Image of γ-Al-1

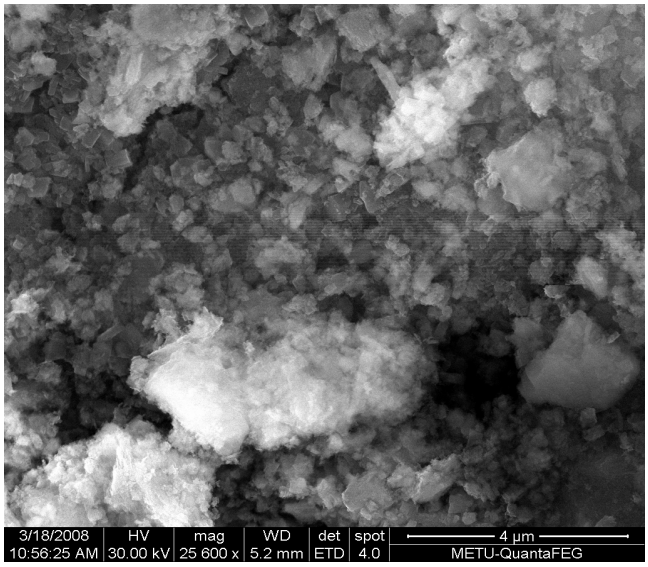


Figure 32. SEM Image of γ-Al-2

7.1.3.3. DRIFTS

DRIFTS spectra of pyridine adsorbed α-Al, γ-Al-1 samples are presented in Fig.32 and Fig.33, respectively. According to DRIFTS spectra of α-Al, Lewis acid site was observed at the band of 1447 cm^{-1}. From Fig.33, for the spectra of γ-Al-1, much less intense Lewis acid site band was observed. The intensities of the aluminum oxides were lower than that of AlSi3 of the synthesized aluminum silicates and Nafion SAC-13. However, for the Bronsted acid sites, a broad and large band was observed at 1510 cm^{-1}. This result indicated that α-Al had strong Bronsted acidity.

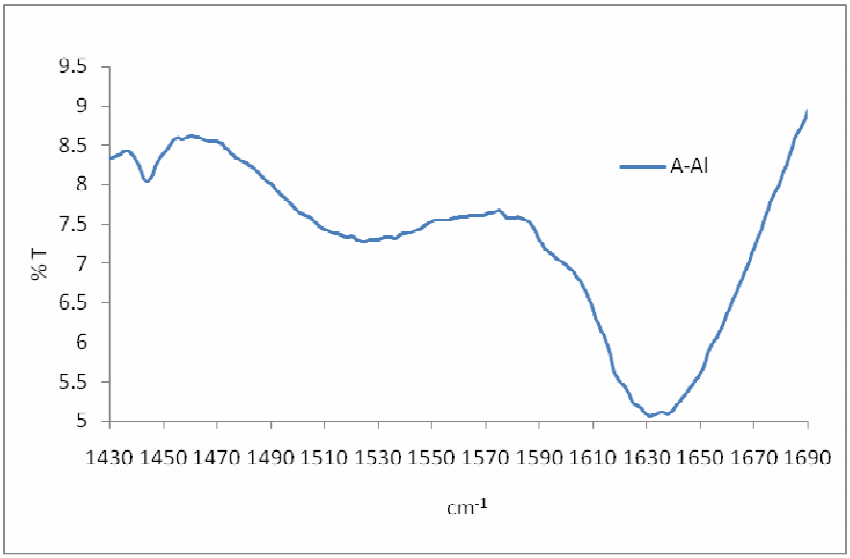


Figure 32. DRIFTS Spectra of α-Al

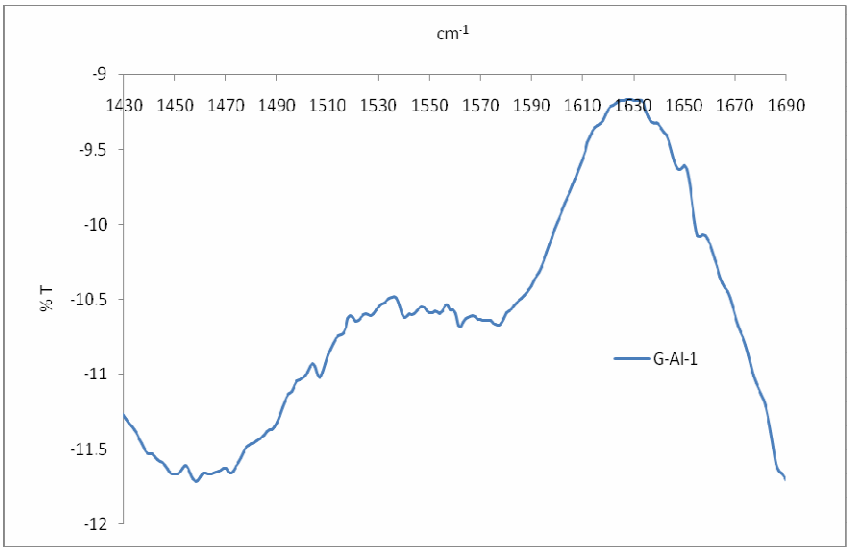


Figure 33. DRIFTS Spectra of γ-Al-1

7.1.4. Characterization Results of Nafion Catalysts

7.1.4.1. N_2 Physisorption

The adsorption and desorption isotherms of Nafion NR-50 and Nafion SAC-13 are presented in Fig.35.

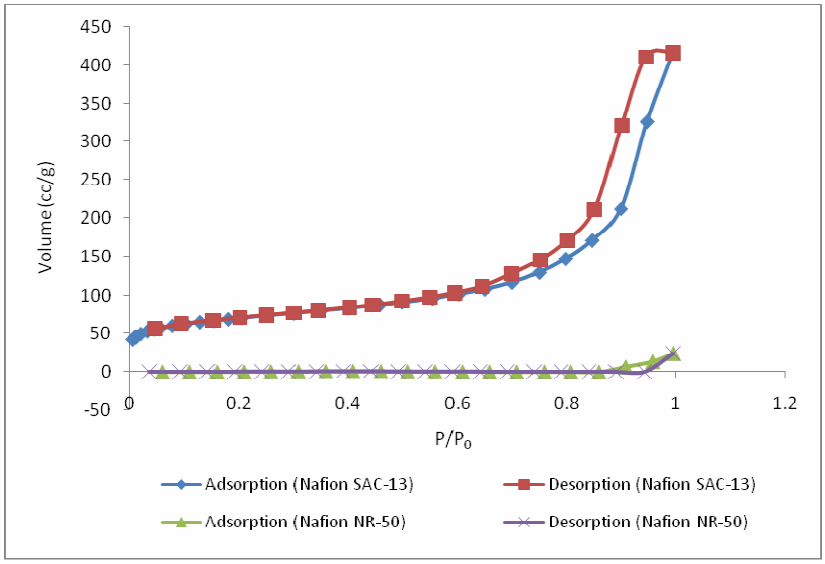


Figure 35. Adsorption-Desorption Isotherm of Nafion NR-50 and SAC-13

The nitrogen adsorption isotherm of Nafion SAC-13 indicated Type V as described by the IUPAC classification. Because of the non porous property of Nafion NR-50, it has limited adsorption and desorption capacity. A much wider pore size distribution was observed with Nafion SAC-13 than Nafion NR-50 due to the stated non-porosity of the material (Fig.36). The presence of larger pores in the order of magnitude of 1000 nm verified the higher adsorption capacity of SAC-13 than that of NR-50.

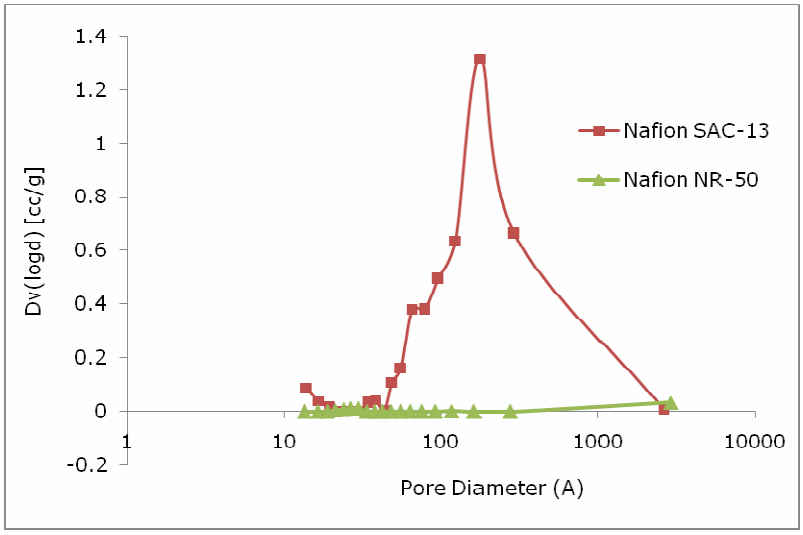


Figure 36. Pore Size Distribution of Nafion NR-50 and SAC-13

Among the two Nafion type catalysts, since NR-50 is essentially nonporous, it had a very low surface area. However, the BET surface area of SAC-13 was over 200 m^2/g. BJH adsorption surface area, pore volume and pore diameter values are also presented in Table 9. Not only BJH adsorption pore diameter of SAC-13 was larger than that of NR-50, but also average pore diameter of SAC-13 (11 nm) was much larger than that of NR-50.

Table 9. Physical Properties of the Catalysts.

Catalyst	Single Point Surface Area(m^2/g)	BET Surface Area (m^2/g)	BJH Ads. Surface Area (m^2/g)	BJH Ads. Pore Volume (cc/g)	BJH Ads. Pore Diameter(nm)
Nafion NR-50	1.30	0.27	4	0.04	-
Nafion SAC-13	208	235	324	0.65	0.90

7.1.4.2. SEM

SEM images of Nafion NR-50 and SAC-13 are shown in Fig. 37 and 38, respectively. Nonporous surface of NR-50 can easily be seen by comparing the images. Average particle size of NR-50 and SAC-13 is 2.5 mm and 1 cm, respectively. Also, some other images of these Nafion catalysts are presented in Appendix A.2.

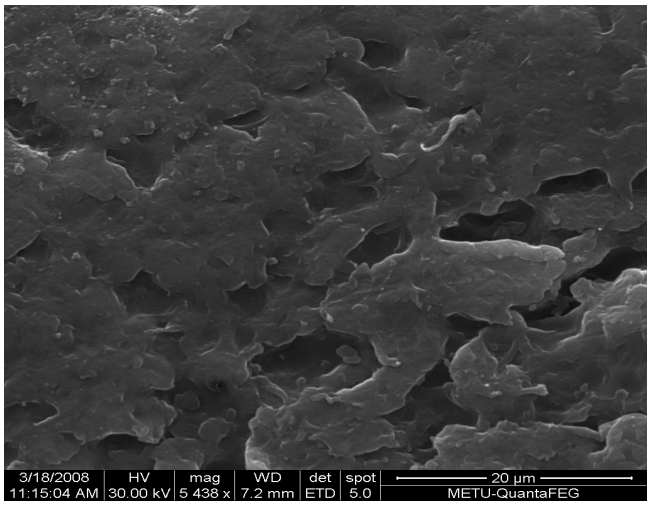


Figure 37. SEM Image of Nafion NR-50

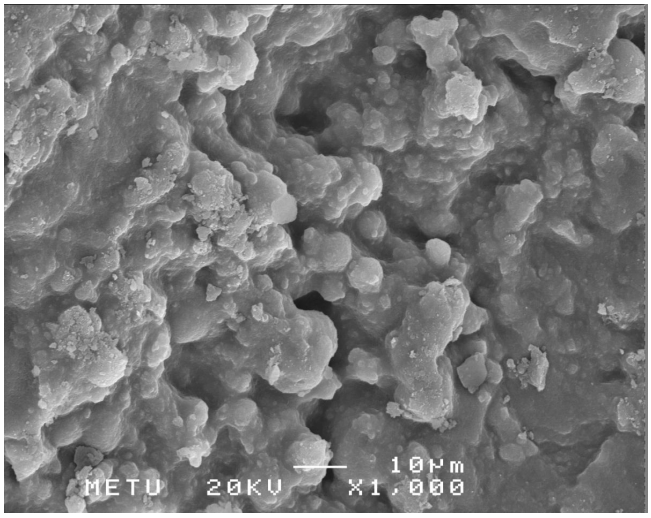


Figure 38. SEM Image of Nafion SAC-13

7.1.4.3. DRIFTS

DRIFTS spectra of pyridine adsorbed Nafion SAC-13 is presented in Fig.39. At the band of 1447 and 1597 cm^{-1}, Lewis acid sites were observed. Bronsted acid sites were observed at the band of 1544 cm^{-1}. Also, a less intense Bronsted acid band in respect of 1544 cm^{-1} were present at 1640 cm^{-1}. The band observed at 1489 was due to both Lewis and Bronsted acid sites. These results indicated the presence of highly strong Bronsted acid sites as well as less strong Lewis acid sites in Nafion SAC-13.

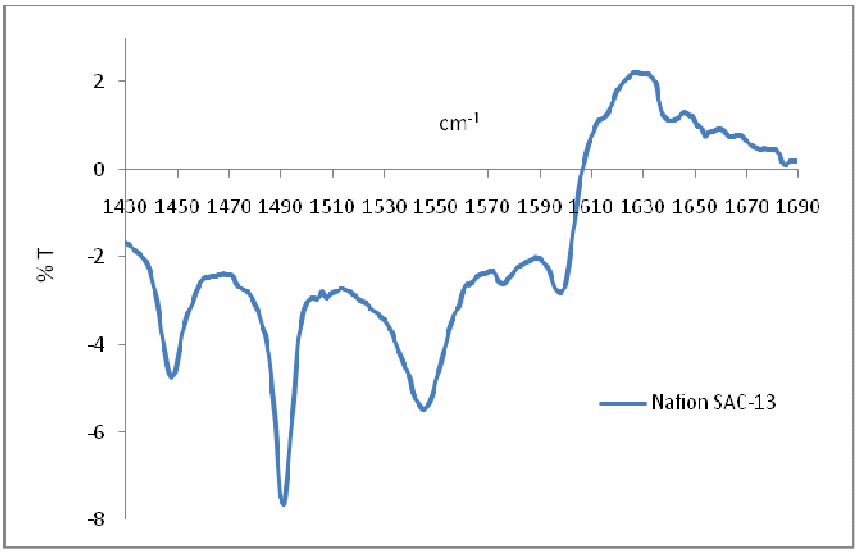


Figure 39. DRIFTS Spectra of Nafion SAC-13

7.2. Results of Methanol Dehydration Reactions

Following methanol dehydration reaction, two main products of DME and water (from reaction 1) and a by-product of formaldehyde (from reaction 2) were observed. According to the basic objective of finding the most suitable catalyst for methanol dehydration reaction that was tested; catalytic activity results of methanol conversion, selectivity and yield of DME were graphed and tabulated.

$2CH_3OH \longrightarrow CH_3OCH_3 + H_2O$ Methanol dehydration (1)

$CH_3OH \longrightarrow CH_2O + H_2$ Formaldehyde formation (2)

In order to evaluate the conversion, selectivity and yield values, mole fractions of the products and unreacted methanol were calculated by multiplying the peak areas obtained from chromatogram of gas chromatography and the calibration factors of each species.

The total conversion of methanol was calculated by using equation below where, n_{MeOH} is the moles of unreacted methanol, n^0_{MeOH} is the moles of methanol fed to the reactor. n^0_{MeOH} was calculated according to the carbon balance of methanol dehydration reaction as seen in equations 4 and 5.

$$X_{MeOH} = \frac{(n^0_{MeOH} - n_{MeOH})}{n^0_{MeOH}} \quad (3)$$

$$n^0_{MeOH} = \beta_{methanol} \times A_{methanol} + 2\beta_{DME} \times A_{DME} + \beta_{Formaldehyde} \times A_{Formaldehyde} \quad (4)$$

$$n^0_{MeOH} = n_{MeOH} + 2n_{DME} + n_{Formaldehyde} \quad (5)$$

Selectivity of DME and formaldehyde was calculated from the following equation;

$$S_{DME} = \frac{2 \times n_{DME}}{(n^0_{MeOH} - n_{MeOH})} \quad (6)$$

$$S_{Formaldehyde} = \frac{n_{Formaldehyde}}{(n^0_{MeOH} - n_{MeOH})} \quad (7)$$

Yield expression was obtained by multiplying selectivity and conversion terms. Yield of DME is the moles of DME produced per mole of methanol fed to the reactor. Maximum DME yield can be 0.5.

$$Y_{DME} = S_{DME} \times X_{DME} \times \frac{1}{2} \quad (8)$$

$$Y_{Formaldehyde} = S_{Formaldehyde} \times X_{Formaldehyde} \quad (9)$$

7.2.1. Results of Methanol Dehydration Reaction over Aluminum Based Catalysts

Activity tests including synthesized AlSi1, AlSi2, AlSi3, Al-SBA-15 and α and γ forms of aluminum oxides were performed with the conditions shown in Table 10. The comparison of the activities; methanol conversion to DME, selectivity and yield values of DME and formaldehyde were given for both among aluminum silicates and aluminum oxides, separately. In addition to these, the effects of reaction temperature and catalyst loading were also analyzed. The activity tests were carried out in a temperature interval of 200-400^{0}C with different space times of 0.136, 0.2 (Appendix B.3), 0.27 s.g/cm^3.

Table 10. Experimental Conditions for Aluminum Based Catalysts

Catalyst	Amount (g)	Feed Flow Rate (MeOH) (mL/min)	He Flow Rate (mL/min)	Total Flow Rate (mL/min)	y_{MetOH}	τ (space time)	Reaction Temp (^{0}C)
AlSi1	0.1	22	22.2	44.2	0.5	0.136	200-400
	0.15	22	22.2	44.2	0.5	0.2	200-400
	0.2	22	22.2	44.2	0.5	0.27	200-400
AlSi2	0.1	22	22.2	44.2	0.5	0.136	200-400
	0.15	22	22.2	44.2	0.5	0.2	200-400
	0.2	22	22.2	44.2	0.5	0.27	200-400
AlSi3	0.1	22	22.2	44.2	0.5	0.136	200-400
	0.15	22	22.2	44.2	0.5	0.2	200-400
	0.2	22	22.2	44.2	0.5	0.27	200-400
Al-SBA-15	0.2	22	22.2	44.2	0.5	0.27	200-400
α-Al	0.1	22	22.2	44.2	0.5	0.136	200-400
	0.15	22	22.2	44.2	0.5	0.2	200-400
	0.2	22	22.2	44.2	0.5	0.27	200-400
γ-Al-1 (2.36-3.33mm)	0.1	22	22.2	44.2	0.5	0.136	200-400
	0.15	22	22.2	44.2	0.5	0.2	200-400
	0.2	22	22.2	44.2	0.5	0.27	200-400
γ-Al-2 (3mm)	0.1	22	22.2	44.2	0.5	0.136	200-400
	0.15	22	22.2	44.2	0.5	0.2	200-400
	0.2	22	22.2	44.2	0.5	0.27	200-400
γ-Al-3 (3.96-4.7 mm)	0.2	22	22.2	44.2	0.5	0.27	200-400

7.2.2. Results of Methanol Dehydration Reaction over Synthesized Aluminum Silicates and Aluminum Impregnated SBA-15 (Al-SBA-15)

MeOH conversions over AlSi1 and AlSi2 at 0.136 s.g/cm^3 space time are plotted against temperature in Fig.40.

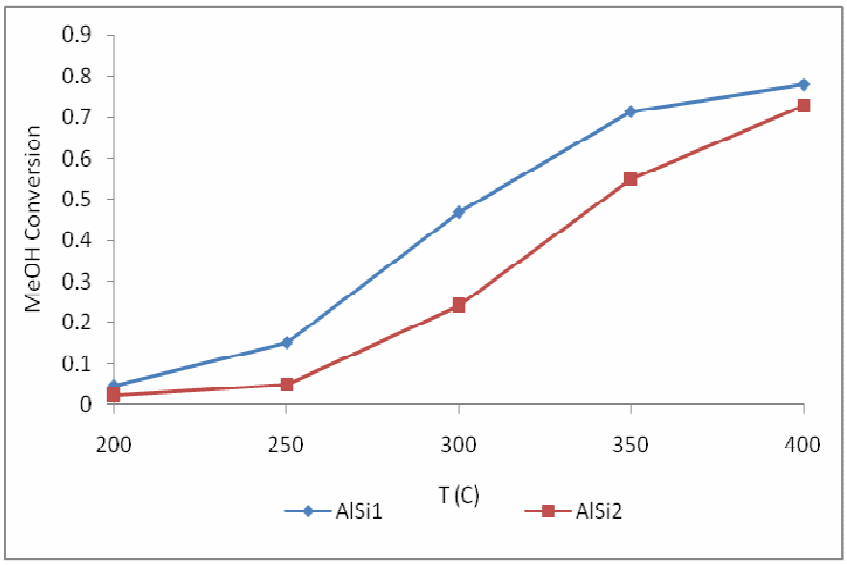


Figure 40. Conversion of Methanol over AlSi1 and AlSi2 at 0.136 s.g/cm^3.

Synthesized mesoporous aluminum silicate catalysts showed high activity in methanol dehydration reaction at temperatures higher than 220^{0}C. Higher conversion of methanol was reached after 250^{0}C. Increasing the reaction zone temperature favored the dehydration reaction for each catalyst. Fractional conversion of methanol approached to 0.78 for AlSi1 and 0.73 for AlSi2 over 350^{0}C. Catalytic activity of AlSi1 was much higher especially between the temperatures of 250-350^{0}C. For instance, MeOH conversion of AlSi1 approximately doubled the conversion of AlSi2 at 300^{0}C with the values of 0.47 and 0.24, respectively. Although catalytic activity of AlSi1 was much higher than

that of AlSi2 at all the temperatures that were tested, methanol conversions of AlSi1 and AlSi2 converged to each other at 400^0C.

Also, synthesized aluminum silicate 3 (AlSi3) and aluminum impregnated SBA-15 (Al-SBA-15) were tested with the catalyst loading of 0.2 g. Methanol conversion against temperature is plotted in Fig.41.

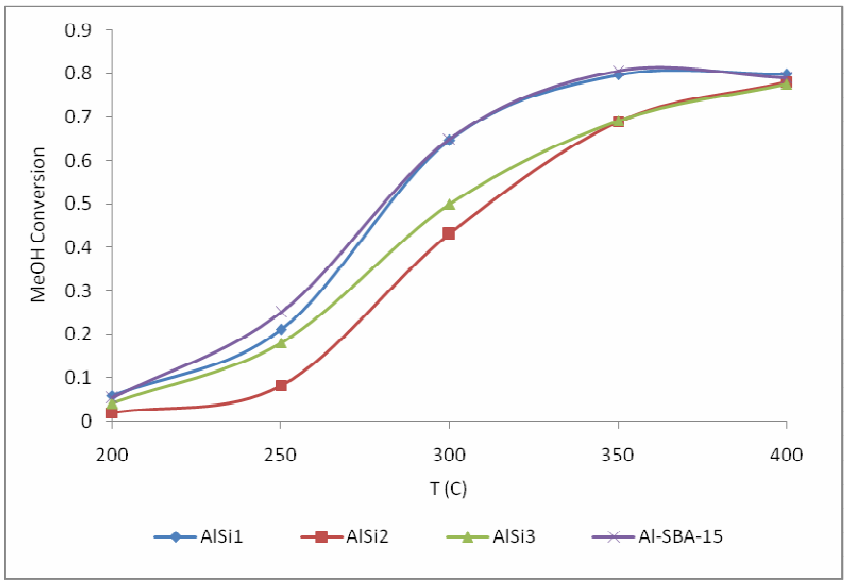


Figure 41. Conversion of Methanol over Synthesized Aluminum Silicates and Al-SBA-15 at 0.27 s.g/cm^3.

Similar conversion trend was obtained with 0.27 s.g/cm^3 compared to 0.136 s.g/cm^3 at lower temperatures for both AlSi1 and AlSi2. The catalytic activity of AlSi1 was again much higher than that of AlSi2 at all the temperatures that were tested. Again, aluminum silicates showed high catalytic activity at temperatures higher than 220^0C. At 300^0C, methanol conversion reached about 0.65 and 0.43 for AlSi1 and AlSi2 respectively. AlSi1's activity was highly stable. Fractional conversion of methanol approached to 0.8 for AlSi1 and 0.78 for AlSi2 over 350^0C, which was very close to the equilibrium conversion. AlSi3 showed similar performance with AlSi1 at lower temperatures and with AlSi2 at higher

temperatures. Although AlSi1 and AlSi3 prepared with the same Al/Si ratio of 0.1, AlSi1 showed higher catalytic activity. This was the case as silica sources were different. Sodium silicate that was used in AlSi1 estimated to enhance catalytic activity than that of TEOS in AlSi3. Besides, Al-SBA-15's catalytic activity was almost same with AlSi1 especially after 300^0C.

As it was discussed in the previous section, aluminum had been successfully incorporated into the matrix of the catalyst when sodium silicate was used as the silica source. In fact, the Al/Si ratio of AlSi1 incorporated in the structure of the catalyst was much higher than the Al/Si ratio of AlSi3. Also, the strength of Bronsted acid sites of AlSi1 was found to be much higher than the corresponding value for AlSi3.

Also, variation of methanol conversion with increasing temperature at different space times is plotted in Fig.42. The increase in space time enhanced methanol conversion (Table 11).

For AlSi1, 65 percent of methanol was converted with a space time of 0.27 s.g/cm^3 at 300^0C, while only 47 percent of methanol was converted with 0.136 s.g/cm^3. Also, at the same temperature methanol conversion increased to 0.43 from 0.24 by increasing the amount of catalyst from 0.1 to 0.2 g. Conversion values were close to each other at 400^0C for both 0.1 g. and 0.2 g. catalyst loading because they reached maximum conversion, as the reaction is thermodynamically limited.

Table 11. Variation of Methanol Conversion with Different Space Times.

Temp. (°C)	**MeOH Conversion**							
	AlSi1		AlSi2		AlSi3		Al-SBA-15	
	0.136 s.g/cm^3	0.27 s.g/cm^3	0.136 s.g/cm^3	0.27 s.g/cm^3	0.136 s.g/cm^3	0.27 s.g/cm^3	0.136 s.g/cm^3	0.27 s.g/cm^3
200	0.05	0.06	0.02	0.02	-	0.04	-	0.05
250	0.15	0.21	0.05	0.08	-	0.18	-	0.25
300	0.47	0.65	0.24	0.43	-	0.50	-	0.65
350	0.71	0.80	0.55	0.69	-	0.69	-	0.80
400	0.78	0.80	0.73	0.78	-	0.78	-	0.79

Higher catalytic activity was obtained with Al/Si ratio of 0.1 (AlSi1) than that of Al/Si ratio of 0.2 (AlSi2). So, it can be said that finding the optimum amount of aluminum loading was crucial for getting better catalytic activity. In fact, the acid strengths of AlSi2 observed by pyridine adsorption were lower than the corresponding values of AlSi1, as indicated in the characterization part. Also, much lower surface area of AlSi2 than AlSi1 caused lower adsorption capacity.

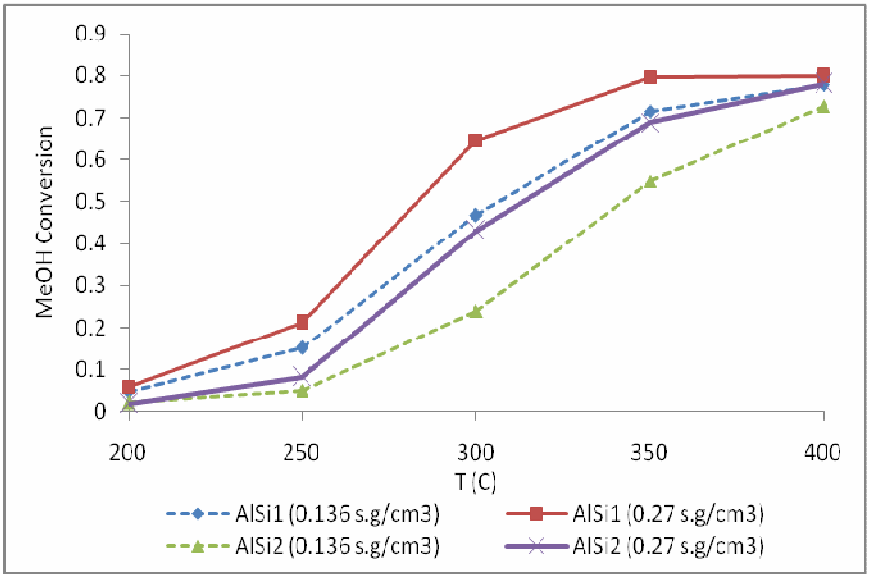


Figure 42. Variation of MeOH Conversion Over AlSi1 and AlSi2 at Different Space Times

Very little amount of coke formation was observed for the aluminum Silicates even at temperatures as high as 400^0C. Therefore, no activity decrease is observed for the aluminum silicates at temperatures as high as 400^0C.

Product selectivities indicated that the main reaction product was DME (Table 12). Experiments carried out with aluminum silicates having different Al/Si molar ratios showed that DME formation was observed even at low temperatures, around 200^0C. However, formation of some formaldehyde was also

observed at lower temperatures (Fig.43). Variation of DME and formaldehyde selectivity over AlSi1, AlSi2 and AlSi3, and Al-SBA-15 with different space times are reported in Table 12 and Table 13. In the case of AlSi1, selectivity of formaldehyde reduced from 0.63 to 0.19 with an increase of temperature from 200^0C to 250^0C. Also, AlSi2 performed similar trend with the decrease of formaldehyde selectivity from 0.81 to 0.24. After 300^0C, very little amount of formaldehyde was observed for both AlSi1 and AlSi2, that is because the entire methanol was converted to DME. These situations were not different for 0.27 s.g/cm^3 space time (Fig.44). High DME selectivity was obtained at temperatures higher than 250^0C. No by-product for AlSi2 was obtained at 350^0C and 400^0C. Also effect of aluminum content of the catalyst on the product selectivity was investigated. Increasing the molar ratio of Al to Si from 0.1 to 0.2 caused a decrease in DME selectivity at low temperatures and space time. Similar DME selectivity of AlSi3 and Al-SBA-15 that were higher than that of AlSi1 and AlSi2 especially at 200^0 C was observed. However, no effect of aluminum content was observed at higher space time at low temperatures. Also, DME selectivity increased with increasing aluminum content at higher temperatures of the higher space time. As reported in the previous section, increase of Al/Si ratio causes a significant decrease in the surface area of the catalyst.

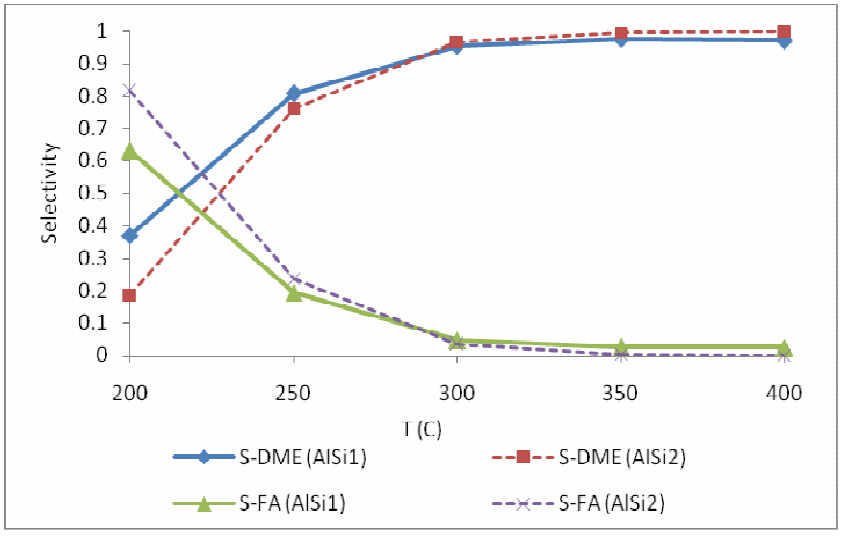


Figure 43. Selectivity of DME and Formaldehyde with AlSi1 and AlSi2 at 0.136 s.g/cm^3.

Table 12. Variation of DME and FA Selectivity Over AlSi1 and AlSi2 with Different Space Times.

Temp. (°C)	**DME Selectivity**						**FA Selectivity**					
	AlSi1		AlSi2		AlSi3		AlSi1		AlSi2		AlSi3	
	0.136 s.g/cm^3	0.27 s.g/cm^3	0.136 s.g/cm^3	0.27 s.g/cm^3	0.136 s.g/cm^3	0.27 s.g/cm^3	0.136 s.g/cm^3	0.27 s.g/cm^3	0.136 s.g/cm^3	0.27 s.g/cm^3	0.136 s.g/cm^3	0.27 s.g/cm^3
200	0.37	0.55	0.19	0.54	-	0.72	0.63	0.45	0.81	0.46	-	0.28
250	0.81	0.88	0.76	0.92	-	0.94	0.19	0.12	0.24	0.08	-	0.06
300	0.95	0.95	0.97	0.99	-	0.99	0.04	0.05	0.03	0.006	-	0.01
350	0.97	0.95	1	1	-	1	0.03	0.05	0.003	0	-	0.002
400	0.97	0.95	1	1	-	1	0.02	0.05	0	0	-	0.001

Table 13. Variation of DME and FA Selectivity Over Al-SBA-15 with 0.27 s.g/cm^3

Temp. (^{0}C)	Al-SBA-15	
	DME Selectivity	FA Selectivity
200	0.76	0.24
250	0.95	0.05
300	1	0
350	1	0
400	1	0

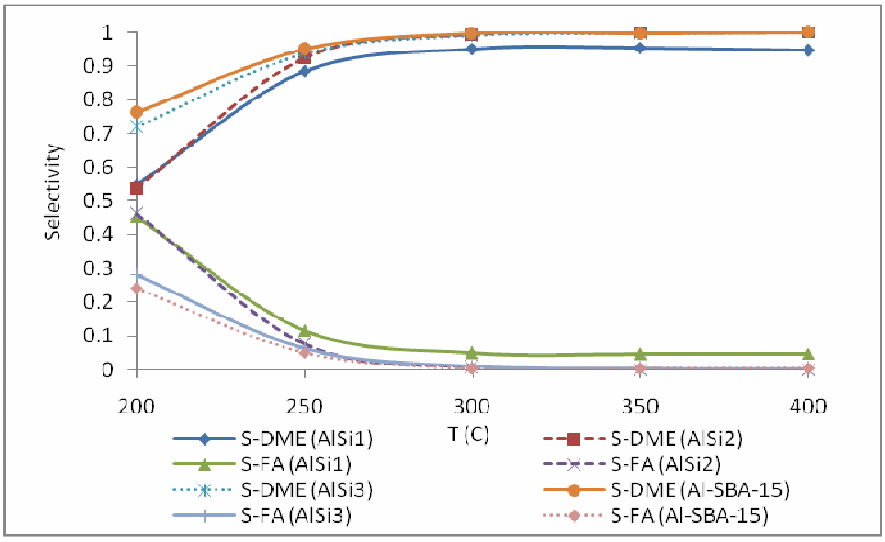


Figure 44. Selectivity of DME and Formaldehyde with Aluminum Silicates and Al-SBA-15 at 0.27 s.g/cm^3.

Yield values of DME and formaldehyde calculated from equation (8,9) are tabulated in Table 14 and Table 15. It can be seen from Fig.45. that yield of DME for both AlSi1 and AlSi2 increased with increasing temperature due to the increase in conversion and selectivity profiles (Fig.41 and Fig.43).

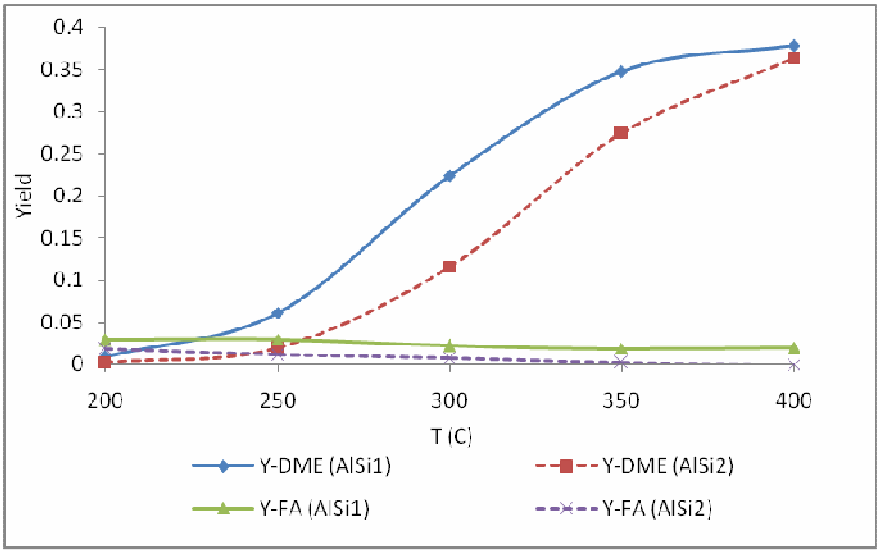


Figure 45. Yield of DME and Formaldehyde with AlSi1 and AlSi2 at 0.136 s.g/cm^3

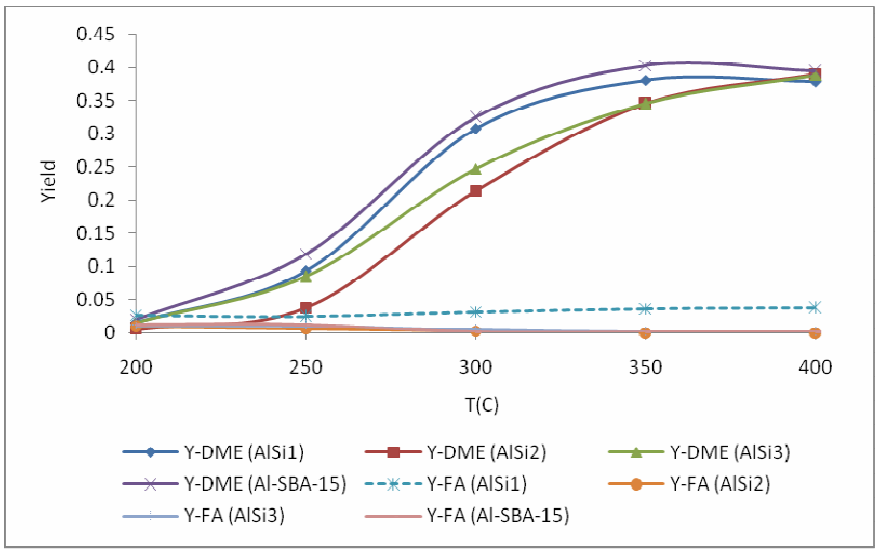


Figure 46. Yield of DME and Formaldehyde with Aluminum Silicates and Al-SBA-15 at 0.27 s.g/cm^3

High DME yields were obtained at temperatures higher than 300^{0}C (Table 13, 14). It reached a value of about 0.38 at 400^{0}C for AlSi1 at lower and higher

space times. For AlSi2 at 400^0C, DME yield had a value of 0.37 and 0.39 at space times of 0.136 and 0.27 s.g/cm^3. At lower temperatures (i.e. 250^0C), a DME yield of 0.02 and 0.04 were obtained respectively. The trend of DME yield of AlSi3 were very similar to those of AlSi2 after 300^0C. Higher DME yield was obtained with Al-SBA-15 compared to those of aluminum silicates at all the temperatures that were tested. However, formaldehyde yield was very low and almost stayed constant during the whole reaction not only for Al-SBA-15 but also for the aluminum silicates.

Table 14. Variation of DME and FA Yield Over Al-SBA-15 with 0.27 s.g/cm^3

Temp. (^{0}**C**)	Al-SBA-15	
	DME Yield	FA Yield
200	0.02	0.012
250	0.12	0.013
300	0.33	0
350	0.40	0
400	0.40	0

Table 15. Variation of DME and FA Yields Over Aluminum Silicates with Different Space Times.

Temp. (°C)	**DME Yield**						**FA Yield**					
	AlSi1		AlSi2		AlSi3		AlSi1		AlSi2		AlSi3	
	0.136 s.g/cm^3	0.27 s.g/cm^3	0.136 s.g/cm^3	0.27 s.g/cm^3	0.136 s.g/cm^3	0.27 s.g/cm^3	0.136 s.g/cm^3	0.27 s.g/cm^3	0.136 s.g/cm^3	0.27 s.g/cm^3	0.136 s.g/cm^3	0.27 s.g/cm^3
200	0.01	0.02	0.002	0.005	-	0.02	0.03	0.03	0.017	0.09	-	0.012
250	0.06	0.01	0.02	0.04	-	0.09	0.03	0.02	0.012	0.006	-	0.011
300	0.23	0.31	0.12	0.22	-	0.25	0.02	0.03	0.008	0.003	-	0.005
350	0.35	0.38	0.28	0.35	-	0.35	0.02	0.04	0.002	0	-	0.002
400	0.38	0.38	0.37	0.39	-	0.39	0.02	0.04	0	0	-	0.001

7.2.3. Results of Methanol Dehydration Reaction Over α and γ Forms of Aluminum Oxides

According to the activity tests performed with aluminum oxide based catalysts, methanol conversion was plotted at 0.136 s.g/cm^3 space time at temperatures ranging between 200 and 400^{0}C as shown in Fig.47. Also, methanol conversion variations are tabulated in Table 16.

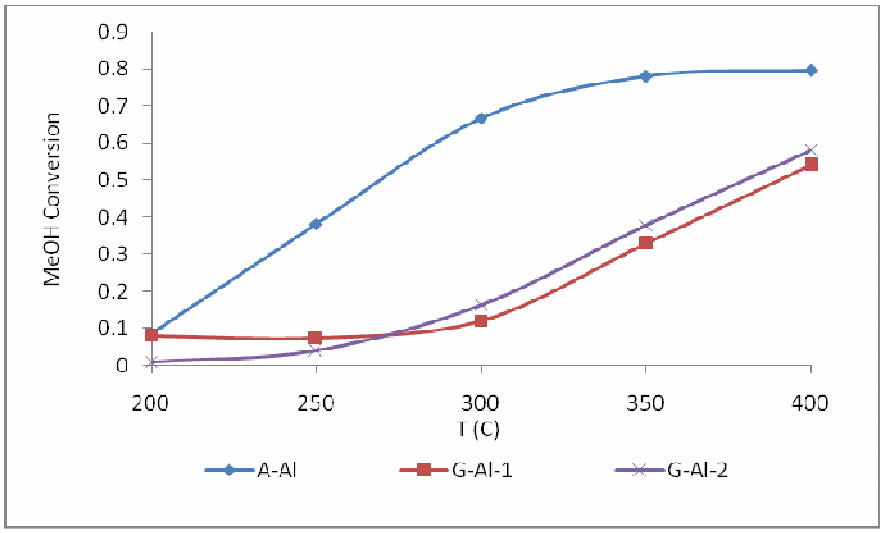


Figure 47. Conversion of Methanol over α and γ Forms of Aluminum Oxides at 0.136 s.g/cm^3.

Higher catalytic activity was obtained with α-Al which was obtained from Toyo Engineering in Japan. Although α-Al has slightly lower surface area than that of γ forms of aluminum oxides, better catalytic activity was obtained right away from 200^{0}C through to 400^{0}C. This was attributed to the high Bronsted acidity and also high pore diameter of this catalyst than that of the other γ forms. Methanol could easily diffuse into the pores of α-Al without much diffusion resistance.

Table 16. Variation of Methanol Conversion over α and γ Forms of aluminum oxides with Different Space Times.

	MeOH Conversion									
Temp. (°C)	200		250		300		350		400	
τ s.g/cm^3	0.136	0.27	0.136	0.27	0.136	0.27	0.136	0.27	0.136	0.27
α-Al	0.09	0.11	0.38	0.52	0.67	0.76	0.78	0.82	0.79	0.81
γ-Al-1	0.08	0.03	0.07	0.05	0.12	0.19	0.33	0.52	0.54	0.73
γ-Al-2	0.01	0.04	0.04	0.08	0.16	0.24	0.38	0.59	0.58	0.77
γ-Al-3	-	0.02	-	0.04	-	0.11	-	0.54	-	0.76

This α-Al catalysts' activity enhanced with increasing temperature until 350^{0}C and it reached almost equilibrium conversion at that temperature with a conversion value of 0.79. While catalytic conversion of γ forms of aluminum oxides was negligible, almost 40 percent of methanol converted to the products with α-Al at 250^{0}C. At 400^{0}C, the conversion values of γ-Al-1 and γ-Al-2 reached 0.54 and 0.58 respectively. On the other hand, tests performed at 0.27 s.g/cm^3 showed that γ forms of aluminum oxides (γ-Al-1, γ-Al-2 and γ-Al-3) caught α-Al at the final test temperature as shown in Fig.48.

Among γ forms of aluminum oxides, γ-Al-2 showed better performance than γ-Al-1 and γ-Al-3. This was mainly due to the higher surface area of this catalyst. γ-Al-1 showed better performance than γ-Al-3 between 250 and 350^{0}C but after this temperature, the activity of γ-Al-3 slightly improved. However, they showed similar performance at 400^{0}C.

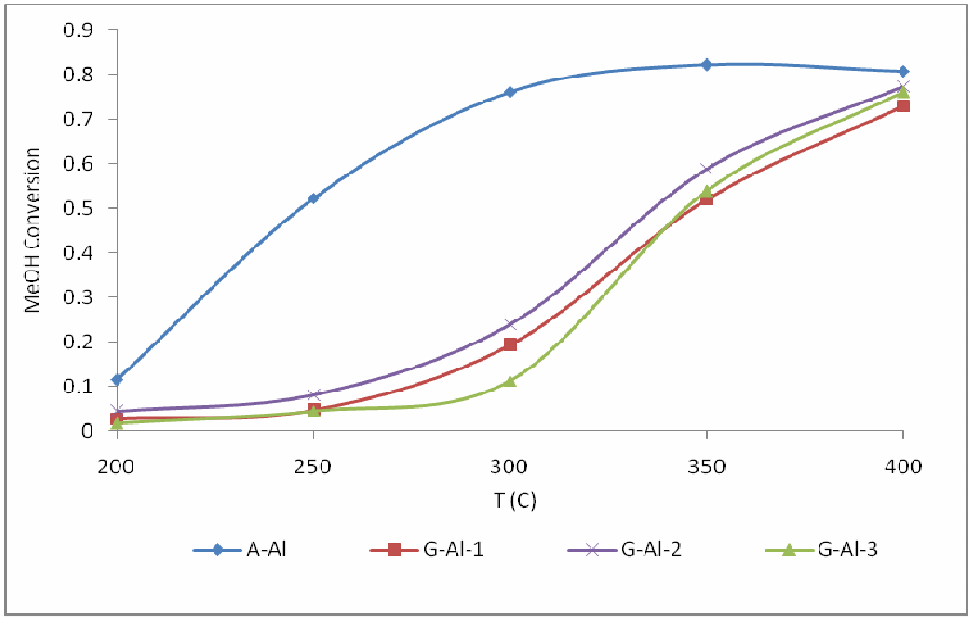


Figure 48. Conversion of Methanol over α and γ Forms of Aluminum Oxides at 0.27 s.g/cm^3.

According to the calculation of selectivity of DME and formaldehyde, the results are plotted in Fig.49 and Fig.50 and tabulated in Table 17 at 0.136 and 0.27 s.g/cm^3, respectively. The highest DME selectivity was obtained with γ-Al-2 at 0.136 s.g/cm^3 at 300^{0}C. But at lower temperatures such as 200 and 250^{0}C, DME selectivity was much higher with α-Al than the other γ forms. This is also due to the high Bronsted acidity of this catalyst. The DME selectivity of γ-Al-1 followed a lower trend till 350^{0}C but after that temperature it reached the value that was obtained for α-Al.

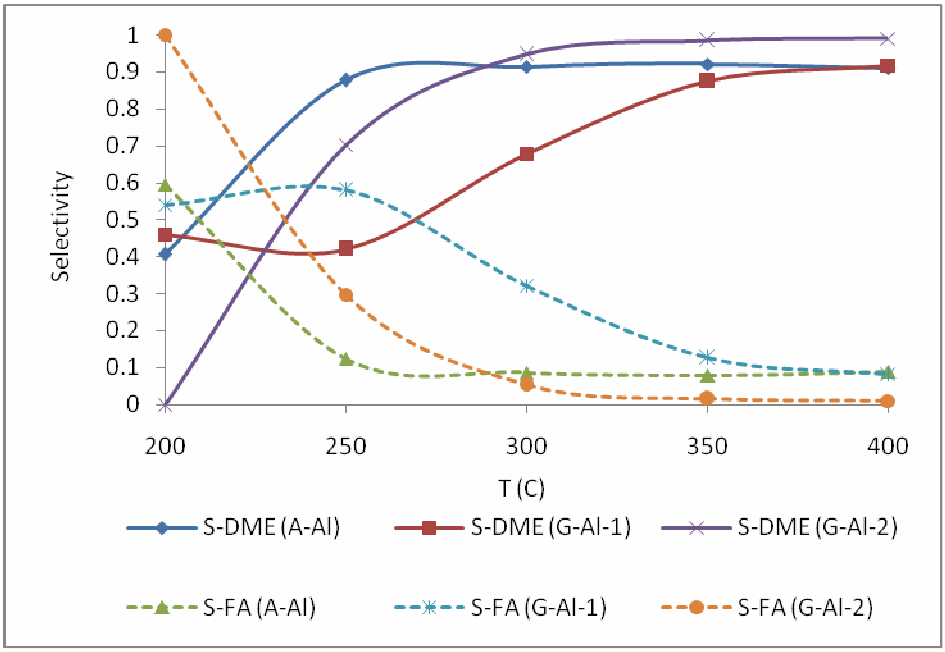


Figure 49. Selectivity of DME and Formaldehyde with α and γ Forms of Aluminum Oxides at 0.136 s.g/cm^3.

Table 17. Variation of DME Selectivity over α and γ Forms of Aluminum Oxides with Different Space Times

	DME Selectivity									
Temp. (°C)	200		250		300		350		400	
τ s.g/cm^3	0.136	0.27	0.136	0.27	0.136	0.27	0.136	0.27	0.136	0.27
α-Al	0.41	0.56	0.88	0.89	0.91	0.92	0.92	0.92	0.91	0.90
γ-Al-1	0.46	0	0.42	0.45	0.68	0.89	0.87	0.95	0.92	0.96
γ-Al-2	0	0.04	0.70	0.58	0.95	0.86	0.98	0.93	0.99	0.95
γ-Al-3	-	0	-	0.70	-	0.91	-	0.99	-	0.99

At 0.27 s.g/cm^3, different from 0.136 s.g/cm^3, DME selectivities of all aluminum oxides approached to each other after 300^{0}C.

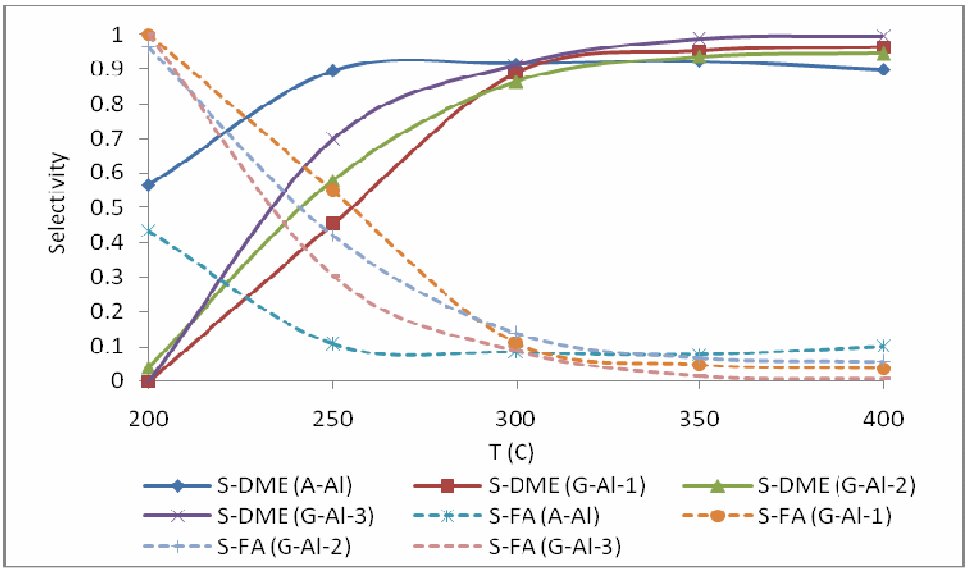


Figure 50. Selectivity of DME and Formaldehyde with α and γ Forms of Aluminum Oxides at 0.27 s.g/cm^3

Among formaldehyde selectivities as shown in Fig.49 and Fig.50, γ-Al-2 had higher formaldehyde selectivity at lower temperatures for both space times. Since formaldehyde is the main by-product; the lower the formaldehyde selectivity, the more the formation of DME. In other words, obtaining a lower formaldehyde selectivity during the whole reaction period enhanced DME yield, and gave a sign for obtaining the most suitable catalyst for methanol dehydration reaction. α-Al showed the lowest formaldehyde selectivity at the very beginning of the reactions and the selectivity further decreased with increasing temperature, reaching a value of about 0.1 after 300^{0}C. The same trend was observed for the other catalysts but the selectivities were much higher at the beginning especially with 0.27 s.g/cm^3.

Table 18. Variation of FA Selectivity over α and γ Forms of Aluminum Oxides with Different Space Times

	FA Selectivity									
Temp. (°C)	200		250		300		350		400	
τ s.g/cm^3	0.136	0.27	0.136	0.27	0.136	0.27	0.136	0.27	0.136	0.27
α-Al	0.59	0.43	0.12	0.11	0.09	0.08	0.08	0.08	0.09	0.10
γ-Al-1	0.54	1	0.58	0.55	0.32	0.11	0.13	0.05	0.08	0.04
γ-Al-2	1	0.96	0.30	0.42	0.05	0.14	0.02	0.07	0.01	0.05
γ-Al-3	-	0.93	-	0.48	-	0.10	-	0.01	-	0.01

Yields of DME and formaldehyde were calculated according to the conversion and selectivity results. Related with the results of conversion and selectivity, yields of DME increased with increasing temperature as shown in Fig.51 and Fig.52. Variation of DME and formaldehyde yield over α and γ forms of aluminum oxides with different space times are presented in Table 19 and 20.

DME yields were very high with α-Al compared to the other γ forms of aluminum oxides. Besides, DME yields came closer to each other with higher space time. Formaldehyde yields were very low at both lower and higher temperatures.

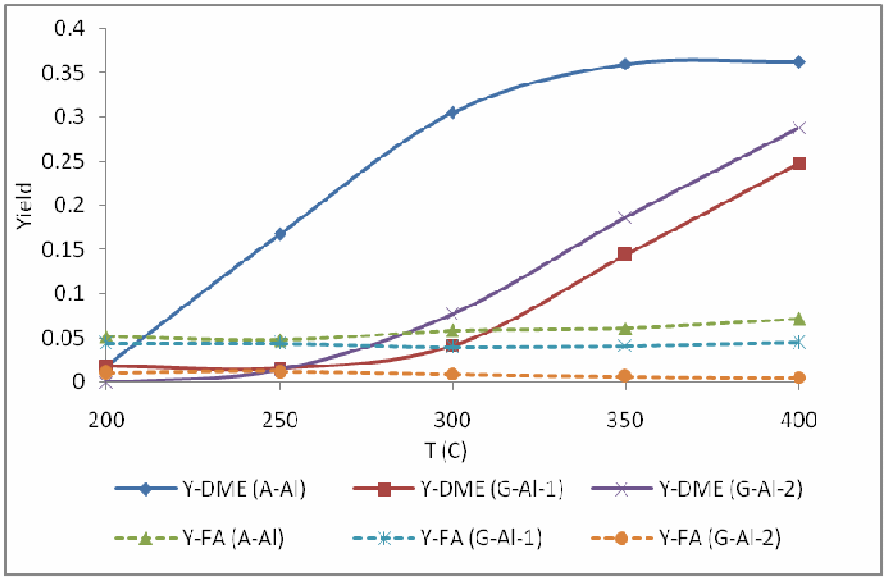


Figure 51. Yield of DME and Formaldehyde with α and γ Forms of Aluminum Oxides at 0.136 s.g/cm^3

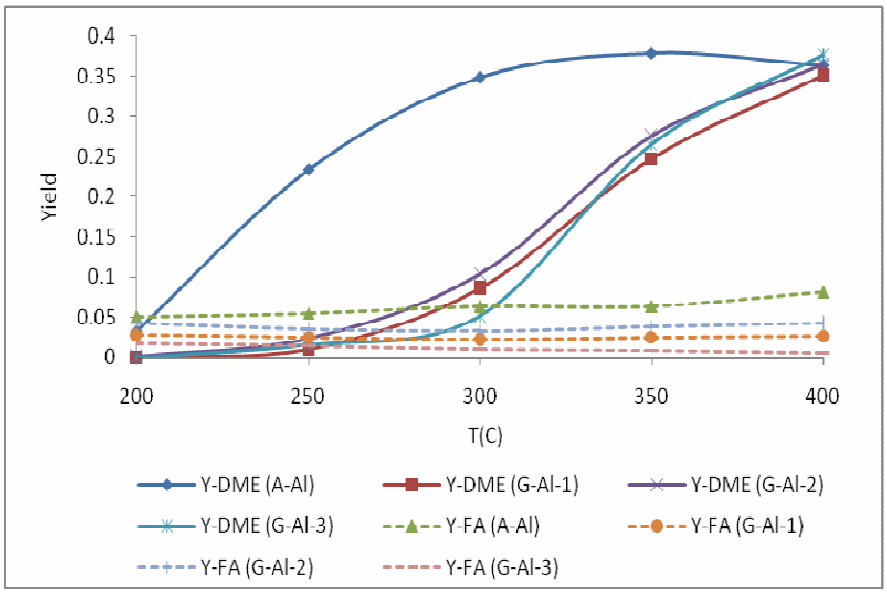


Figure 52. Yield of DME and Formaldehyde with α and γ Forms of Aluminum Oxides at 0.27 s.g/cm^3

Table 19. Variation of DME Yield over α and γ Forms of Aluminum Oxides with Different Space Times

	DME Yield									
Temp. (°C)	200		250		300		350		400	
τ s.g/cm^3	0.136	0.27	0.136	0.27	0.136	0.27	0.136	0.27	0.136	0.27
α-Al	0.02	0.03	0.17	0.24	0.3	0.35	0.36	0.38	0.36	0.37
γ-Al-1	0.02	0	0.02	0.01	0.04	0.09	0.15	0.25	0.25	0.35
γ-Al-2	0	0.001	0.02	0.03	0.08	0.1	0.19	0.28	0.29	0.37
γ-Al-3	-	0	-	0.02	-	0.05	-	0.27	-	0.38

Table 20. Variation of FA Yield over α and γ Forms of Aluminum Oxides with Different Space Times

	FA Yield									
Temp. (°C)	200		250		300		350		400	
τ s.g/cm^3	0.136	0.27	0.136	0.27	0.136	0.27	0.136	0.27	0.136	0.27
α-Al	0.05	0.05	0.05	0.05	0.06	0.06	0.06	0.06	0.07	0.08
γ-Al-1	0.04	0.03	0.04	0.02	0.04	0.02	0.04	0.02	0.04	0.03
γ-Al-2	0.01	0.04	0.01	0.03	0.01	0.03	0.006	0.04	0.005	0.04
γ-Al-3	-	0.02	-	0.01	-	0.01	-	0.01	-	0.01

In addition to these, the best catalytic activity among synthesized aluminum silicates was compared to those of the commercial aluminum oxides (Fig.53). The best activity was obtained with AlSi1 and α-Al among aluminum silicates and aluminum oxides respectively. From Fig.53, it can be seen that the activity of α-Al was much higher than that of AlSi1 at temperatures between 200

and 300^{0}C. Both of them almost reached an equilibrium conversion of about 0.8 after 350^{0}C.

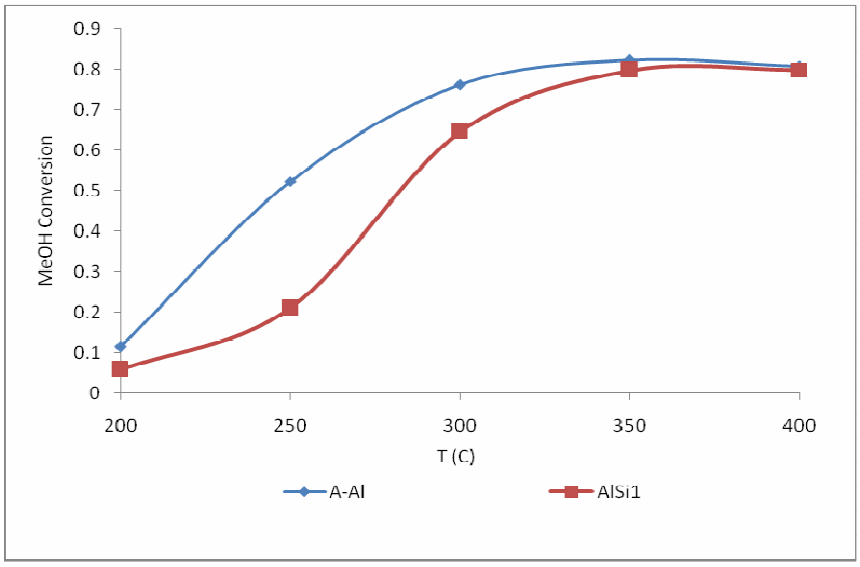


Figure 53. Conversion of Methanol over A-Al and AlSi1 at 0.27 s.g/cm^3.

7.2.4. Results of Methanol Dehydration Reaction over Nafion Catalysts

Activity tests of Nafion based catalysts were performed with the conditions given below in Table 21. In these experiments, 0.2, 0.5 and 1 g. (Appendix B.3) of catalysts were packed into the reactor with the same experimental conditions except temperature. In the vapor phase methanol dehydration reaction, Nafion type catalysts showed activity in the temperature range of 120-220^{0}C. In order to understand the effect of water on dehydration reaction of methanol, a methanol-water mixture was prepared by a methanol water ratio of 1 to 5 (20%) by volume, respectively. Reactions of methanol-water mixture were also tested with Nafion NR-50 and the results were compared with the reactions that were performed with pure methanol.

Table 21. Experimental Conditions for Nafion Catalysts

Catalyst	Amount (g)	Feed Flow Rate (MeOH) (mL/min)	He Flow Rate (mL/min)	Total Flow Rate (mL/min)	y_{MetOH}	τ (space time)	Reaction Temp. (^{0}C)
Nafion SAC-13	0.2	22	22.2	44.2	0.5	0.27	120-220
	0.5	22	22.2	44.2	0.5	0.68	120-220
	1	22	22.2	44.2	0.5	1.36	120-220
Nafion NR-50	0.2	22	22.2	44.2	0.5	0.27	120-220
	0.5	22	22.2	44.2	0.5	0.68	120-220
	1	22	22.2	44.2	0.5	1.36	120-220
Nafion NR-50 (with 20% water)	0.2	22 (with H_2O)	22.2	44.2	0.46	0.27	120-220
	0.5	22 (with H_2O)	22.2	44.2	0.46	0.68	120-220
	1	22 (with H_2O)	22.2	44.2	0.46	1.36	120-220

Conversion of methanol over Nafion SAC-13, Nafion NR-50 catalysts at a space time of 0.27 s.g/cm^3 is plotted in Fig.54. Also, results of conversion at different space times are presented in Table 22. Methanol converted to the main product of DME with increasing temperature and the main by-product was formaldehyde. At lower temperatures, conversion values of each were very low. The conversion values were under 0.1 at 150^{0}C. After about 165^{0}C, SAC-13 had higher conversion rates than the others. At 220^{0}C, SAC-13 reached a conversion value of 0.26. The addition of water in feed stream retarded methanol conversion considerably. This was thought to be mainly due to the strong adsorption of water on the active sites which caused a blocking effect for the adsorption of alcohol.

Table 22. Variation of Methanol Conversion over Nafion Catalysts with Different Space Times.

	MeOH Conversion														
Temp. (°C)	120			150			180			200			220		
τ s.g/cm^3	0.27	0.68	1.36	0.27	0.68	1.36	0.27	0.68	1.36	0.27	0.68	1.36	0.27	0.68	1.36
SAC-13	0.03	0.03	0.02	0.03	0.08	0.12	0.15	0.34	0.70	0.26	0.63	0.82	0.26	0.60	0.76
NR-50	0.03	0.02	0.07	0.06	0.06	0.13	0.10	0.14	0.24	0.16	0.20	0.40	0.23	0.29	0.44
NR-50 (with 20% water)	0.004	0.008	0.004	0.023	0.036	0.03	0.06	0.06	0.10	0.12	0.12	0.11	0.14	0.15	0.21

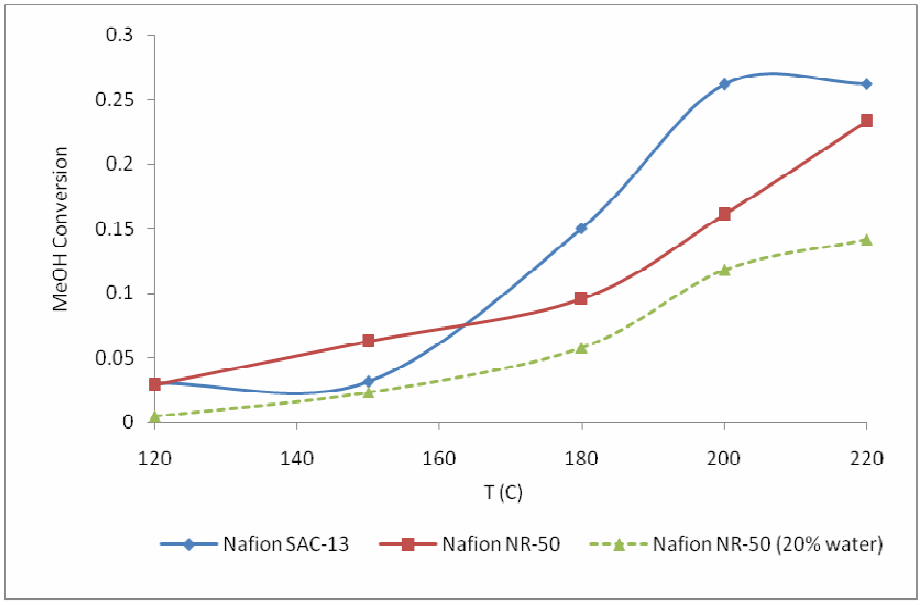


Figure 54. Conversion of Methanol over Nafion Catalysts at 0.27 s.g/cm^3.

In addition, activity tests of Nafion based catalysts were also performed with 0.5 g of catalyst at a space time of 0.68 s.g/cm^3 in order to see the variation of the results with the change in catalyst loading. At lower temperatures, the catalytic activities of SAC-13 and NR-50 showed similar patterns. However, methanol conversion at 180^{0}C with SAC-13 that reached more than twice the value of NR-50 started to separate from that temperature through to the final test temperature of 220^{0}C (Fig.55). Nafion SAC-13 showed much higher activity in DME synthesis. While converted percentage of methanol was 20% at 200^{0}C with NR-50, 63% of methanol conversion was obtained with SAC-13 at the same temperature. This is mainly due to the much higher surface area of this catalyst as compared to the surface area of NR-50. Also, the contribution of Bronsted acidity of SAC-13, according to the pyridine adsorption analysis, enhanced its catalytic activity. After 200^{0}C, SAC-13 showed a tendency to be stable against increasing temperature.

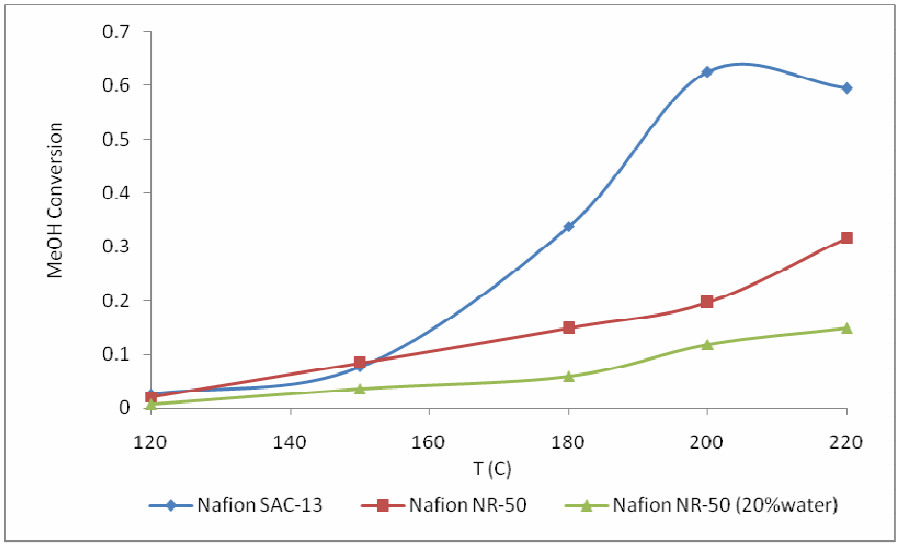


Figure 55. Conversion of Methanol over Nafion Based Catalysts at 0.68 s.g/cm^3.

In addition to the mentioned tests that were conducted at two different space times, all Nafion based catalysts were also tested at a space time of 1.36 s.g/cm^3. As shown in Fig.56 that SAC-13 reached a maximum conversion value of 0.82 at 200^{0}C, while NR-50 had a value of only 0.40. It was also found that water addition in feed stream had negative effects for the catalytic activity o2f NR-50. In every catalyst loading that were tested, NR-50 with water in feed stream could only reach a value of about 0.20 and didn't give the expected reaction with different catalyst loading.

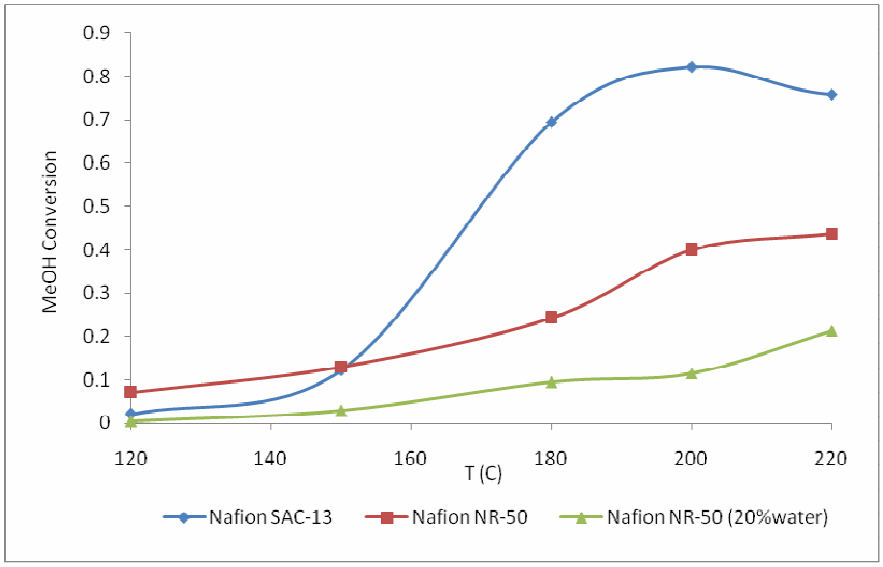


Figure 56. Conversion of Methanol over Nafion Based Catalysts at 1.36 s.g/cm^3

Moreover, SAC-13 was tested at high temperatures and the reactions were carried out with 1 g. of this catalyst from the temperature of 120 to 300 ^{0}C (Fig.57). Since Nafion based catalysts showed activity at relatively lower temparatures, the unexpected higher catalytic activity of SAC-13 even at the temperature of 300^{0}C proved that this catalyst is very suitable not only at lower temperatures but also at the higher ones for the vapor phase methanol dehydration reactions. Also, no coke formation was observed after unloading the catalyst from the reactor.

Selectivities of the products for Nafion based catalysts at 0.27 s.g/cm^3 are presented in Fig.58. Selectivity results are also presented in Table 23. High selectivities of SAC-13 and NR-50 (with water) were obtained after 150^{0}C and reached 0.92 and 0.87 for SAC-13 and NR-50 (with water), respectively. Surprisingly, the highest selectivity was obtained at 0.27 s.g/cm^3 by adding water into the feed stream with the catalyst of NR-50. Although water retarded methanol conversion, it enhanced DME selectivity. By-product selectivity was high at lower temperatures, then it decreased as methanol was converted to the main product of

DME. The lowest selectivity of Formaldehyde value was obtained at 220^{0}C with water tested NR-50.

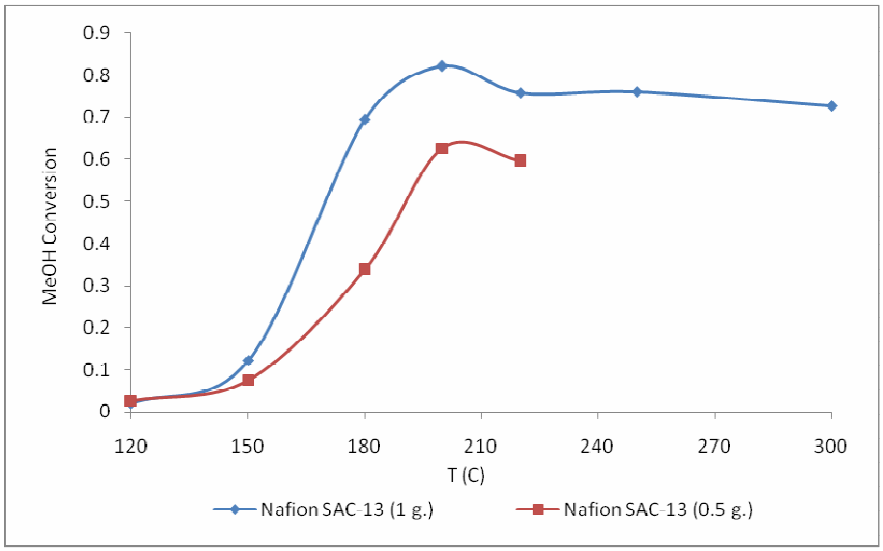


Figure 57. Conversion of Methanol over Nafion SAC-13 at Different Catalyst Loading.

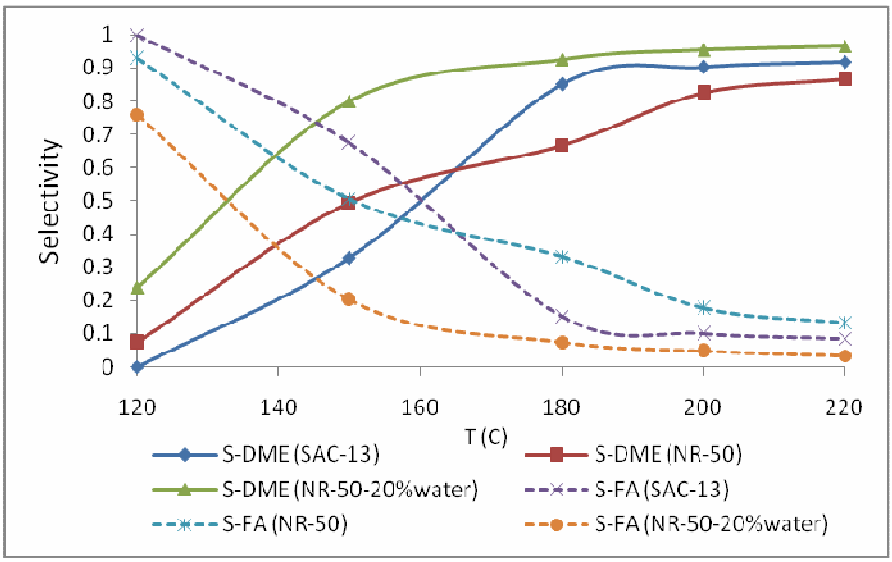


Figure 58. Selectivity of DME and Formaldehyde with Nafion Based Catalysts at 0.27 s.g/cm^3.

Table 23. Variation of DME and Formaldehyde Selectivity over Nafion Catalysts with Different Space Times.

	DME Selectivity									**FA Selectivity**								
	SAC-13			NR-50			NR-50 (with 20% water)			SAC-13			NR-50			NR-50 (with 20% water)		
Temp. (°C) / **τ s.g/cm³**	0.27	0.68	1.36	0.27	0.68	1.36	0.27	0.68	1.36	0.27	0.68	1.36	0.27	0.68	1.36	0.27	0.68	1.36
120	0	0.07	0.7	0.07	0.68	0.92	0.24	0.20	0	1	0.93	0.28	0.93	0.32	0.07	0.76	0.80	1
150	0.33	0.65	0.96	0.49	0.93	0.95	0.8	0.74	0.84	0.67	0.35	0.04	0.51	0.07	0.05	0.20	0.26	0.16
180	0.85	0.92	1	0.67	0.95	0.98	0.93	0.90	0.92	0.15	0.15	0	0.33	0.005	0.02	0.07	0.10	0.08
200	0.90	0.95	1	0.82	0.97	0.99	0.95	0.96	0.95	0.10	0.06	0	0.18	0.03	0.008	0.05	0.04	0.05
220	0.92	0.96	1	0.87	0.98	0.99	0.97	0.98	0.98	0.08	0.05	0	0.13	0.02	0.006	0.03	0.02	0.02

Although, SAC-13 showed better catalytic activity at the space time of 0.68 s.g/cm^3 than that of NR-50 that were tested with pure methanol and water-methanol mixture in feed stream, it couldn't show similar performance for obtaining DME in selectivity profiles comparing with NR-50 at lower temperatures (Fig.59). Nevertheless, after about 190^{0}C, DME selectivities reached about 1 which meant DME was the only product at these temperatures. Again, formaldehyde selectivities decreased with increasing temperature. Formaldehyde selectivity of SAC-13 was higher than that of the others at the beginning of the reaction but it decreased with the others till 200^{0}C. At that temperature, formaldehyde selectivities remained constant near zero.

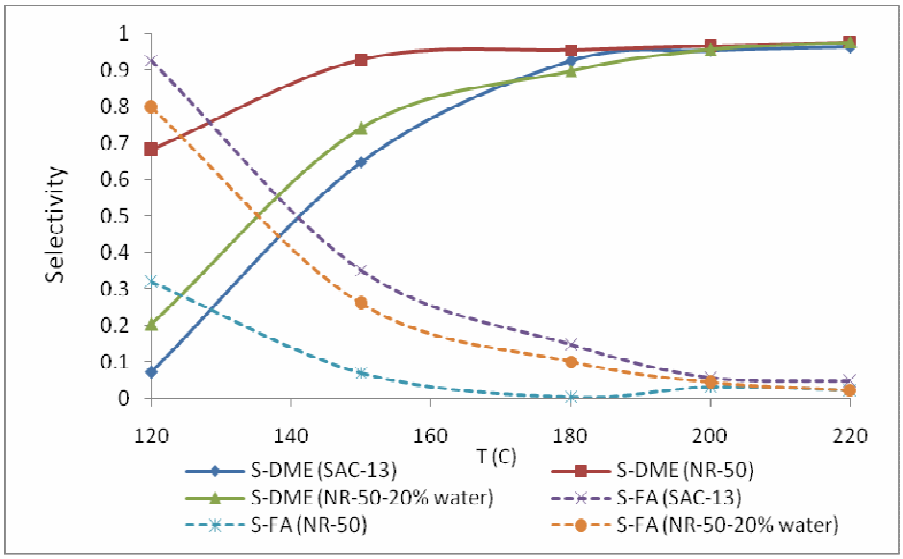


Figure 59. Selectivity of DME and Formaldehyde with Nafion Catalysts at 0.68 s.g/cm^3

Yields of Nafion type catalysts at different space times are presented in Table 24 and plotted at 0.27 s.g/cm^3 against temperature in Fig.60. Yields that were obtained with 0.2 g. of catalyst loading and at a space time of 0.27 s.g/cm^3 were very low due to the low conversion values. Especially at the temperatures

between 120 and 160, the yields were almost negligible. But after 160^0C, DME yield difference between SAC-13 and NR-50 was significant.

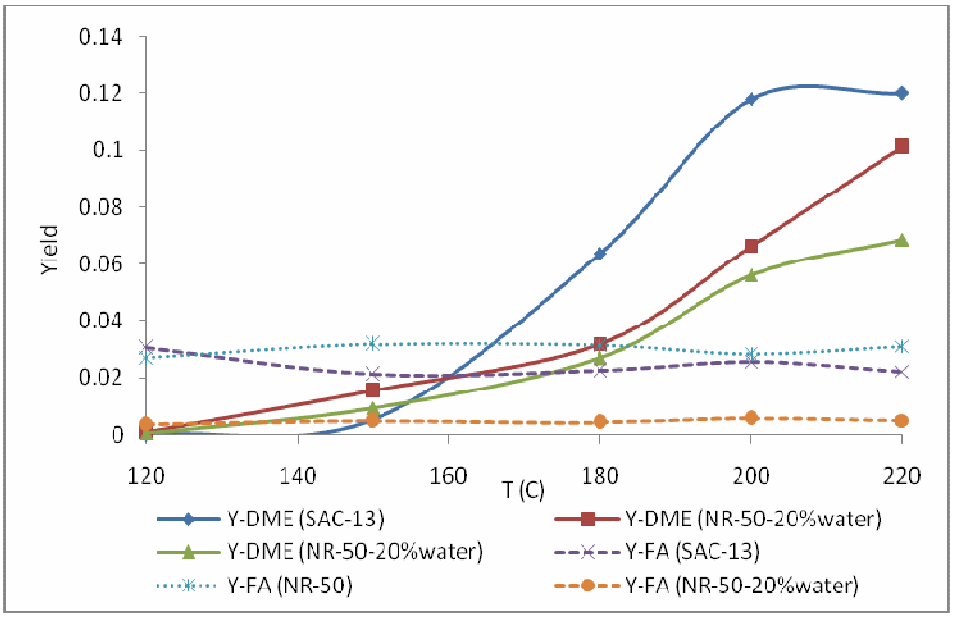


Figure 60. Yield of DME and Formaldehyde with Nafion Based Catalysts at 0.27 s.g/cm^3

Table 24. Variation of DME and Formaldehyde Yield over Nafion Catalysts with Different Space Times.

	DME Yield									**FA Yield**								
	SAC-13			NR-50			NR-50 (with 20% water)			SAC-13			NR-50			NR-50 (with 20% water)		
Temp. (°C) / **τ** / **s.g/cm^3**	0.27	0.68	1.36	0.27	0.68	1.36	0.27	0.68	1.36	0.27	0.68	1.36	0.27	0.68	1.36	0.27	0.68	1.36
120	0	0.001	0.008	0.001	0.005	0.032	0	0.001	0	0.03	0.025	0.006	0.027	0.007	0.005	0.003	0.006	0.004
150	0.005	0.03	0.06	0.016	0.04	0.06	0.01	0.02	0.012	0.021	0.03	0.005	0.032	0.006	0.006	0.005	0.009	0.004
180	0.07	0.16	0.35	0.032	0.07	0.12	0.027	0.03	0.05	0.02	0.05	0	0.03	0.001	0.006	0.004	0.006	0.008
200	0.12	0.30	0.41	0.07	0.10	0.20	0.06	0.06	0.05	0.026	0.04	0	0.03	0.007	0.003	0.005	0.005	0.006
220	0.12	0.29	0.38	0.10	0.16	0.215	0.07	0.08	0.11	0.02	0.03	0	0.031	0.007	0.002	0.005	0.004	0.005

It can be seen from Fig.61 that DME yields increased at 0.68 s.g/cm^3 than that of 0.27 s.g/cm^3 because of the increase in catalyst loading. As DME yields increased, by product formation yields decreased. If formaldehyde yields are compared with those of 0.27 s.g/cm^3, high decreases at formaldehyde yields were obtained for higher catalyst loadings at lower temperatures. On the other hand, when the temperature increased, similar formaldehyde yields were obtained with all of the space times.

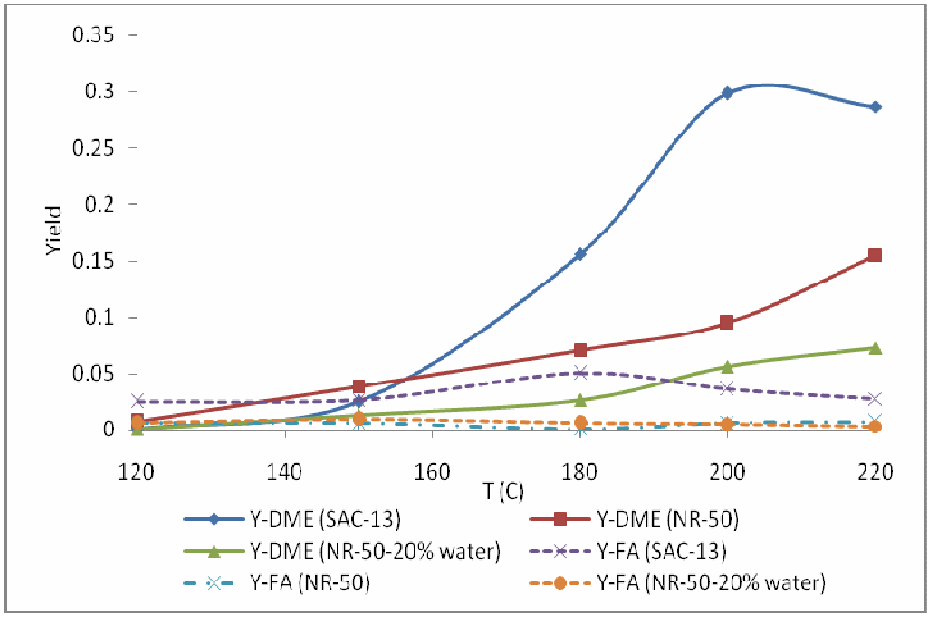


Figure 61. Yield of DME and Formaldehyde with Nafion Based Catalysts at 0.68 s.g/cm^3

CHAPTER 8

CONCLUSION

In this work, methanol dehydration reaction was studied over different solid acid catalysts. For this purpose, three mesoporous aluminum silicate catalysts having different Al/Si ratios and different silica sources were prepared by direct hydrothermal synthesis method. Also, aluminum impregnation was achieved into a synthesized SBA-15 sample and tried in methanol dehydration reaction for the first time in the literature. In addition to this, different types of aluminum oxides, Nafion NR-50 and Nafion SAC-13 of two different Nafion catalysts that were obtained from commercial suppliers were tested. According to the results obtained and comments on these results in "Results and Discussion" part, the following conclusions were reached:

Following the reaction results; among the Nafion type catalysts tested in this work, Nafion SAC-13 showed better activity than that of Nafion NR-50 in DME synthesis from methanol. This was the case as Nafion SAC-13 has much higher surface area value. Due to their higher Bronsted acidity values, Nafion catalysts showed activity at lower temperatures (120-220^{0}C) than the mesoporous aluminum silicates (220-400^{0}C). However, the activities of aluminum silicates were quite stable even at temperatures as high as 400^{0}C. The analyses have shown that AlSi1 is the most active of all the aluminum silicates synthesized in both 0.136 and 0.27 s.g/cm^3 space time, with up to 80% methanol conversion in all temperatures tested. DME selectivity was also found to be significantly improved at higher temperatures for all the catalysts tested. It was concluded that due to the effects of acid strength and surface area values,

there is an optimum Al/Si ratio (about 0.09). Aluminum impregnation also affected the acidity of pure SBA-15. Similar activities with AlSi1 and better activity than that of other synthesized aluminum silicates proved that this Al-SBA-15 is very appropriate for DME synthesis in the temperature range of 200 to 400^0C. Also, higher DME selectivities were obtained even at lower temperatures. As to aluminum oxides, α-alumina was seen to be superior to others in γ forms in terms of conversion, selectivity and yield, especially at low temperatures. This was mainly due to the higher pore diameter of this compared to γ forms of aluminum oxides and also due to its higher Bronsted acidity.

Among synthesized and commercial catalysts that were tested at a common space time of 0.27 s.g/cm^3 and a temperature of 200^0C in this study, Nafion SAC-13 was found to be the most active one with a methanol conversion value of 0.26. Methanol conversion values were 0.06, 0.02, 0.04, 0.05, 0.16, 0.12 for AlSi1, AlSi2, AlSi3, Al-SBA-15, NR-50 and NR-50 (with water), respectively at the same conditions. Also, the two important performance factors of selectivity and yield values were much higher than that of the others.

For the future studies, Nafion SAC-13 will be appropriate for studying reactive distillation of methanol as its reasonable catalytic activity, even at the lower temperatures, is needed for this operation.

Because of the fast diminishing of our fossil fuel resources, the next era will undoubtedly not be the oil era. So, finding renewable energy sources and novel technologies are crucial for the next generation. Whatever the next era will be, alcohols will certainly play more important role in energy sector than they do nowadays.

REFERENCES

[1] Doğu, T., Varışlı, D., Alcohols as Alternates to Petroleum for Environmentally Clean Fuels and Petrochemicals, *Turkish Journal of Chemistry*, 2007, **31**, 551-567.

[2] Ogawa, T., Inoue, N., Shikada, T., Inokoshi, O., Direct Dimethyl Ether Synthesis, *Journal of Natural Gas Chemistry*, 2003, **12**, 219-227.

[3] Varisli, D., Dogu, T., Dogu, G., Ethylene and diethyl-ether production by dehydration reaction of ethanol over different heteropolyacid catalysts, *Chem. Eng. Sci.*, 2007, **62**, 5349-5352.

[4] Olah, G. A., Goeppert, A., Surya Prakash, G.K., Beyond Oil and Gas: The Methanol Economy, Wiley-VCH Verlag GmbH & Co. KGaA, 1st Ed., 2006, Weinheim.

[5] Reed, T.B., Lerner, R.M., Methanol: A varsatile Fuel for Immediate Use, *Science*, 1973, **182**, 1299.

[6] Specht, M., Staiss, F., Bandi, A., Weimer, T., Comparison of the Renewable Transportation Fuels, Liquid Hydrogen and Methanol, With Gasoline-Energetic and Economic Aspects, *Int. J. Hydrogen Energy,* 1998, **23**, 387-396.

[7] Song, J., Huang, Z., Qiao, X., Wang, W., Performance of a controllable premixed combustion Engine fueled with dimethyl ether, *Energy Conversion and Management*, 2004, **45**, 2223-2232.

[8] Semelsberger, T.A., Borup, R.L., Greene, H.L., Dimethyl ether (DME) as an alternative fuel, *Journal of Power Sources*, 2006, **156**, 497-511.

[9] Ogawa, T., Inoue, N., Shikada, T., Inokoshi, O., Ohno Y., Direct Dimethyl Ether synthesis from natural gas, *Studies in Surface Science and Catalysis*, 2004, **147**, 379-384.

[10] http://www.wikipedia.org, http://en.wikipedia.org/wiki/Dimethyl_ether, Last access Date: April 2008.

[11] Crookes, R.J., Bob-Manuel, K.D.H., RME or DME: A preferred alternative fuel option for future diesel engine operation, *Energy Conversion and Management*, 2007, **48**, 2971-2977.

[12] http://www.aboutdme.org, http://eficlient.kma.net/index.asp?bid=219, Last access date: May 2008.

[13] Xu, M., Lunsford, J.H., Goodman, D.W., Synthesis of dimethyl ether (DME) from methanol over solid-acid catalysts, *Applied Catalysis A: General*, 1997, **149**, 289-301.

[14] Ahlgren, S., Baky, A., Bernesson, S., Nordberg, A., Noren, O., Hansson, P.A., Future fuel supply systems for organic production based on Fischer-Tropsch diesel and dimethyl ether from on-farm-grown biomass, *Biosystem Engineering*, 2008, **99**, 145-155.

[15] Wang, L., Fang, D., Huang, X., Zhang, S., Qi, Y., Liu, Z., Influence of Reaction Conditions on Methanol Synthesis and WGS Reaction in the Syngas-to-DME Process*, Journal of Natural Gas Chemistry, 2006,* **15**, 38-44.

[16] Ramos, F.S., Duarte de Farias, A.M., Borges, L.E.P., Monteiro, J.L., Fraga, M.L., Sousa-Aguiar, E.F., Appel, L.G., Role of dehydration catalyst acid properties on one-step DME synthesis over physical mixtures, *Catalysis Today,* 2005, **101**, 39-44.

[17] Yaripour, F., Baghaei, F., Schmidt, I., Perregaard, J., Synthesis of dimethyl ether from methanol over aluminum phosphate and silica-titania catalysts, *Catalysis Communication*, 2005, **6**, 542-549.

[18] Fei, J., Hou, Z., Zhu, B., Lou, H., Zheng, X., Synthesis of dimethyl ether (DME) on modified HY zeolite and modified HY zeolite-supported Cu–Mn–Zn catalysts, *Applied Catalysis*, 2006, **304**, 49-54.

[19] Jiang, S., Hwang, Y.K., Jhung, S.H., Chang, J.S., Hwang, J.S., Cai, T., Park, S.E., Zeolite SUZ-4 as Selective Dehydration Catalyst for Methanol Conversion to Dimethyl Ether, *Chemistry Letters* ,2004, **33**, 1048-1049.

[20] Fu, Y., Hong, T., Chen, J., Auroux, A., Shen, J., Surface acidity and the dehydration of methanol to dimethyl ether, *Thermochimica Acta*, 2005, **434**, 22-26.

[21] Jun, K.W., Lee, H.S., Roh, H.S., Park, S.E., Catalytic Dehydration of Methanol to Dimethyl Ether (DME) over Solid-Acid Catalysts, *Bull. Korean Chem. Soc.,* 2002, **23**, 803-806.

[22] Kim, J.H., Park, M.J., Kim S.J., Joo, O.S., Jung, K.D., DME synthesis from synthesis gas on the admixed catalysts of $Cu/ZnO/Al_2O_3$ and ZSM-5, *Applied Catalysis*, 2004, **264**, 37-41.

[23] Ng, K.L., Chadwick D., Toseland, B.A., Kinetics and modelling of dimethyl ether synthesis from synthesis gas, *Chemical Engineering Science*, 1999, **54**, 3587-3592.

[24] Mao, D., Yang, W., Xia, J., Zhang, B., Lu, G., The direct synthesis of dimethyl ether from syngas over hybrid catalysts with sulfate-modified γ-alumina as methanol dehydration components, *Journal of Molecular Catalysis A: Chemical*, 2006, **250**, 138-144.

[25] Omata, K., Watanabe, Y., Umegaki, T., Ishiguro, G., Yamada M., Low pressure DME synthesis with Cu based hybrid catalysts using temperature gradient reactor, *Fuel*, 2002, **81**, 1605-1609.

[26] Kunpeng Sun, Weiwei Lu, Min Wang, Xianlun Xu, Low-temperature synthesis of DME from CO_2/H_2 over Pd-modified $CuO–ZnO–Al_2O_3–ZrO_2$/HZSM-5 catalysts, *Catalysis Communications*, 2004, **5**, 367-370.

[27] Sun, K., Lu, W., Qiu, F., Liu, S., Xu, X., Direct synthesis of DME over bifunctional catalyst: surface properties and catalytic performance, *Applied Catalysis*, 2003, **252**, 243-249.

[28] Moradi, G.R., Nosrati, S., Yaripor, F., Effect of the hybrid catalysts preparation method upon direct synthesis of dimethyl ether from synthesis gas, *Catalysis Communications*, 2007, **8**, 598-606.

[29] Erena, J., Garona, R., Arandes, J.M., Aguayo, A.T., Bilbao, J., Effect of operating conditions on the synthesis of dimethyl ether over a CuO-ZnO-Al_2O_3/NaHZSM-5 bifunctional catalyst, *Catalysis Today*, 2005, **107-108**, 467-473.

[30] Tan, Y., Xie, H., Cui, H., Han, Y., Zhong, B., Modification of Cu-based methanol synthesis catalyst for dimehyl ether synthesis from syngas in slurry phase, *Catalysis Today*, 2005, **104**, 25-29.

[31] Mao, D., Yang, W., Xia, J., Zhang, B., Song, Q., Chen, Q., Highly effective hybrid catalyst for the direct synthesis of dimethyl ether from syngas

with magnesium oxide-modified HZSM-5 as a dehydration component, *Journal of Catalysis,* 2005, **230**, 140-149.

[32] Shikada T., Ohno, Y., Ogawa, T., Ono, M., Mizuguchi, M., Tomura K., Fujimoto, K., Direct Synthesis of Dimethyl Ether form Synthesis Gas, *Studies in Surface Science and Catalysis,* 1998, **119**, 515-520.

[33] Diep, B.T., Thermodynamic Equilibrium Constants for the Methanol-Dimethyl Ether-Water System, *J. Chem. Eng. Data,* 1987, **32**, 330-333.

[34] Hayashi, H., Moffat, J.B., *J.Catal*, 1982, **77**, 478.

[35] Given, P.H., *J. Chem. Soc.*, 1943, 589.

[36] Øye, G., Sjoblom, J., Stocker, M., Synthesis, characterization and potential applications of new materials in the mesoporous range, *Advances in Colloid and Interface Science,* 2001, **89-90**, 439-466.

[37] Ciesla, U., Schüth, F., Ordered mesoporous materials, *Microporous and Mesoporous Materials*, 1999, **27**, 131-149.

[38] Vartuli, J.C., Roth, W.J., Degnan, T.F., Mesoporous Materials (M41S): From Discovery to Application, Dekker Encylopedia of Nanoscience and Nanotechnology, IMMS2006 Pre School Program Lecture Notes, China.

[39] Taguchi, A., Schüth, F., Ordered mesoporous materials in catalysis, *Microporous and Mesoporous Materials*, 2005, **77**, 1-45.

[40] Russo, P.A., Ribeiro Carrott, M.M.L., Carrott P.J.M., Effect of hydrothermal treatment on the structure, stability and acidity of Al containing MCM-41 and MCM-48 synthesised at room temperature, *Colloids and Surfaces A: Physicochem. Eng. Aspects*, 2007, **310**, 9-19.

(41) Khushalani, D., Kuperman, A., Ozin, G.A., Tanaka, K., Garces, J., Olken, M.M., Coombs, N., Metamorphic materials - restructuring siliceous mesoporous materials, *Adv. Mater.,* 1995, **7,** 842-846.

[42] Ribeiro Carrott, M.M.L., Galacho, C., Conceiçao, F.L., Carrott, P.J.M., Influence of the synthesis conditions on the pore structure and stability of MCM-41 materials containing aluminium or titanium, *Studies in Surface Science and Catalysis*, 2007, **160**, 567-574.

[43] Blanco, C., Pesquera, C., Gonzalez, F., Synthesis and Characterization of MCM-41 with Different Si/Al Molar Ratios and Different Silicon Sources, *Studies in Surface Science and Catalysis*, 2004, **154**, 432-438.

[44] Pasquale F. Fulvio, Pikus, S., Jaroniec, M., Tailoring properties of SBA-15 materials by controlling conditions of hydrothermal synthesis, *Journal of Materials Chemistry,* 2005, **287**, 717-720.

[45] Yu, C., Fan, J., Tian, B., Stucky, G.D., Zhao, D., Synthesis of Mesoporous Silica from Commercial Poly (ethylene oxide)/Poly (butylene oxide) Copolymers: Toward the Rational Design of Ordered Mesoporous Materials, *J. Phys. Chem. B.,* 2003, **107**, 13368-13375.

[46] Zhao, D., Feng, J., Huo, Q., Melosh, N., Fredrickson, G.H., Chmelka B.F., Stucky, G.D., Triblock Copolymer Syntheses of Mesoporous Silica with Periodic 50 to 300 Angstrom Pores, *Science,* 1998, **279**, 548-552.

[47] Kruk, M., Jaroniec, M., Ko, C.H., Ryoo, R., Characterization of the Porous Structure of SBA-15, *Chem. Mater.,* 2000, **12**, 1961-1968.

[48] Kumaran G.M., Garg, S., Soni, K., Kumar, M., Gupta, J.K., Sharma L.D., Rama Rao K.S, Dhar G.M., Synthesis and characterization of acidic properties of Al-SBA-15 materials with varying Si/Al ratios, *Microporous and Mesoporous Materials*, 2008, **114**, 103-109.

[49] Gomez-Cazalillaa, M., Merida-Robles J.M., Gurbanib, A., Rodriguez-Castellon, E., Jimenez-Lopeza, A., Characterization and acidic properties of Al-SBA-15 materials prepared by post-synthesis alumination of a low-cost ordered mesoporous silica, *Journal of Solid State Chemistry*, 2007, **180**, 1130-1140.

[50] Hu, W., Luo, Q., Su, Y., Chen, L., Yue, Y., Ye, C., Deng, F., Acid sites in mesoporous Al-SBA-15 material as revealed by solid-state NMR spectroscopy, *Microporous and Mesoporous Materials*, 2006, **92**, 22-30.

[51] Niemantsverdriet, J.W., Spectroscopy in Catalysis, Wiley-VCH Verlag GmbH & Co. KgaA, 3rd Ed., 2007, Weinheim.

[52] Wachs, I.E., Fitzpatrick, L.E., Characterization of Catalytic Materials, Manning Publications Co., 1992, Greenwich.

[53] Wikipedia the Free Encylopedia, http://en.wikipedia.org/wiki/Main_Page, http://en.wikipedia.org/wiki/Scanning_electron_microscope, Last Access Date: March 2008.

[54] Şener, C**.,** Synthesis and Characterization of Pd-MCM-Type Mesoporous Nanocomposite Materials, Master Thesis, METU, 2006.

[55] Wikipedia the Free Encylopedia, http://en.wikipedia.org/wiki/Main_Page, http://en.wikipedia.org/wiki/Nafion, Last Access Date: June 2008.

[56] Harmer M.A., Farneth W.E., Sun Q., High Surface Area Nafion† Resin/Silica Nanocomposites: A New Class of Solid Acid Catalyst**,** *J. Am. Chem. Soc.,* 1996, **118**, 7708-7715.

[57] Varisli D., Dogu T., Dogu G., Silicotungstic Acid Impregnated MCM-41-like Mesoporous Solid Acid Catalysts for Dehydration of Ethanol, *Ind. Eng. Chem.Res*,2008,**47(12)**,4071-40

APPENDIX A.1

EDS RESULTS

AlSi1

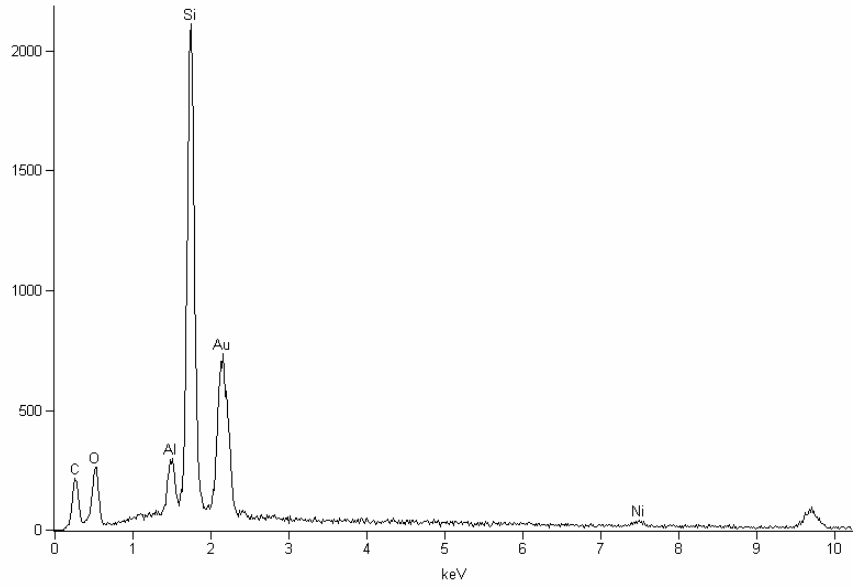


Figure 62. EDS of AlSi1

Element	*Weight Conc %*	*Atom Conc %*
Al	8.24	8.55
Si	91.76	91.45

AlSi2

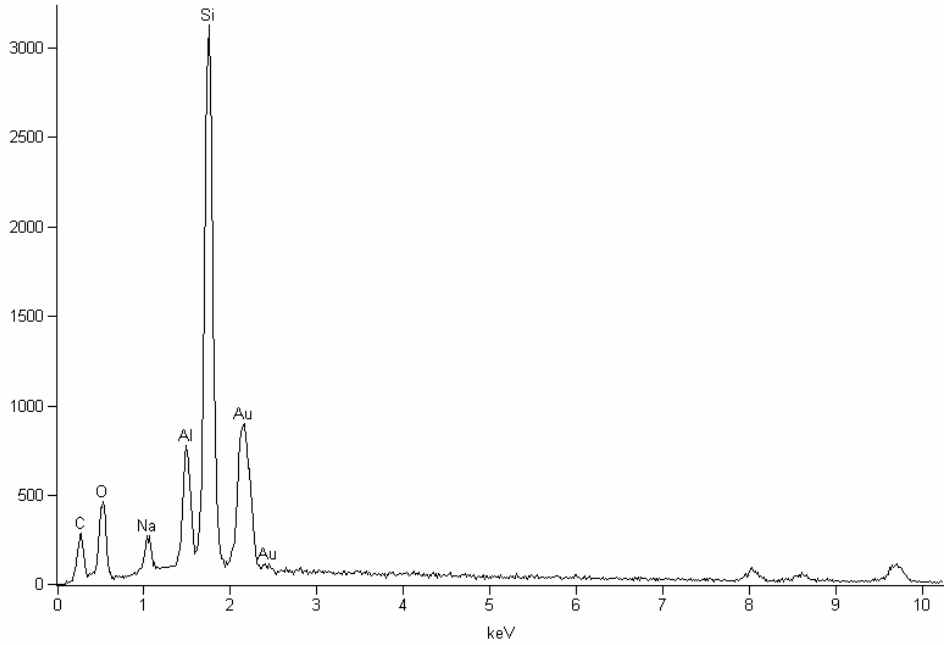


Figure 63. EDS of AlSi2

Element	*Weight Conc %*	*Atom Conc %*
Al	14.91	15.43
Si	85.09	84.57

AlSi3

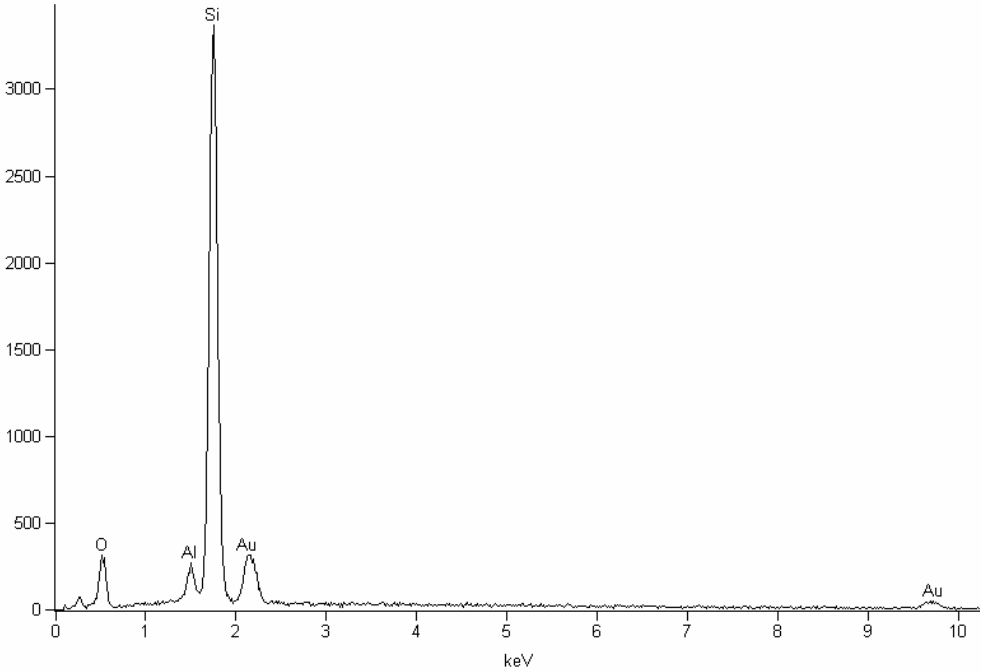


Figure 64. EDS of AlSi3

Element	*Weight Conc %*	*Atom Conc %*
Al	4.26	4.43
Si	95.74	95.57

Al-SBA-15

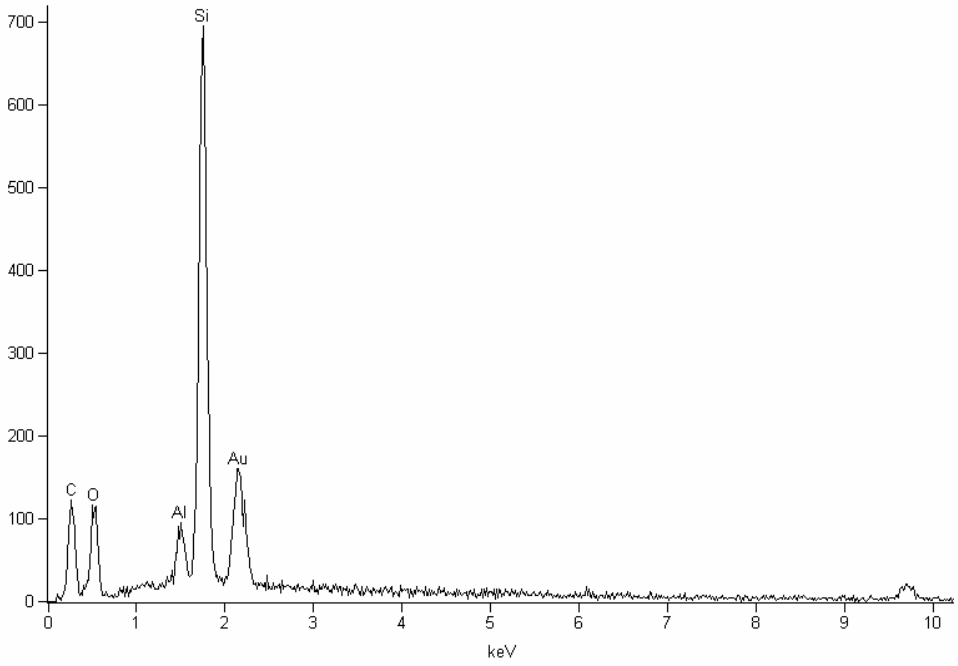


Figure 65. EDS of Al-SBA-15

Element	***Weight Conc %***	***Atom Conc %***
Al	8.87	9.20
Si	91.13	90.80

APPENDIX A.2

SEM IMAGES

SEM Images of AlSi1

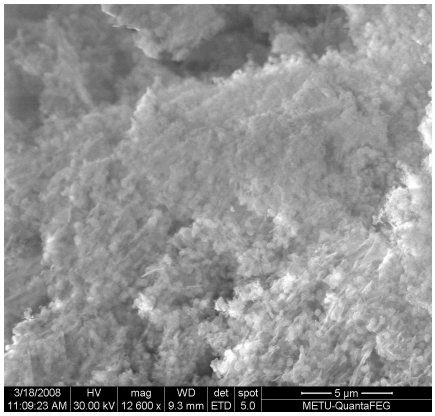


Figure 66. SEM Image of AlSi1 (a)

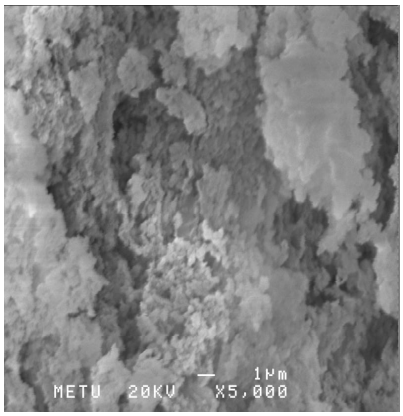


Figure 67. SEM Image of AlSi1 (b)

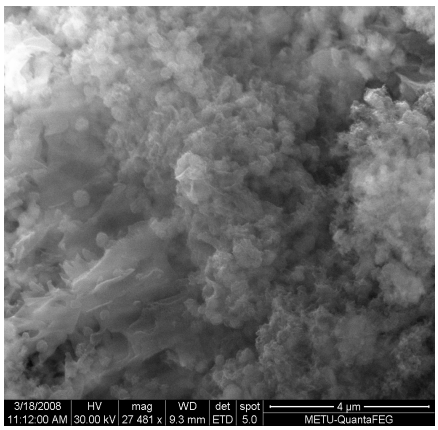


Figure 68. SEM Image of AlSi1 (c)

SEM Images of AlSi2

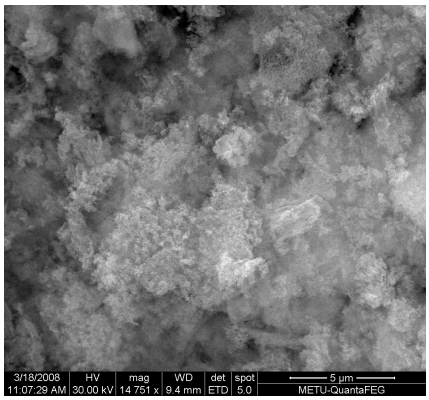


Figure 69. SEM Image of AlSi2 (a)

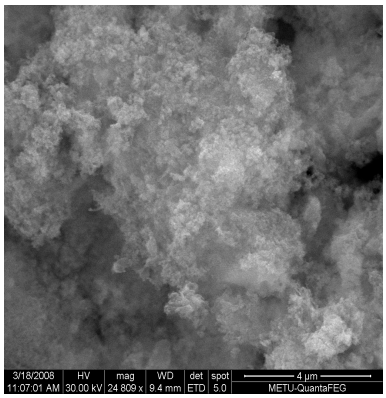


Figure 70. SEM Image of AlSi2 (b)

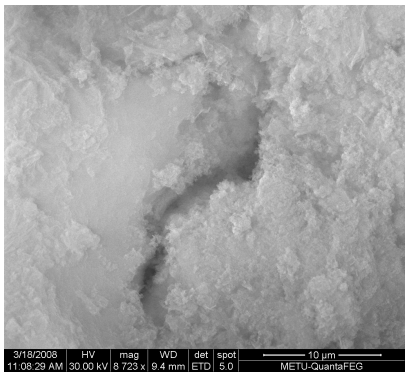


Figure 71. SEM Image of AlSi2 (c)

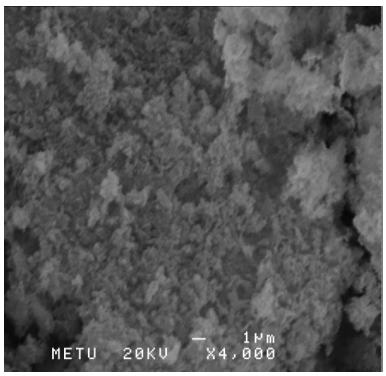


Figure 72. SEM Image of AlSi2 (d)

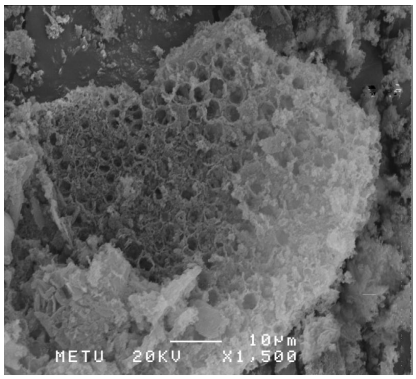


Figure 73. SEM Image of AlSi2 (e)

SEM Images of AlSi3

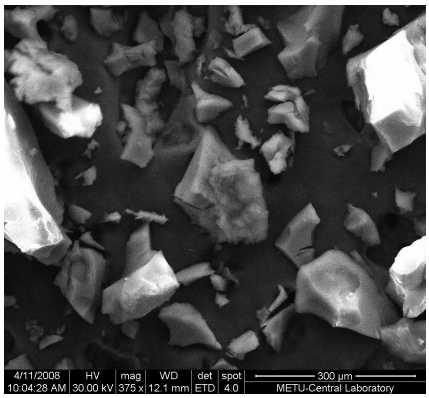


Figure 74. SEM Image of AlSi3 (a)

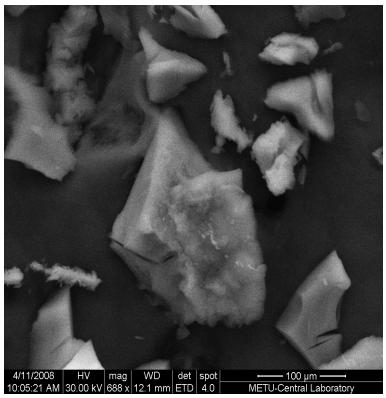


Figure 75. SEM Image of AlSi3 (b)

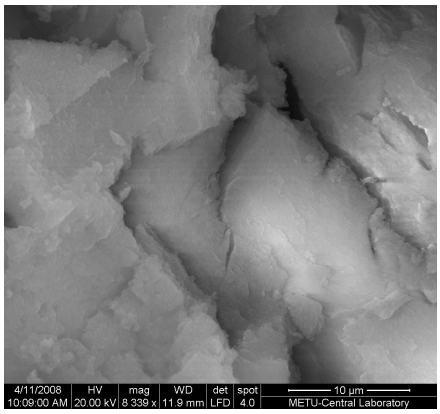


Figure 76. SEM Image of AlSi3 (c)

SEM Images of α-Al

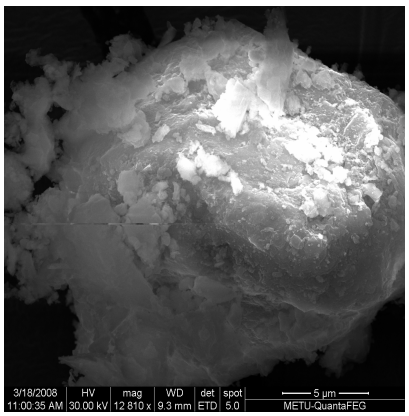


Figure 77. SEM Image of α-Al (a)

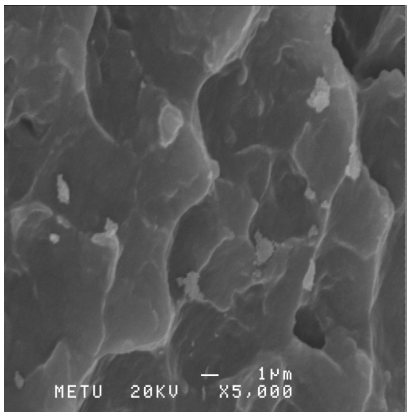


Figure 78. SEM Image of α-Al (b)

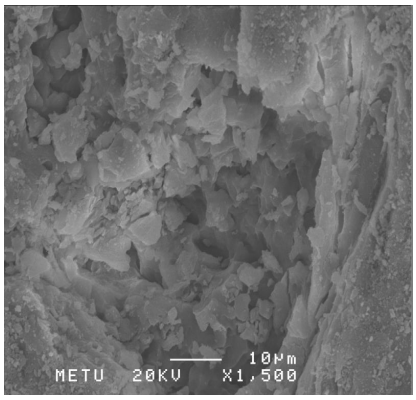


Figure 79. SEM Image of α-Al (c)

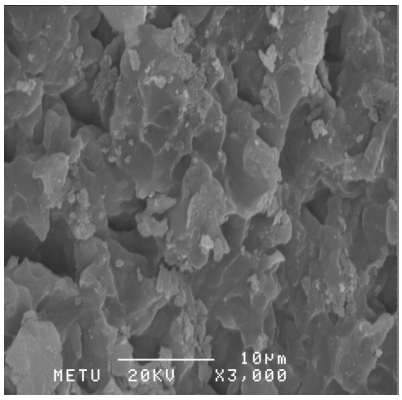


Figure 80. SEM Image of α-Al (d)

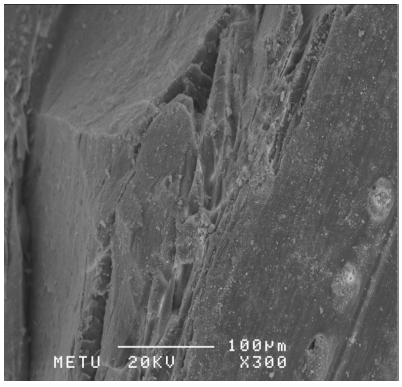


Figure 81. SEM Image of α-Al (e)

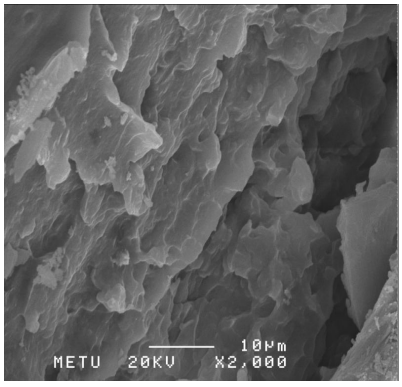


Figure 82. SEM Image of α-Al (f)

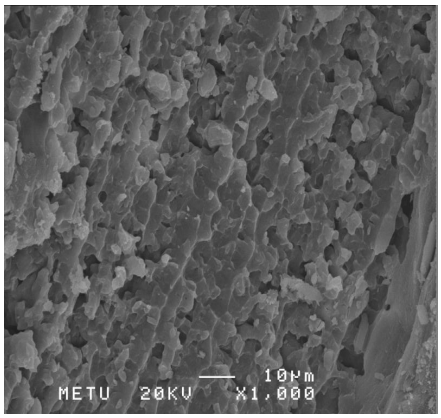


Figure 83. SEM Image of α-Al (g)

SEM Images of γ-Al-1

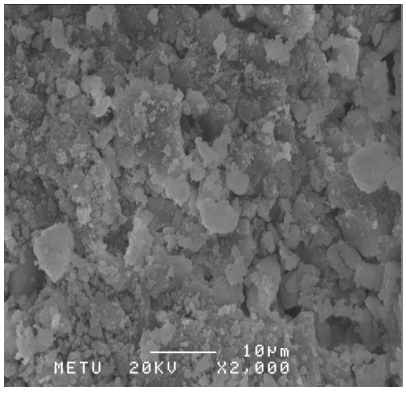


Figure 84. SEM Image of γ-Al-1 (a)

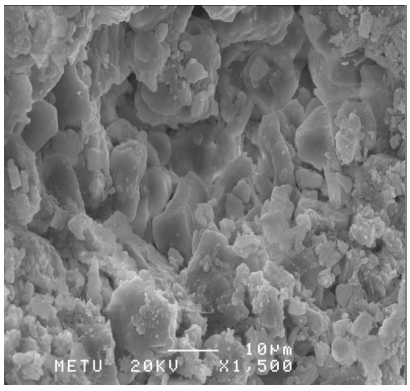


Figure 85. SEM Image of γ-Al-1(b)

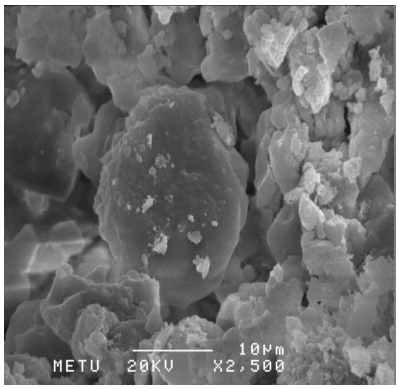


Figure 86. SEM Image of γ-Al-1(c)

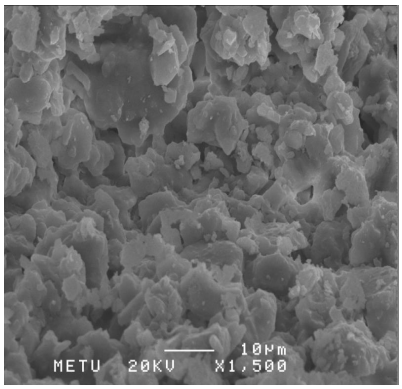


Figure 87. SEM Image of γ-Al-1(d)

SEM Images of γ-Al-2

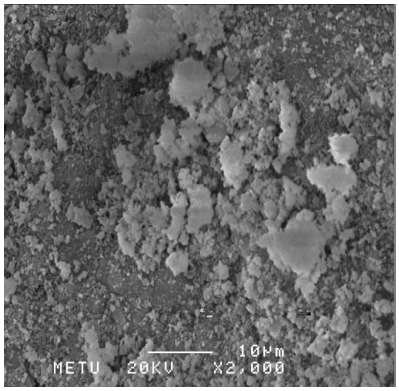


Figure 88. SEM Image of γ-Al-2 (a)

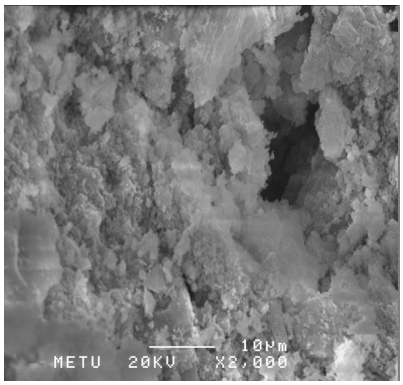


Figure 89. SEM Image of γ-Al-2 (b)

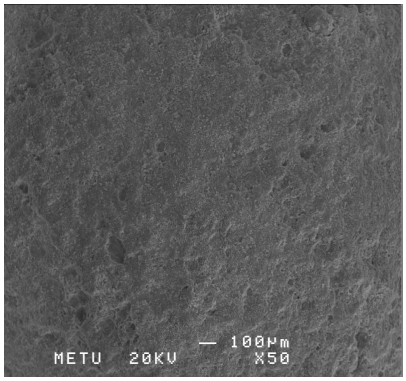


Figure 90. SEM Image of γ-Al-2 (c)

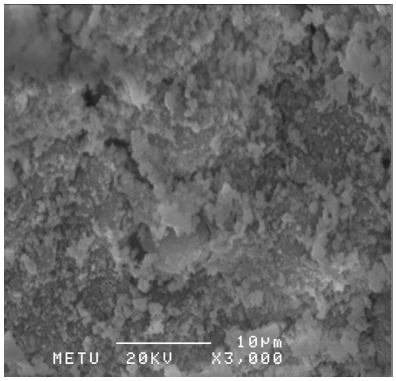


Figure 91. SEM Image of γ- Al-2 (d)

SEM Images of Nafion NR-50

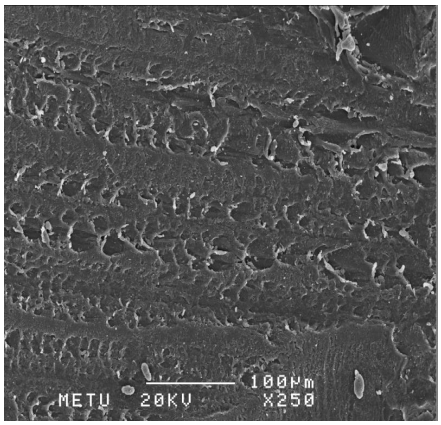


Figure 92. SEM Image of NR-50 (a)

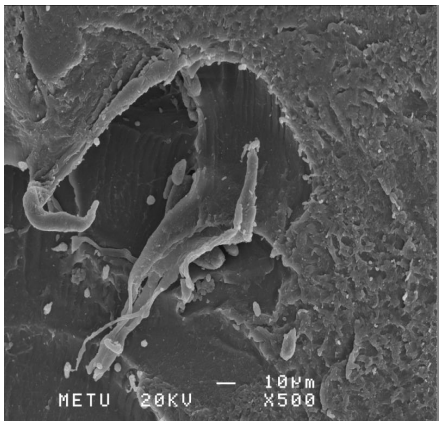


Figure 93. SEM Image of NR-50 (b)

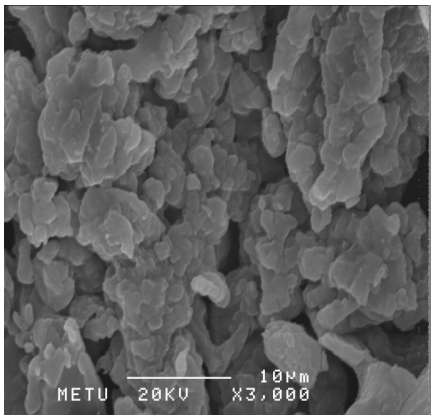


Figure 94. SEM Image of NR-50 (c)

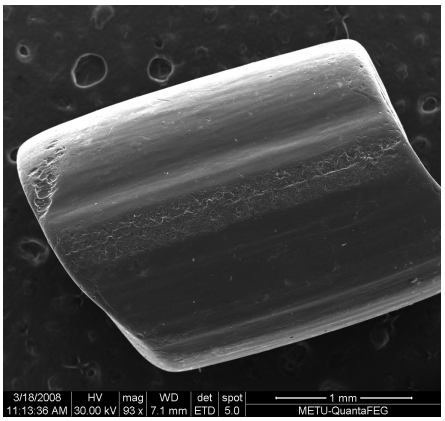


Figure 95. SEM Image of NR-50 (d)

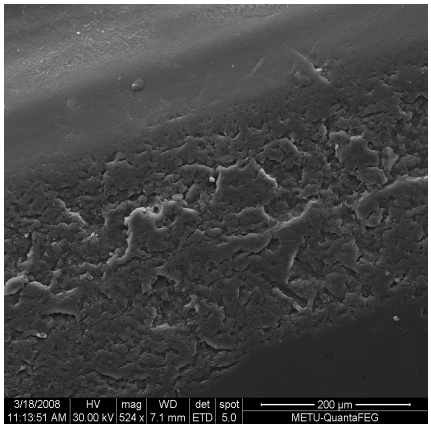


Figure 96. SEM Image of NR-50 (e)

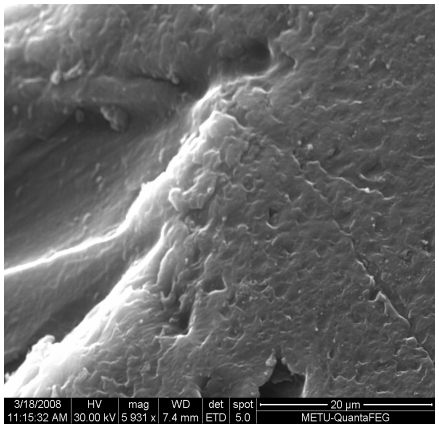


Figure 97. SEM Image of NR-50 (f)

SEM Images of Nafion SAC-13

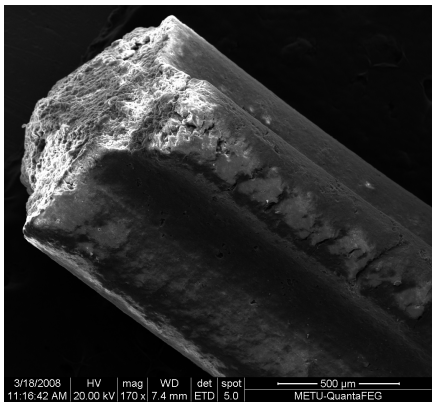


Figure 98. SEM Image of SAC-13 (a)

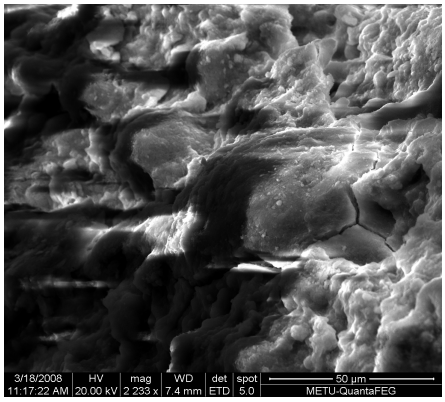


Figure 99. SEM Image of SAC-13(b)

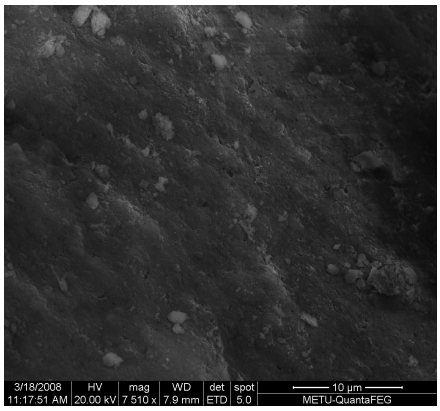


Figure 100. SEM Image of SAC-13 (c)

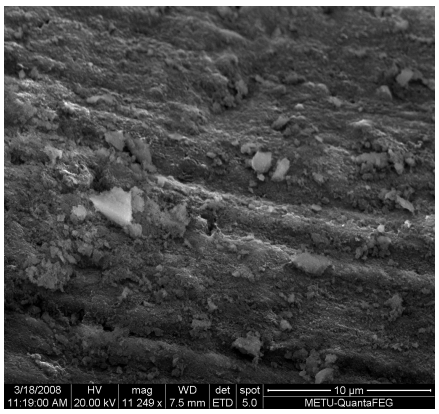


Figure 101. SEM Image of SAC-13 (d)

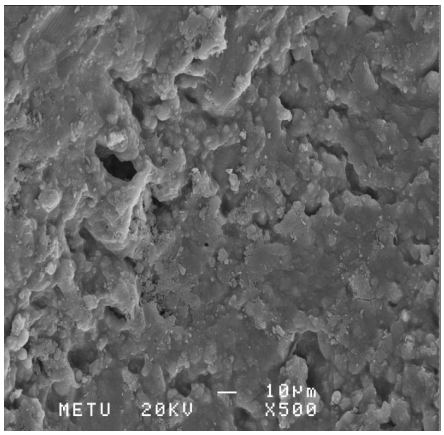


Figure 102. SEM Image of SAC-13(f)

SEM Images of SBA-15

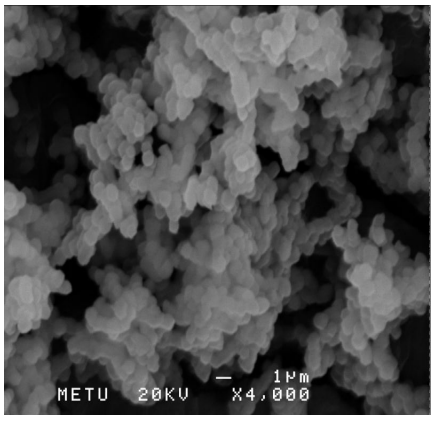


Figure 103. SEM Image of SBA-15 (a)

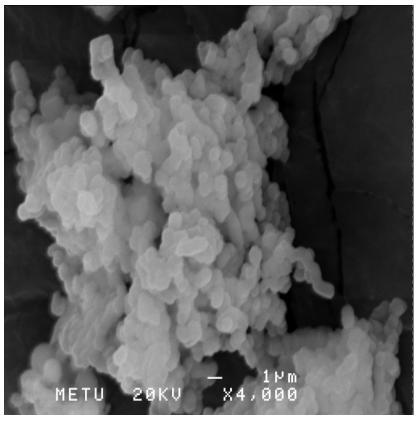


Figure 104. SEM Image of SBA-15 (b)

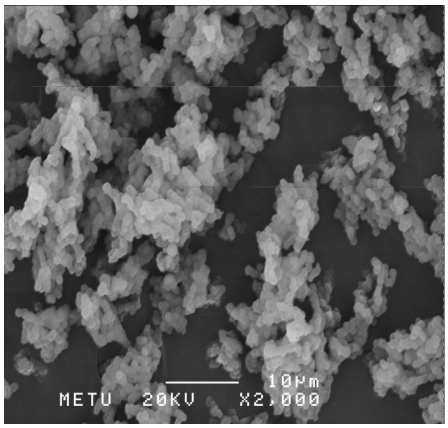


Figure 105. SEM Image of SBA-15 (c)

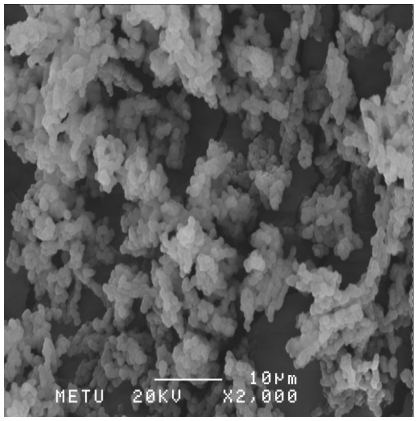


Figure 106. SEM Image of SBA-15 (d)

SEM Image of Al-SBA-15

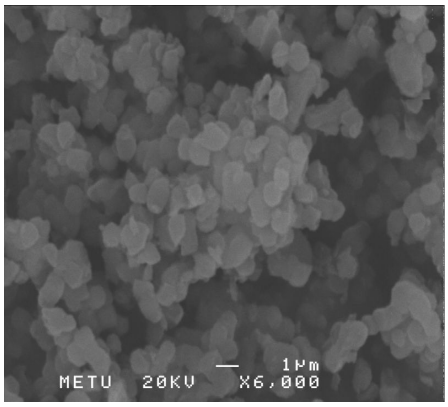


Figure 107. SEM Image of Al-SBA-15 (a)

APPENDIX B.1

CALIBRATION FACTORS OF THE SPECIES FOR CHROMOTOGRAPHIC ANALYSIS

Table 25. Calibration Factors of the Components

Component	Calibration factor
Methanol (C_2H_5OH)	1
DME (CH_3OCH_3)	0.76
Water (H_2O)	2.53
Formaldehyde (CH_2O)	1.33

Carrier Gas: Helium

Column: Poropak T

Gas Flow Rate: 22.2 ml/min

APPENDIX B.2

SAMPLE CALCULATIONS OF THE REACTION PARAMETERS

Calculation of MeOH Flow Rate

$$c = \frac{P}{RT}$$

$$\Rightarrow \rho = \frac{PM}{RT} = \frac{0.96atm \times 32.07}{82.05 \times 298} = 0.001259 g/cm^3 \text{ (at room temperature)}$$

When 20 cc syringe is used with flow rate of $0.035 cm^3/\min$ in the syringe pump,

$$\frac{\rho_{liq}}{\rho_{vap}} = \frac{0.792}{0.001259} = 629$$

$$629 \times 0.035 cm^3/\min = 22 cm^3/\min = 22 ml/\min$$

Calculation of He flowrate

$$\frac{10ml}{27\sec} \times 60\sec/\min = 22.2 ml/\min$$

Calculation of Total Flowrate

$$F_{MeOH} + F_{He} = 22 ml/\min + 22.2 ml/\min = 44.2 ml/\min$$

Ratio

$$\frac{F_{MeOH}}{F_{MeOH}+F_{He}}=\frac{22ml/\min}{44.2ml/\min}=0.497\cong 0.5$$

Conversion of MeOH and Selectivities of Products

$$n_{TOTAL}=\beta_{formaldehyde}\times A_{formaldehyde}+\beta_{MeOH}\times A_{MeOH}+2\times\beta_{DME}\times A_{DME}$$

$$X_{MeOH}=\frac{(n^{0}_{MeOH}-n_{MeOH})}{n^{0}_{MeOH}}$$

$$S_{DME}=\frac{2\times n_{DME}}{(n^{0}_{MeOH}-n_{MeOH})}$$

$$Y_{DME}=X_{MeOH}\times S_{DME}\times\frac{1}{2}$$

$$S_{formaldehyde}=\frac{n_{formaldehyde}}{(n^{0}_{MeOH}-n_{MeOH})}$$

$$Y_{formaldehyde}=X_{MeOH}\times S_{formaldehyde}$$

APPENDIX B.3

OTHER MEOH DEHYDRATION REACTION RESULTS

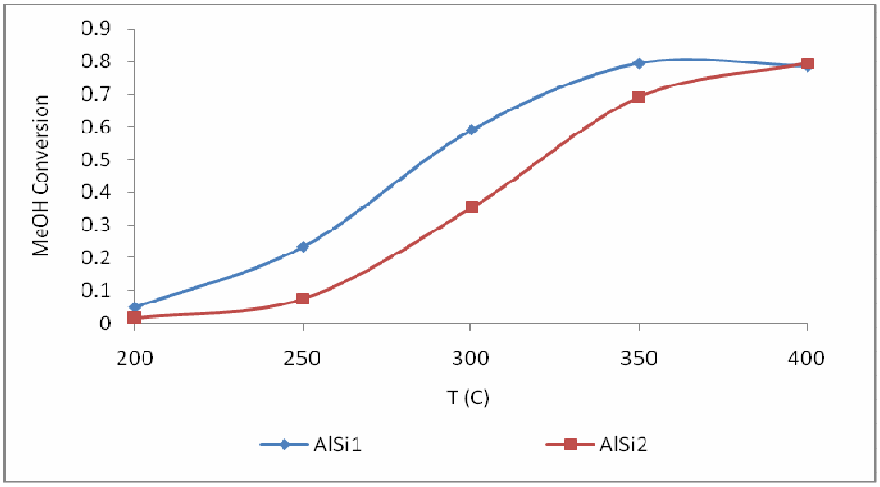


Figure 108. Conversion of Methanol over AlSi1 and AlSi2 at 0.2 s.g/cm^3.

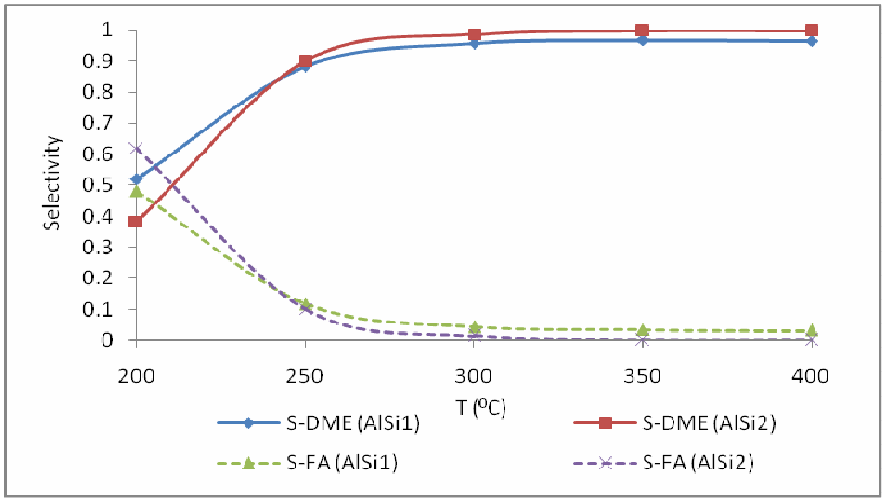


Figure 109. Selectivity of DME and Formaldehyde with AlSi1 and AlSi2 at 0.2 s.g/cm^3.

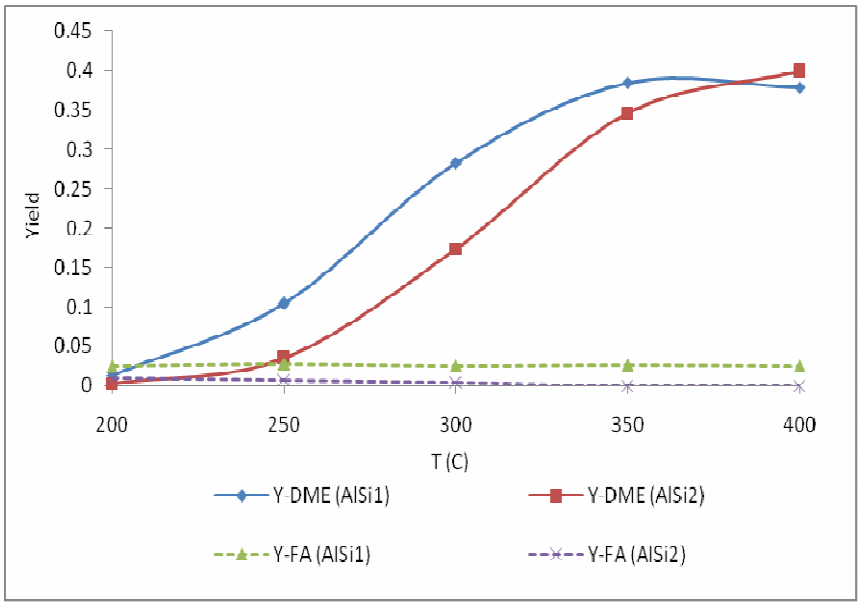


Figure 110. Yield of DME and Formaldehyde with AlSi1 and AlSi2 at 0.2 s.g/cm^3.

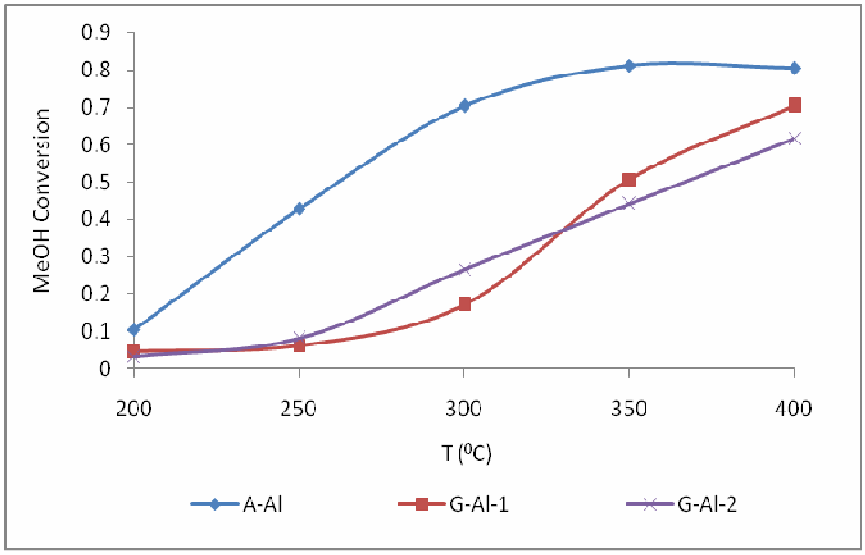


Figure 111. Conversion of Methanol over α and γ Forms of Aluminum Oxides at 0.2 s.g/cm^3.

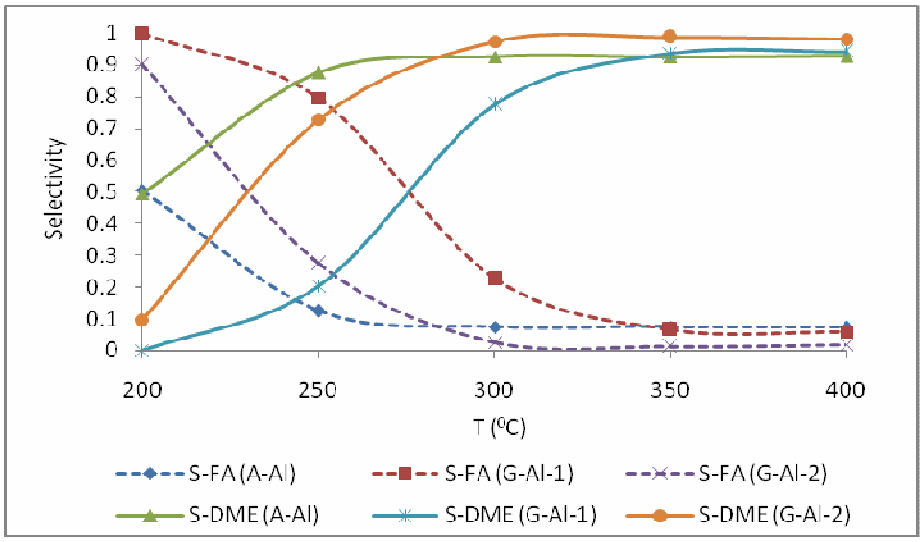


Figure 112. Selectivity of DME and Formaldehyde with α and γ Forms of Aluminum Oxides at 0.2 s.g/cm^3.

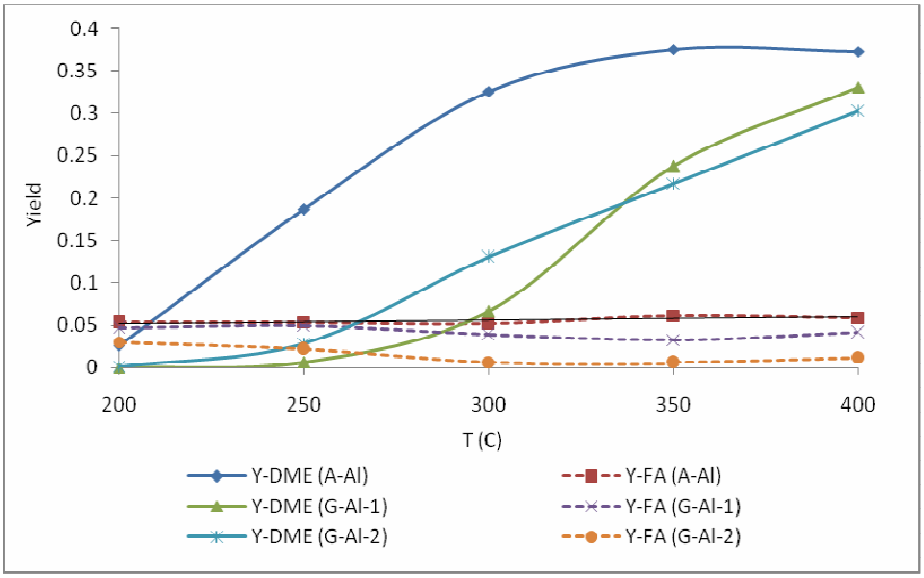


Figure 113. Yield of DME and Formaldehyde with α and γ Forms of Aluminum Oxides at 0.2 s.g/cm^3.

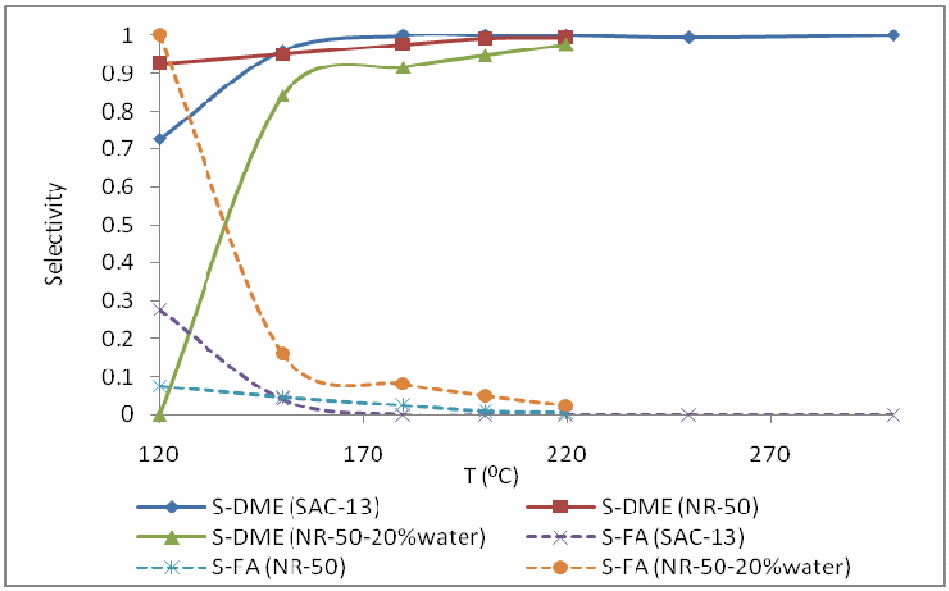


Figure 114. Selectivity of DME and Formaldehyde with Nafion Based Catalysts at 1.36 s.g/cm^3

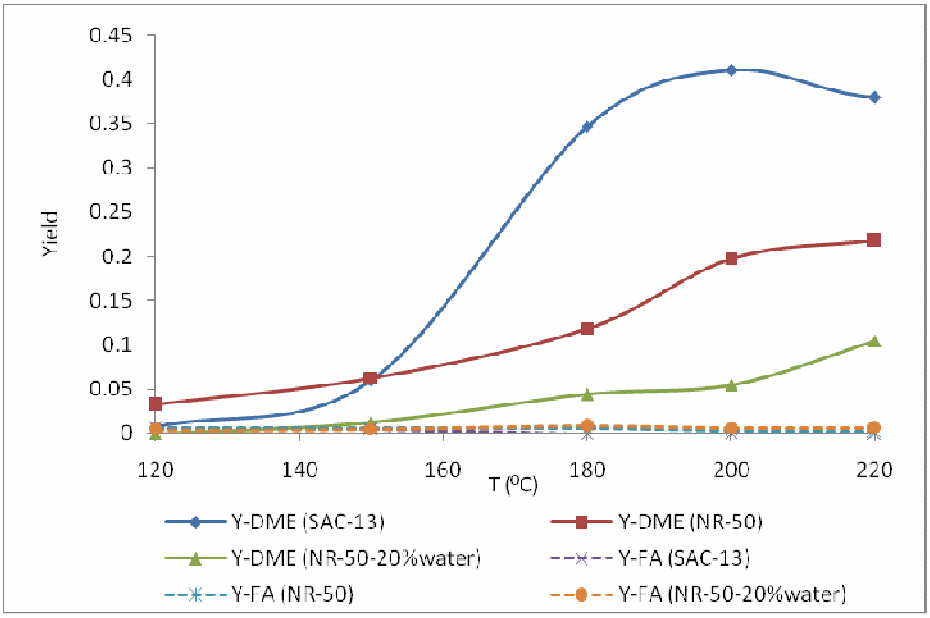


Figure 115. Yield of DME and Formaldehyde with Nafion Based Catalysts at 1.36 s.g/cm^3